Stem Cells International

Cell-Instructive Microenvironment to Direct Stem Cell Fate

Lead Guest Editor: Monica Montesi
Guest Editors: Silvia Panseri, Carla Cunha, Francesca Taraballi, and Marita Bosticardo

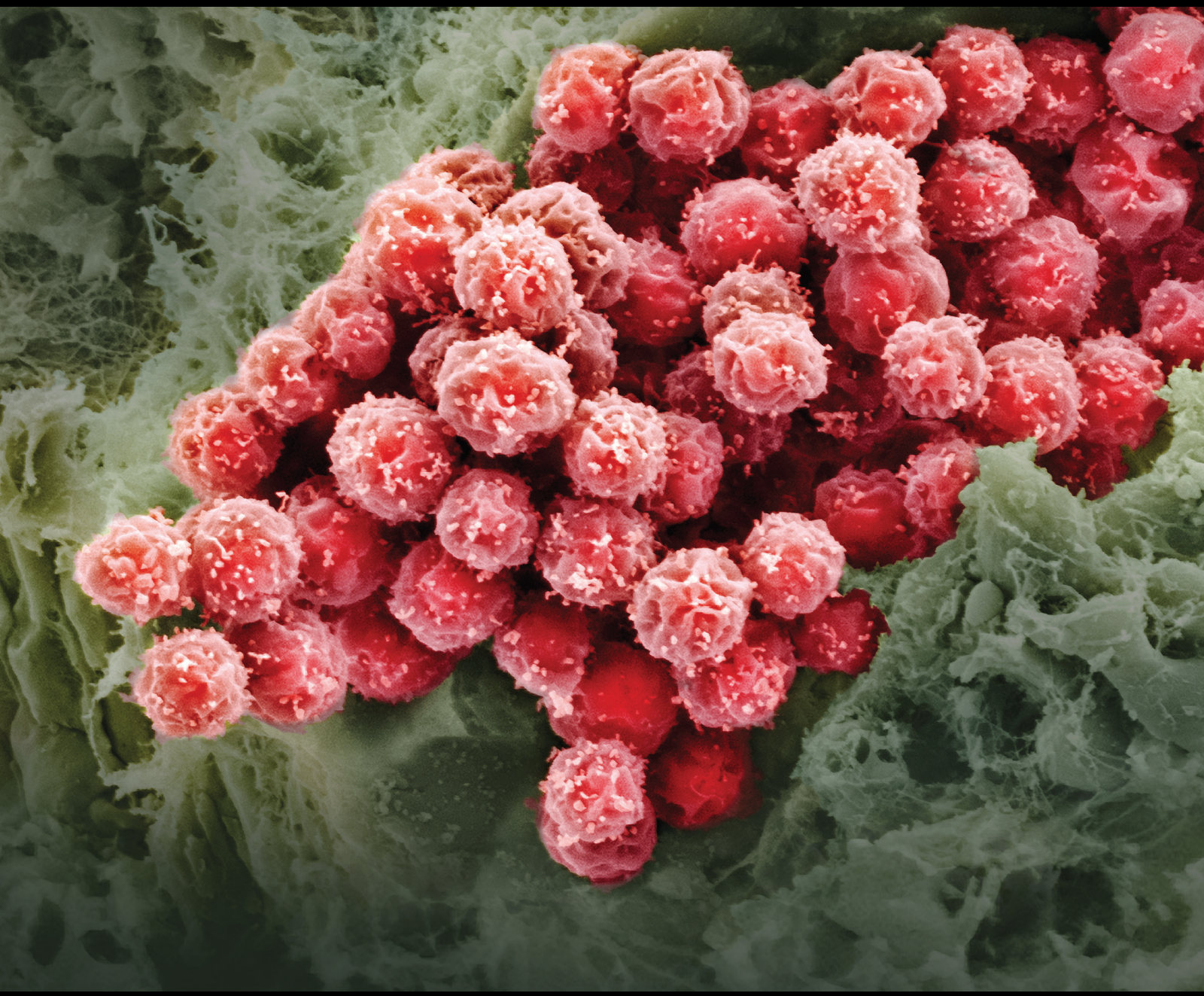

Cell-Instructive Microenvironment to Direct Stem Cell Fate

Stem Cells International

Cell-Instructive Microenvironment to Direct Stem Cell Fate

Lead Guest Editor: Monica Montesi
Guest Editors: Silvia Panseri, Carla Cunha, Francesca Taraballi, and Marita Bosticardo

Contents

Hindawi
Stem Cells International
Volume 2019, Article ID 2180925, 16 pages
https://doi.org/10.1155/2019/2180925

Review Article

Regulation and Directing Stem Cell Fate by Tissue Engineering Functional Microenvironments: Scaffold Physical and Chemical Cues

Fei Xing,[1] Lang Li,[2] Changchun Zhou,[3] Cheng Long,[1] Lina Wu,[3] Haoyuan Lei,[3] Qingquan Kong,[1] Yujiang Fan,[3] Zhou Xiang,[1] and Xingdong Zhang[3]

[1]*Department of Orthopaedics, West China Hospital, Sichuan University, No. 37 Guoxue Lane, Chengdu, 610041 Sichuan, China*
[2]*Department of Pediatric Surgery, West China Hospital, Sichuan University, No. 37 Guoxue Lane, Chengdu, 610041 Sichuan, China*
[3]*National Engineering Research Center for Biomaterials, Sichuan University, 610064 Chengdu, Sichuan, China*

Correspondence should be addressed to Changchun Zhou; changchunzhou@scu.edu.cn

Received 15 October 2019; Accepted 5 December 2019; Published 27 December 2019

Guest Editor: Monica Montesi

It is well known that stem cells reside within tissue engineering functional microenvironments that physically localize them and direct their stem cell fate. Recent efforts in the development of more complex and engineered scaffold technologies, together with new understanding of stem cell behavior in vitro, have provided a new impetus to study regulation and directing stem cell fate. A variety of tissue engineering technologies have been developed to regulate the fate of stem cells. Traditional methods to change the fate of stem cells are adding growth factors or some signaling pathways. In recent years, many studies have revealed that the geometrical microenvironment played an essential role in regulating the fate of stem cells, and the physical factors of scaffolds including mechanical properties, pore sizes, porosity, surface stiffness, three-dimensional structures, and mechanical stimulation may affect the fate of stem cells. Chemical factors such as cell-adhesive ligands and exogenous growth factors would also regulate the fate of stem cells. Understanding how these physical and chemical cues affect the fate of stem cells is essential for building more complex and controlled scaffolds for directing stem cell fate.

1. Introduction

Stem cells have the ability of self-renewal and differentiation; they can be used to repair the bone, cartilage, and skin and play an important role in regenerative medicine [1, 2]. Stem cells are generally classified into embryonic stem cells and adult stem cells. Embryonic stem cells are more primitive, but some studies have shown that they may turn into tumor cells, which dramatically limits their application. At present, adult stem cells, such as bone marrow-derived mesenchymal stem cells (BMMSCs), adipose-derived stromal cells (ASCs), umbilical cord-derived mesenchymal stem cells (UC-MSCs), and even urine-derived mesenchymal stem cells (U-MSCs), have attracted more and more attention and are widely used in the field of regenerative medicine [3]. In the field of tissue engineering regeneration, regulating the proliferation and differentiation of stem cells has been an important research direction for stem cells [4, 5].

The fate of stem cells includes cell proliferation, differentiation, migration, and adhesion. Proliferation and differentiation of stem cells are influenced by the surface of scaffold materials, which have been studied by many researchers in the past decades. Ideal scaffolds for cell survival have the following specific characteristics: firstly, the materials show good biocompatibility; secondly, the materials could be degradable in vivo; thirdly, the fundamental characteristics of materials could mimic the extracellular matrix (ECM) as much as possible [6, 7].

Previous researchers suggested that the scaffold surface microenvironment influenced the fate of stem cells. And the surface microenvironments mainly include physical and biochemical factors [8, 9]. For example, scaffolds with different pore sizes and porosity would lead to different

properties and affect the fate of stem cells. Previous studies have shown that scaffolds with pore sizes of 370-400 μm are more conducive to promote the chondrogenic differentiation for ASCs [10, 11]. Also, scaffolds with different materials also affect the fate of stem cells, including cell proliferation, differentiation, and adhesion [12]. It is essential to have a comprehensive understanding of the regulation of the fate of stem cells by physical, biochemical, and other factors, so that we can better design scaffolds with specific microenvironment characteristics to regulate cells for promoting tissue regeneration.

This review summarizes the factors affecting the fate of stem cells which are mainly discussed in terms of physical and chemical aspects: the material stiffness, surface topography, three-dimensional space, mechanical stimulation, and adhesion proteins, growth factors, and substances secreted by cells on the surface of materials. This review is aimed at highlighting the effects of the surface microenvironment of biomaterials in directing stem cell fate.

2. Advanced Technology for the Manufacturing of Biomimetic Biomaterials

2.1. 3D Printing of Porous Biomimetic Scaffolds. The ideal biomimetic scaffold for tissue reconstruction should resemble natural tissue in both material composition and geometrical properties. For bone tissue biomimetic scaffold, the three-dimensional (3D) porous structure plays a crucial role for bone regeneration [13–16] (Figure 1). This biomimetic porous structure contains interconnected and micro pores and provides a temporary support for cell proliferation and tissue infiltration, as well as a microenvironment for transportation of nutrients and waste products which can function well [17–20]. At the same time, the surface topography of scaffolds also plays an important role in bone tissue regeneration and regulation of cell behaviors. Numerous methods, such as solvent casting/particle leaching [21, 22], phase separation [23, 24], emulsion freeze drying [25], chemical foaming, electrospun, 3D printing, and micropattern techniques [26–29], have been developed to fabricate different porous scaffolds for tissue engineering.

Advances in computational design and 3D printing (3DP) have resulted in quick and accurate fabrication of 3D porous scaffolds with well-controlled geometrical architectures [30–33]. 3DP can fabricate scaffolds with complex internal and external structures in various materials [34–36]. 3DP produces complex scaffolds from a 3D design file by decomposing an object's structures into a series of parallel slices. Internal 3D structures are then fabricated by reproducing these slices one layer at a time by using a sized nozzle (direct extrusion printing) or a programmed selective sintering laser (selective laser melting, SLM), electron beam melting (EBM), or a specific curing light (stereo lithography apparatus, SLA). So far, 3D printing technology has successfully printed various bioceramics, polymers, metal materials, and other biocompatible materials for bone tissue engineering scaffolds [37–39]. These printed scaffolds have highly complicated geometrical architectures with personal-customized shape for different patients in accordance with their CT data. However, the printing capability is limited. For most 3D printing technologies, objects with an accurate porosity of less than 10 μm are difficult to fabricate due to printing accuracy and printing efficiency [40–42].

2.2. Electrospinning of Biomimetic Biomaterials. Electrospinning is curing nanofibers by high-voltage electrostatic force (5-30 kV), which has the advantages of rapid and efficient preparation. In recent years, it has received great attention in the field of tissue engineering. Electrospinning could change the properties by regulating the voltage, conductivity of the solution, distance between the injector and the collector, temperature, and humidity [43]. Common electrospinning materials, including PCL, PLGA, and PLA, have been widely used for tissue regeneration [44–46] (Figure 2). In tendon repairing, orderly arrangement of electrospun nanofibers can guide the arrangement of cells, improve the deposition for ECM, and promote the differentiation of stem cells to regenerate tendon [47]. In addition, electrospun nanofibers could be a suitable carrier, and stem cell could have myogenic differentiation after adding the platelet-derived growth factor (PDGF) [48]. And the arrangement of electrospun nanofibers could be regulated according to requirements. Compared with the random arrangement, the orderly and aligned arrangement of scaffolds showed advantages in neural differentiation of stem cells and migration of neural cell in a rat T9 dorsal hemisection spinal cord injury model, which provided great promise for biomaterial design for applications in nerve regeneration [49].

2.3. Micropattern of Biomaterial Surface Topography. As important factors, the physical and topographical surface of the scaffold could regulate the cell behaviors and control cell function [53, 54]. In addition, a previous study found that the different shapes and sizes of cell could play a role in directing the fates of stem cells [55]. Round cells promoted adipogenesis while cells with high spreading preferred an osteoblast fate by activating MAP kinase pathways and Wnt signaling [53]. In addition, the increased myosin contractility enhances osteogenesis of stem cells. Therefore, the micropatterns of scaffolds could affect the cell behavior by altering the shapes of stem cells [56]. However, these microscopic structures are difficult to fabricate by conventional methods. Literatures reported that the combined uniaxial pressing method and templates may fabricate HA ceramics with regular concaves [57, 58] and grooves [59]. In that work, HA powders were compacted into disc-shaped pellets *via* uniaxial pressing and polystyrene resin microspheres of different sizes were used as poroshifters to form patterned surfaces with a series of regular concaves; the circular holes with diameters of about 50, 200, and 500 μm were patterned uniformly as shown in (Figure 3(a)). *In vitro* studies found that HA bioceramics with 50 μm concaves showed the strongest ability to induce osteogenic differentiation of human osteosarcoma MG-63 cells, as evidenced by the highest alkaline phosphatase (ALP) activity and Cbfa-1 gene expression [57]. Wang et al. reported that HA disc-shaped pellets with micropatterned grooves of ~20, 40, and 60 μm in width were patterned by transferring patterns from different aluminum

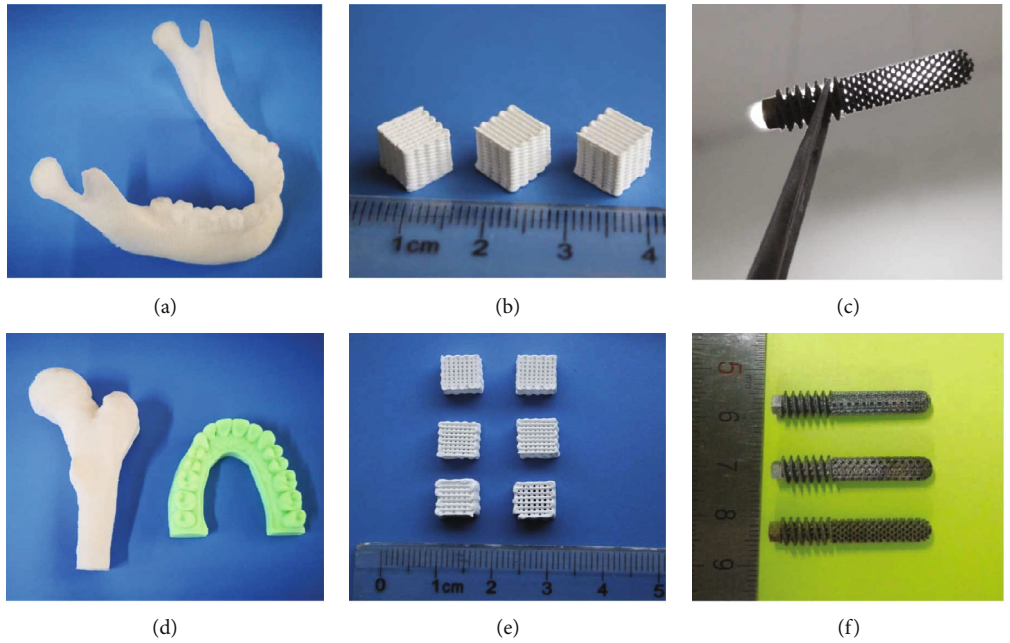

Figure 1: (a, d) Different 3D-printed bone tissue engineering scaffolds. Fused deposition modeling of polymer bone tissue models. (b, e) Direct extrusion 3D printing of calcium phosphate bioceramics. (c, f) Selected laser melting 3D printing of titanium femoral head nail prosthesis [12, 18, 29, 35].

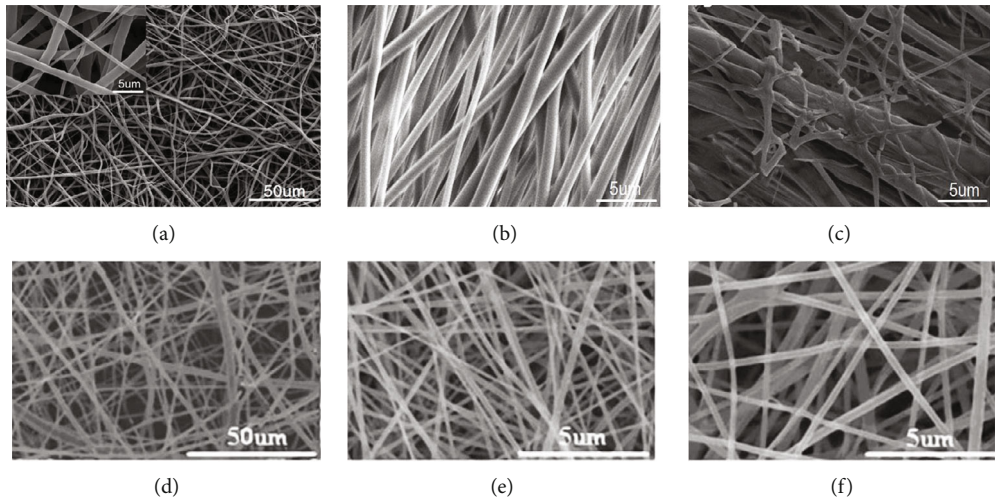

Figure 2: SEM micrographs of different electrospun nanofibers. (a) Electrospun PCL nanofiber [50]. (b) Electrospun-aligned PLGA nanofiber [51]. (c) Electrospun-aligned PLGA/gelatin nanofiber [51]. (d) Electrospun PLA nanofiber [52]. (e) Electrospun silk fibroin-gelatin nanofiber (50 : 50) [52]. (f) Electrospun silk fibroin-gelatin nanofiber (70 : 30) [52].

alloy templates (Figure 3(b)). The HA ceramics with microgrooved patterns showed increased water wettability with decrease of groove width. The microgrooves evidently affected cell elongation, as MC3T3-E1 preosteoblasts were oriented along the direction of grooves, and the cell orientation angles were decreased by decreasing groove width [59]. Zhao et al. [60] fabricated HA ceramics that exhibited micropatterned structured surfaces with quadrate convexes of different sizes *via* uniaxial pressing method by using ordered micropatterned nylon sieves as templates (Figure 3(c)). Compared to the flat one, the micropatterned surface could enhance the adhesion, proliferation, and osteogenic differentiation of rat BMSCs. These studies indicated that bioceramics with regular micropattern of size close to cell size (20-50 μm) showed the best stimulation of cell response.

Furthermore, Wang and Hu [61] created ordered HA patterns with spherical (Figure 3(d)) and hexagonal (Figure 3(e)) shapes on Si and Ti substrates *via* electrophoretic deposition technique. Teshima et al. [62] prepared aligned CaP microstructured patterns with HA nanocrystals by using a hydrophilic/hydrophobic Si-based template photochemically made by VUV light irradiation to provide micro reaction cells for HA crystal growth. Tseng et al. [63] fabricated uniform single-crystal HA nanorods onto specific

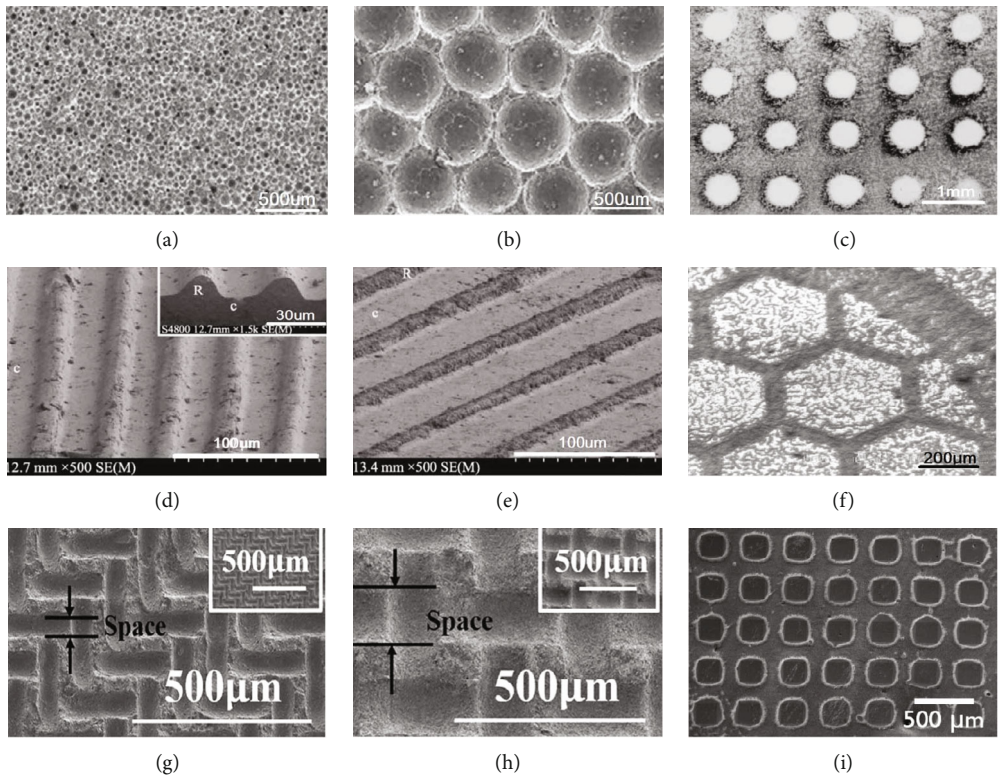

Figure 3: Typical orderly micropatterned scaffold surface. HA bioceramic micropatterned surface with regular small concaves (a) and larger concaves (b) [57]. HA ceramics with spherical array (c) [61]. Micropatterned vertical grooves (d) and inclined grooves (e) [59]. Ordered hexagonal-shape patterns (f) [61]. Quadrate convexes with smaller space (g) and larger space (h) [60]. Grid-shaped patterns (i) [63].

sites of grid-shaped substrate patterned by hexagonal microcontact printing (Figure 3(f)). However, clear cell behaviors or regulation mechanism of these micropatterned scaffolds remains unidentified, but almost all of the highly ordered patterns close to the diameter of the cells show effective regulation of cell fate.

Surface micropatterning has been widely studied in the preparation of biological functional materials. The patterning methods include photolithography [64], electron beam etching [65], and microcontact transfer method [66, 67]. Traditional methods are usually complicated process and cost high, which limit its application in large-area patterning. The inkjet printing technology is easy to realize direct writing of large-area complex patterns and composite functional materials, which makes it to be a promising method of patterning [68, 69].

3. Regulation and Directing of Stem Cell Fate

3.1. Scaffold Physical Cues

3.1.1. Pore Size and Porosity Effects. The pore diameter is an essential parameter of the physical structure for porous scaffolds. Pores may determine the nutrition exchange inside of scaffolds, affect the skeletal tension of cell proliferation process, and regulate the fate of stem cells (Table 1). Cells can recognize micropores of 5 nm in the scaffolds. If the pore size is much larger than the cell diameter, the growth situation of the cells will be similar to that on the plate [70]. The pore diameter will affect the adhesion and migration of cells. It is generally believed that scaffolds with a small pore diameter were facilitating the adhesion of cells, while scaffolds with a large pore diameter are more conducive to the migration of cells from the outer layer of scaffolds to the inner layer of scaffolds. In the experiments of osteogenic differentiation of stem cells, it is generally believed that the diameter of 100-300 μm is more conducive to the osteogenic differentiation of bone marrow-derived mesenchymal stem cells [71]. Some scholars have proposed that the pore size of 200 μm is the optimal condition for the osteogenic differentiation of cells [72]. However, 350 μm is considered to be the optimal condition for cell proliferation [73]. When the diameter is larger than 500 μm, cell adhesion will be reduced, which is not conducive to cell proliferation [11]. In terms of cartilage formation, scholars believe that when the diameter is close to 400 μm, it is conducive to cartilage repairing [74]. As for the differentiation of hematopoietic stem cells, it is believed that less than 150 μm is more conducive to the differentiation of stem cells into hematopoietic stem cells [75]. In addition, high porosity could promote the transport of nutrition and oxygen, making it easier for cells to grow inward. However, due to a large number of pores, the mechanical properties of scaffolds will be decreased [76]. The optimal porosity has not been determined, and many studies have shown that scaffolds with high porosity (96.7%) can promote cell proliferation, which may be due to high porosity to promote the transport of nutrients. Some studies showed that when porosity was 86%, cell proliferation was better, which may

Table 1: Proposed optimal pore sizes and porosities affecting the fate of stem cell.

Material	Optimal pore size (μm)	Optimal porosity (%)	Target stem cell(s)	Potential application(s)	Reference
β-Tricalcium phosphate	200-600	65	BMMSCs	Osteogenic	[78]
Sintered titanium fiber mesh	250	86	BMMSCs	Osteogenic	[79]
PCL	200		ASCs	Proliferation	[74]
PCL	400		ASCs	Chondrogenic	[74]
Polycaprolactone	370–400	80–97	BMMSCs	Chondrogenic	[11]
Poly(lactic-*co*-glycolic acid)	120–200	50	ASCs	Hepatogenesis	[80]
Poly(lactic-*co*-glycolic acid)	50–200		BMMSCs	Myogenic	[81]
Coralline hydroxyapatite	200	75	BMMSCs	Osteogenic	[82]
β-Tricalcium phosphate	400–500	70	BMMSCs	Osteogenic	[83]
ZrO_2 ceramic	600	80–89	ASCs	Osteogenic	[84]
Polycaprolactone	100–150		BMMSCs	Chondrogenic	[85]

be because different scaffold materials have different effects on different cells [77].

3.1.2. Stiffness Effects. The fate of cells is also affected by the stiffness of the surface microenvironment. Firstly, studies have shown that the stiffness of matrix could affect the differentiation spectrum of stem cell (Figure 4). Stem cells differentiate into muscle cells on soft substrates and osteoblasts on harder substrates [86, 87]. Another study supported this finding, and stem cell on soft materials when stiffness is less than 0.05 kPa could promote neural differentiation effectively, while hard stiffness materials (>40 kPa) promoted osteogenic differentiation effectively [88, 89], which could be related to the Wnt signal pathway [90]. However, there is no agreement on the optimal stiffness for stem cells to differentiate into neurons, muscle cells, cartilage cells, and osteoblasts [86, 91]. Secondly, the stiffness of the material also affects stem cell migration. Stem cells tend to migrate to harder matrix [92]. However, the specific matrix of stem cell migration to the high stiffness matrix is unknown and may be associated with contractility of stem cells [93]. Moreover, the surface stiffness also affects the proliferation of stem cells [94]; a previous study has shown that hydrogels with very soft modulus (~10 Pa) decreased cell proliferation and differentiation [95]. In addition, stiffness is an important factor to maintain the survival rate for stem cells; studies have shown that stem cell on the matrix with a stiffness of 200 Pa survived more than 90% compared to 80% in cultures (100 Pa) [96]. Another study showed that the hardness of 2.5 MPa increased pluripotency [97]. However, the optimal stiffness to maintain pluripotency of stem cells has not been determined, which may be related to different stem cells and material properties from different sources.

3.1.3. Topography Effects. Surface topography plays a vital role in regulating stem cell behavior. In vivo, the topography of the extracellular matrix (ECM) is the basis for cell survival and affects stem cell behavior [99]. In vitro, the surface topography of scaffolds influences the fate of stem cells, including gene expression, cell adhesion, cell proliferation, and extracellular matrix secretion. The scaffold is the cornerstone and directly contacts with stem cell, so the effect of surface topography on stem cells has been widely studied. Surface topography such as roughness and texture is very important in regulating cell response and determining cell fate.

The roughness of the material's surface also plays a role in the fate of stem cells, with a rougher surface reducing the proliferation rate of stem cell compared to a smooth surface. On rough surfaces, cells are more likely to form composite layers, so stem cells are more likely to accumulate in grooves, holes, canyons, and craters, forming bone nodules and ultimately osteogenic differentiation. In the study of Graziano et al., stem cells differentiated faster on concave surfaces and showed nuclear polarity and a high expression of bone-specific proteins, and the interaction between cells and scaffolds is better. However, when cultured on the convex surface, the proliferation activity of stem cells was low, and the extracellular matrix secretion was reduced [100]. Some studies have found that topography can also affect the differentiation lineages of cells. Several lineages including chondrogenic differentiation, osteogenic differentiation, and neuronal differentiation have been studied [101–103].

In the past decades, the rapid development of nanotechnology has promoted the development of material surface topography modification [104]. Different surface topographies have been reported, such as porous silicon, TiO_2 nanotube, binary colloidal crystal, colloidal lithography, nanopillars, and nanopillar topographies [105–107] (Figure 5). Nanoscale surface topographies can be constructed by means of electrochemical etching [108, 109], lithography [110, 111], sputtering [112], and colloidal lithography [105, 113, 114]. Each of these methods has advantages and limitations. According to topography forms, nanotech surface topographies could be divided into nanopits, nanocolumns, nanogrooves, and nanotubes. Previous studies have found that ordered nanopits can reduce cell adhesion [115]. However, disordered nanopits can better promote the osteogenic differentiation of embryonic stem cells [116]. Previous studies have found that the height of nanoliths has a great impact on the osteogenic differentiation of stem cells. The height of nanoliths less than 50 nm can stimulate the adhesion of stem cells and improve the osteogenic differentiation, while nanoliths with height of 95 nm were not good for adhesion of stem cells

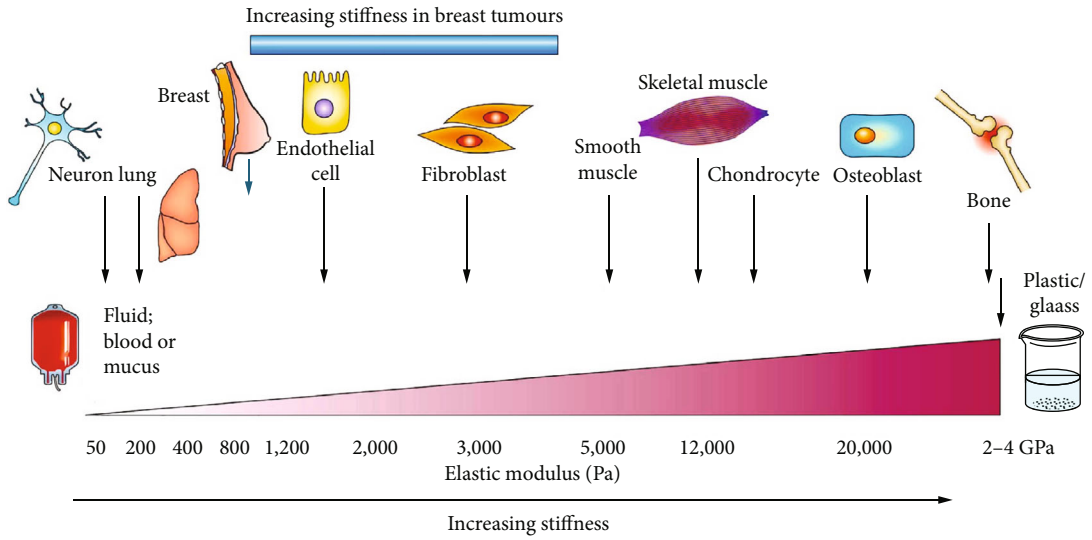

Figure 4: The stiffness affecting the fate of stem cell in vivo, adopted figure from Butcher et al. [98]; the brain is softer than bone, and stem cells are more likely to differentiate into neural differentiation on a soft cell matrix. By contrast, osteogenic differentiation is more likely to occur on scaffolds, which are harder and have material properties similar to those of newly formed bones.

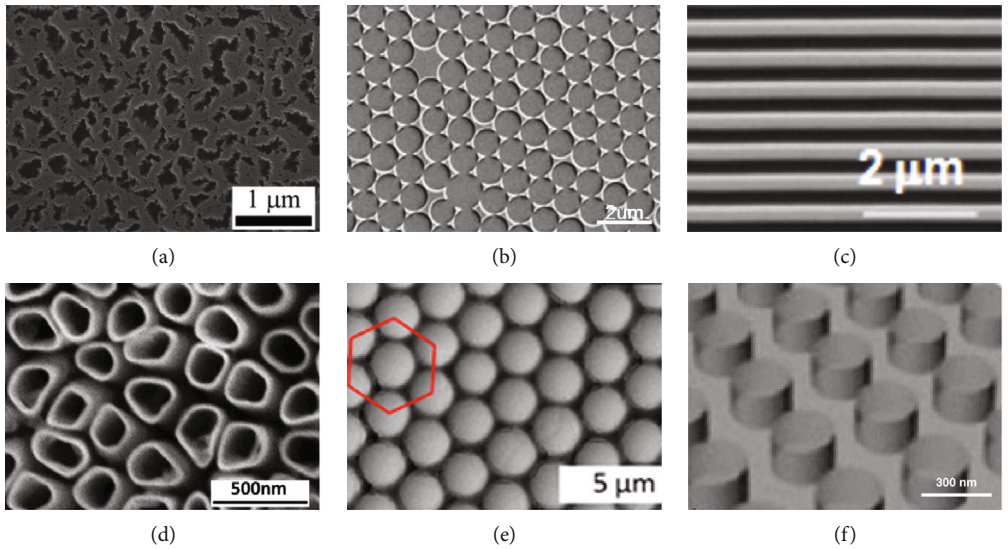

Figure 5: Nanotechnology on different materials with different topographies. (a) Porous silicon fabricated by electrochemical etching, adopted figure from Wang et al. [123]. (b) Colloidal lithography fabricated by self-assembly and sputtering [105]. (c) Nanogrooves fabricated by UV-assisted capillary force lithography [124]. (d) TiO_2 nanotube fabricated by anodization [125]. (e) Binary colloidal crystals fabricated by self-assembly [126]. (f) Nanopillars (polyurethane acrylate) fabricated by nanoimprinting [127].

[115]. Nanogrooves are the most common nanoscaffold material, which could promote cell extension or migration, fix cell arrangement, and affect cell differentiation. The arrangement of nanoscale grooves also has an effect on cell fate, and compared with the parallel groove, vertical groove retracted faster [117]. In nanoscale grooves, the ratio of grooves to ridges also influences cell differentiation, and grooves : ridges = 3 : 1 could promote stem cell osteogenesis [118]. In addition, some scholars have discussed the width of groove, and the width of the groove may have an effect on the differentiation spectrum of stem cells, but there is no unified conclusion [116, 119]. As for the limiting sensitivity to grooves, studies have shown that stem cell is sensitive to grooves in 8 nm [120]. However, because of the complexity of manipulating and evaluating cell fate, it is difficult to construct nanoscale materials systematically, and its clinical application is still limited.

In addition, hydrophobicity and chemical moieties are also important factors influencing stem cell behavior. Hydrophilic biomaterial is more conducive to protein adsorption, promoting the transport and excretion of nutrients. Therefore, it is more conducive to tissue regeneration [121, 122]. The chemical composition of the material is similar to that of the host tissue, which is more conducive to the integration of the tissue. For example, calcium phosphate ceramics are chemically similar to natural bone tissue, so they are widely

used in bone repair. It was found that this calcium phosphate material could integrate well with bone tissue [16, 37].

3.1.4. Spatial and Dimensional Influences. Cells cultured by a two-dimensional (2D) culture lose their original characteristics in vivo gradually. However, 3D culture could better simulate the living environment of cells in vivo. The cells obtained from a 3D culture were significantly different from those obtained from the 2D culture in terms of morphological structure, proliferation and differentiation, gene expression, and cell function [128]. The 3D cell culture can not only retain the material structure foundation of natural cell microenvironment but also simulate the microenvironment of cell growth *in vivo* (Figure 6), which overcomes the defects of the previous two methods and provides a simpler, safer, and more reliable method for cell research. More and more researches adopt 3D scaffolds for stem cell culture. Some studies have shown that the proliferation and differentiation potential of ASCs is significantly stronger than that in 2D environment when cultured about 21 days [129, 130]. 3D environment prevented the reduction of osteogenic differentiation efficiency of stem cells caused by aging or passage [130]. In the field of tissue engineering, 3D culture could promote the differentiation of stem cells into bone and cartilage compared with 2D culture, which is widely used in the osteochondral tissue engineering [16, 30]. 3D culture also provides a good scaffold for neuron growth, in which neurons could grow in all directions and form a neural network, providing a better method for neuron regeneration [131, 132]. 3D culture can also improve survival of stem cells, as shown in a study by Lee et al., which also found that 3D culture has the advantage of maintaining genomic stability [133]. In the study of Adil et al., 3D culture could generate more neurons with electrophysiological activity, increase cell activity, and integrate well with host tissues after implantation [134].

3.2. Scaffold Chemical Cues

3.2.1. Phytochemical Cue Stimulation. The chemical signal of the cell microenvironment can regulate the fate of stem cells. The chemical properties of the surface of the material, such as the characteristics of the material itself, cell coculture, and adhesion between cells could affect the proliferation and differentiation behavior of the cells. For example, many studies have reported that hydroxyapatite itself could promote osteogenic differentiation of stem cells [59]. Some growth factors such as VEGF could promote the differentiation of stem cells into vascular endothelial cells [136]. In our previous study, we have shown that cell coculture could affect the fate of stem cells [137]. Another study showed that coinjection of MSCs and VEGF could affect the fate of stem cell and improve cell implantation myocardial infarction [136, 138].

A large number of studies have been conducted on the effects of phytochemicals on the fate of stem cells. Currently, the phytochemicals studied mainly fall into the following categories: icariin [139], resveratrol [140], quercetin [141], and curcumin [142] (Table 2). Icariin is extracted from the plant herba epimedii and helps improve male fertility [143]. Icariin is associated with phosphorylation of ERK and p38 and activates the ERK and p38 MAPK signaling pathways, leading to the upregulation of MAPK target downstream transcription factors Elk1 and C-MYC, promoting the proliferation of rat BMMSCs. In addition, the optimal concentration of icariin in medium for the proliferation of BMMSCs is 320 μg/L. However, these findings need to be further confirmed in vivo [143]. As a phytoestrogen, resveratrol is a naturally occurring polyphenolic compound in red wine and numerous plants. In addition, resveratrol could activate estrogen receptor signaling selectively. For human mesenchymal stem cells, resveratrol upregulated the expression of osteolineage genes RUNX2 and osteocalcin while suppressing adipolineage genes PPARγ2 and LEPTIN in adipogenic medium, which was mediated mainly through the SIRT1/-FOXO3A axis with a smaller contribution from the estrogenic pathway [144]. As an inflammatory demyelinating disease, experimental autoimmune encephalitis is a useful model providing considerable insights into the pathogenesis of multiple sclerosis. The combination of resveratrol and BMMSCs could effectively alleviate the symptoms of autoimmune encephalitis, which is associated with its immunomodulatory effects. The combination of resveratrol and BMMSCs could effectively suppress proinflammatory cytokines (IFN-γ, TNF-α) and increase anti-inflammatory cytokines (IL-4, IL-10) [145]. Quercetin is one of the most ubiquitous bioflavonoids, widely found in many kinds of plants [141]. Quercetin has a positive pharmacological effect on bone metabolism, which could play a leading role in the quercetin-promoted osteogenic proliferation and differentiation of MSCs by activating the ERK1/2 and JNK signaling pathways [146]. Curcumin is a natural phenolic component of yellow curry spice, which is used in some cultures for the treatment of diseases associated with oxidative stress and inflammation. In addition, curcumin could prevent the death of neurons in animal models of neurodegenerative disorders [142]. Kim et al. conducted a research to investigate the effects of curcumin on mouse multipotent neural progenitor cells and adult hippocampal neurogenesis. The results showed that curcumin could promote the proliferation and neural differentiation of hippocampal embryonic stem cells at low concentrations and be cytotoxic at high concentrations. In addition, curcumin could activate cellular signal transduction pathways, including ERK and p38MAPK pathways, which could regulate neuronal plasticity and stress responses [147]. In conclusion, phytochemical stimulation regulates the fate of stem cells by regulating signal pathways such as Wnt, protein kinase, and PI3K/Akt signaling pathways.

3.2.2. Cell-Adhesive Ligand Effects. The adhesion of cells and their surroundings is very important to the fate of stem cells, which can regulate the apoptosis, migration, and differentiation of stem cells [158]. This cellular adhesion to the microenvironment is mediated by transmembrane matrix receptors (Figure 7). Integrin is an important transmembrane receptor that plays an important role in signal transduction by mediating the main link between cells and ECM [159]. Integrin is a heterodimer transmembrane molecule

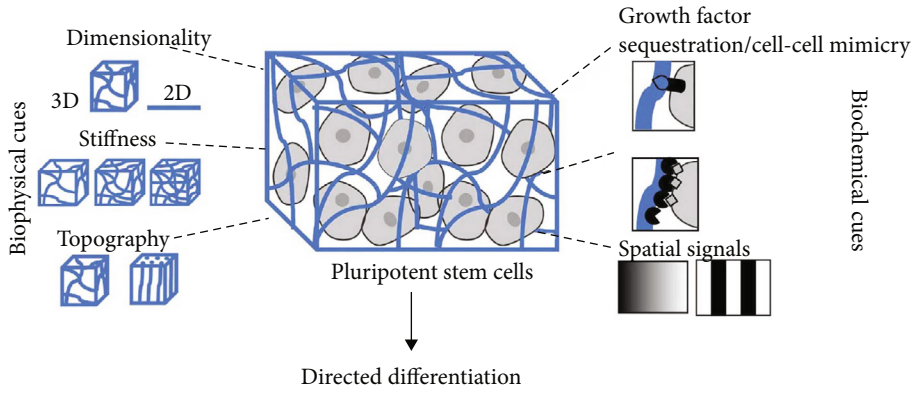

Figure 6: Compared with 2D environment, 3D environment could carry growth factors, maintain stiffness, and promote stem cell differentiation [135].

Table 2: The applications of phytochemicals for stem cell.

Phytochemical	Affecting signal transduction pathway	Target stem cell(s)	Potential application(s)	Reference
Icariin	PI3K/Akt and STAT3	ASCs	Diabetes-associated erectile dysfunction	[148]
	ERK and p38 MAPK	BMMSCs	Proliferation	[143]
	SDF-1alpha/HIF-1alpha/CXCR4	BMMSCs	Migration	[139]
	PI3K and ERK1/2	BMMSCs	Angiogenesis and neurogenesis	[149]
Resveratrol	SIRT1/FOXO3A	Human embryonic stem cells	Osteoblastic differentiation	[144]
	AMPK	BMMSCs	Osteogenic differentiation	[140]
	AMPK/Ulk1	Embryonic stem cells	Pluripotency	[150]
	SIRT1	Umbilical cord-derived mesenchymal stem cells	Neural repair of Alzheimer's disease	[151]
Quercetin	p38 MAPK, ERK1/2, and JNK	BMMSCs	Osteogenesis	[141]
	TNF-alpha	BMMSCs	Osteogenesis	[152]
	BMP2, Smad1, Smad4, RUNX2, OSX, and OPN expression and Smad1 phosphorylation	BMMSCs	Differentiation	[153]
Curcumin	Self-renewal genes, Notch1 and Hes1	Neural stem cells	Proliferation	[154]
	Caveolin-1	Epidermal stem cells	Proliferation	[155]
	Glucocorticoid receptor and STAT3	Embryonic neural stem cells	Proliferation	[156]
	TERT gene	ASCs	Improve lifespan	[157]

composed of different alpha and beta subunits that binds directly to ECM proteins such as collagen, laminin, and fibronectin. Integrins bind to adhesion molecules (CD54 or ICAM1) on the cell surface and adhesion molecules (CD106 or VCAM1) which are present in stem cells. However, in in vitro culture, the expression of integrin is different due to different cell sources and culture methods. RGD is an integrin-binding ligand, which could be used to explore the interaction between cells and ECM [160]. Studies have shown that changing the coupling strength of RGD peptide on substrates could regulate the adhesion, diffusion, and differentiation of MSCs [161]. By adding RGD-related polypeptide into hydrogel, cell adhesion and diffusion could be promoted while high concentrations of RGD also inhibit cell detachment [162]. Due to the importance of adhesion between cells and matrix, strategies for adding binding ligands to hydrogels have been studied. Luo et al. discovered an agarose hydrogel which could react with RGD peptides by exposure to light [163]. In addition to RGD, other adhesion peptides, such as YIGSR and IKVAV, could also influence the fate of stem cell [164, 165]. Integrin, adaptor, and signal proteins together form the adhesive plaque complex, which contains more than 100 proteins which connect actomyosin and ECM and form the signaling pathway [166, 167]. In addition to integrins, cadherins are important receptors on cell surfaces and are involved in stem cell migration and homing [168]. Cadherins play an important role in stem cell early adhesion and self-renewal [169]. The study of cadherins is limited now, and more researchers are needed in the future. In addition to integrin and cadherin, other cell surface

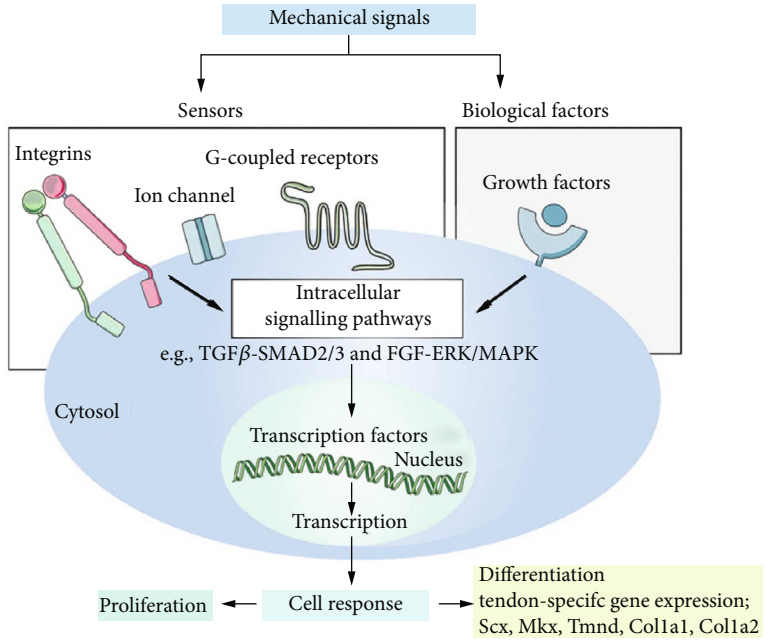

Figure 7: Mechanical signal transduction. Mechanical signaling influences the proliferation and differentiation of stem cells through integrins, ion channels, receptors or exogenous growth factors, and complex intracellular pathways [171].

receptors are also considered important for stem-niche interactions, including EGF, Notch, curl, TGF beta, gap junction, c-kit, CD44, and VCAM1 [170].

3.2.3. Growth Factor Effects. The development and differentiation of stem cells are affected by various internal mechanisms and microenvironmental factors, and growth factors are often used as inducers of differentiation (Figure 7). Therefore, it is very important to clarify their role in the survival or differentiation of stem cells. There are also growth factors that mobilize stem cells to return home for tissue repair. The most common growth factor includes platelet-derived growth factor, insulin-like growth factor-1, hepatocyte growth factor (HGF), EGF, and angiopoietin [172–176]. Currently, growth factor is widely used in the field of regeneration, such as bone regeneration and cartilage regeneration. There are many cytokines that promote bone formation, such as BMP, PDGF, TGF-beta, FGF, and IGF [177]. Among them, BMP is the most widely used osteogenic factor. BMP could induce MSC proliferation and differentiation into chondrocytes and osteoblasts [178]. In terms of heart repair, literatures reported that coinjection of MSCs and VEGF into the heart with myocardial infarction increased cell implantation and resulted in better cardiac function than either VEGF or MSC alone [136, 179]. Mesenchymal stem cells with IGF-1 overexpression promote bone marrow stem cell mobilization through paracrine activation of SDF-1alpha/CXCR4 signaling so as to promote cardiac repair [138]. The combination of laminin and platelet-derived growth factor could promote neuronal differentiation of U-MSCs [180]. Hepatocyte growth factor could promote the differentiation of stem cells, which may be associated with the activation of Wnt signaling [181]. Another study found that this hepatocyte growth factor significantly promotes the viability of embryo-derived mesenchymal stem cells and prevents its senescence, which is associated with transcription of RAD51 [182]. All of the above growth factors have an impact on the proliferation and differentiation of stem cells. Loading growth factors onto the scaffold material could affect the growth of stem cells, which could be the direction of tissue engineering research. Local sustained release is an important part of how to use growth factors efficiently.

4. Conclusion and Future Perspective

The fate of stem cells in the body is complicated and much remains unknown. The fate of stem cells is regulated not only by the genetic material but also by the microenvironment. The ideal microenvironment is a combination of various conditions to simulate the extracellular matrix as much as possible, to construct the physicochemical conditions suitable for the growth of stem cells, and to meet the requirements of proliferation, differentiation, adhesion, and other aspects of stem cells. Ideal microenvironments include a proper mechanical stiffness, porosity, aperture, topography, 3D environment, proper mechanical stimulation, and orderly/disordered arrangement. It is generally believed that scaffolds with a pore diameter of 100-300 μm are more conducive to the osteogenic differentiation of bone marrow-derived mesenchymal stem cells. When the diameter is larger than 500 μm, cell adhesion will be reduced, which is not conducive to cell proliferation. In terms of cartilage formation, it is generally accepted that when the diameter is close to 400 μm, it is conducive to cartilage repairing. Stiffness is an important factor to maintain the survival rate for stem cells. Stem cells tend to migrate to harder matrix. Different substrates with varied stiffness would affect stem cell

differentiation. In addition, exogenous phytochemicals, peptides, and growth factors will stimulate stem cells through a series of complex signaling pathways, affecting the fate of stem cells. Changing the microenvironment to guide stem cell behavior is challenging because of the complex structure of cells and some unknown signaling pathways, which require greater efforts in the future. With the development of fabrication techniques, there are many advance fabrication methods, such as 3D printing, electrospinning, and micropatterning, which were successfully applied to design and fabricate scaffolds with specific microenvironment [183].

At present, many researchers have promoted stem cell differentiation and tissue regeneration by adding growth factors. However, studies have shown that matrix characteristics may be more important than exogenous addition of growth or differentiation factors, which may provide a direction for future research [86]. This review highlights the contribution of physical and chemical cues that influence stem cell fate. Most of the current studies are preclinical, and their progress in clinical applications requires additional testing to demonstrate safety and efficacy. In addition, it was found that the same materials have different effects on the fate of stem cells from different sources. Proper stem cell and matched surface microenvironment remain the focus of future research. By combining these strategies with existing material properties to guide cell fate, stem cells could be an important option in tissue engineering. Although there are many factors and cues that can regulate the release of growth factors, they have advantages and disadvantages and need to be selected according to the specific situation.

Conflicts of Interest

The authors declare that they have no conflicts of interest.

Authors' Contributions

Fei Xing and Lang Li contributed equally to this work.

Acknowledgments

This work was supported by the National Key Research and Development Program of China (Nos. 2018YFC1106800 and 2018YFB1105600), the National Natural Science Foundation of China (31971251), the Sichuan Province Science & Technology Department Projects (2019YFH0079, 2016CZYD0004, 2017SZ0001, 2018GZ0142, and 2019JDTD0008), and the "111" Project (No. B16033).

References

[1] J. Saroia, W. Yanen, Q. Wei, K. Zhang, T. Lu, and B. Zhang, "A review on biocompatibility nature of hydrogels with 3D printing techniques, tissue engineering application and its future prospective," *Bio-Design and Manufacturing*, vol. 1, no. 4, pp. 265–279, 2018.

[2] S. Ding and P. G. Schultz, "A role for chemistry in stem cell biology," *Nature biotechnology*, vol. 22, no. 7, pp. 833–840, 2004.

[3] M. F. Pittenger, A. M. Mackay, S. C. Beck et al., "Multilineage potential of adult human mesenchymal stem cells," *Science*, vol. 284, no. 5411, pp. 143–147, 1999.

[4] E. M. Andre, C. Passirani, B. Seijo, A. Sanchez, and C. N. Montero-Menei, "Nano and microcarriers to improve stem cell behaviour for neuroregenerative medicine strategies: Application to Huntington's disease," *Biomaterials*, vol. 83, pp. 347–362, 2016.

[5] I. Armentano, E. Fortunati, S. Mattioli, N. Rescignano, and J. M. Kenny, "Biodegradable composite scaffolds: a strategy to modulate stem cell behaviour," *Recent patents on drug delivery & formulation*, vol. 7, no. 1, pp. 9–17, 2013.

[6] J. S. Katz and J. A. Burdick, "Hydrogel mediated delivery of trophic factors for neural repair," *Wiley Interdisciplinary Reviews: Nanomedicine and Nanobiotechnology*, vol. 1, no. 1, pp. 128–139, 2009.

[7] Y. Li, H. Meng, Y. Liu, and B. P. Lee, "Fibrin gel as an injectable biodegradable scaffold and cell carrier for tissue engineering," *The Scientific World Journal*, vol. 2015, Article ID 685690, 10 pages, 2015.

[8] L. Ding, T. L. Saunders, G. Enikolopov, and S. J. Morrison, "Endothelial and perivascular cells maintain haematopoietic stem cells," *Nature*, vol. 481, no. 7382, pp. 457–462, 2012.

[9] X. Chen, H. Fan, X. Deng et al., "Scaffold structural microenvironmental cues to guide tissue regeneration in bone tissue applications," *Nanomaterials*, vol. 8, no. 11, p. 960, 2018.

[10] K. Odelius, A. Hoglund, S. Kumar et al., "Porosity and pore size regulate the degradation product profile of polylactide," *Biomacromolecules*, vol. 12, no. 4, pp. 1250–1258, 2011.

[11] S. H. Oh, T. H. Kim, G. I. Im, and J. H. Lee, "Investigation of pore size effect on chondrogenic differentiation of adipose stem cells using a pore size gradient scaffold," *Biomacromolecules*, vol. 11, no. 8, pp. 1948–1955, 2010.

[12] S. H. McBride and M. L. Knothe Tate, "Modulation of stem cell shape and fate A: the role of density and seeding protocol on nucleus shape and gene expression," *Tissue engineering Part A*, vol. 14, no. 9, pp. 1561–1572, 2008.

[13] C. Zhou, K. Yang, K. Wang et al., "Combination of fused deposition modeling and gas foaming technique to fabricated hierarchical macro/microporous polymer scaffolds," *Materials & Design*, vol. 109, pp. 415–424, 2016.

[14] X. Pei, L. Ma, B. Zhang et al., "Creating hierarchical porosity hydroxyapatite scaffolds with osteoinduction by three-dimensional printing and microwave sintering," *Biofabrication*, vol. 9, no. 4, p. 045008, 2017.

[15] H. Yoshikawa, N. Tamai, T. Murase, and A. Myoui, "Interconnected porous hydroxyapatite ceramics for bone tissue engineering," *Journal of the Royal Society Interface*, vol. 6, Supplement 3, 2009.

[16] B. Zhang, H. Sun, L. Wu et al., "3D printing of calcium phosphate bioceramic with tailored biodegradation rate for skull bone tissue reconstruction," *Bio-Design and Manufacturing*, vol. 2, no. 3, pp. 161–171, 2019.

[17] I. Henriksson, P. Gatenholm, and D. Hagg, "Increased lipid accumulation and adipogenic gene expression of adipocytes in 3D bioprinted nanocellulose scaffolds," *Biofabrication*, vol. 9, no. 1, p. 015022, 2017.

[18] S. Chen, J. C. Huang, C. T. Pan et al., "Microstructure and mechanical properties of open-cell porous Ti-6Al-4V fabricated by selective laser melting," *Journal of Alloys and Compounds*, vol. 713, pp. 248–254, 2017.

[19] M. Ansari and M. Eshghanmalek, "Biomaterials for repair and regeneration of the cartilage tissue," *Bio-Design and Manufacturing*, vol. 2, no. 1, pp. 41–49, 2019.

[20] P. Song, C. Zhou, H. Fan et al., "Novel 3D porous biocomposite scaffolds fabricated by fused deposition modeling and gas foaming combined technology," *Composites Part B: Engineering*, vol. 152, pp. 151–159, 2018.

[21] S. Sarkar, G. Y. Lee, J. Y. Wong, and T. A. Desai, "Development and characterization of a porous micro-patterned scaffold for vascular tissue engineering applications," *Biomaterials*, vol. 27, no. 27, pp. 4775–4782, 2006.

[22] A. Sadiasa, T. Nguyen, and B. Lee, "In vitro and in vivo evaluation of porous PCL-PLLA 3D polymer scaffolds fabricated via salt leaching method for bone tissue engineering applications," *Journal of Biomaterials Science-polymer Edition*, vol. 25, no. 2, pp. 150–167, 2014.

[23] H. Lee, G. Jin, U. S. Shin, J. Kim, and H. Kim, "Novel porous scaffolds of poly(lactic acid) produced by phase-separation using room temperature ionic liquid and the assessments of biocompatibility," *Journal of Materials Science: Materials in Medicine*, vol. 23, no. 5, pp. 1271–1279, 2012.

[24] R. Akbarzadeh and A. Yousefi, "Effects of processing parameters in thermally induced phase separation technique on porous architecture of scaffolds for bone tissue engineering," *Journal of Biomedical Materials Research Part B*, vol. 102, no. 6, pp. 1304–1315, 2014.

[25] N. Sultana and M. Wang, "PHBV/PLLA-based composite scaffolds fabricated using an emulsion freezing/freeze-drying technique for bone tissue engineering: surface modification and in vitro biological evaluation," *Biofabrication*, vol. 4, no. 1, p. 015003, 2012.

[26] S. A. Riboldi, M. Sampaolesi, P. Neuenschwander, G. Cossu, and S. Mantero, "Electrospun degradable polyesterurethane membranes: potential scaffolds for skeletal muscle tissue engineering," *Biomaterials*, vol. 26, no. 22, pp. 4606–4615, 2005.

[27] J. Rnjakkovacina, S. G. Wise, Z. Li et al., "Tailoring the porosity and pore size of electrospun synthetic human elastin scaffolds for dermal tissue engineering," *Biomaterials*, vol. 32, no. 28, pp. 6729–6736, 2011.

[28] R. Geetha Bai, K. Muthoosamy, S. Manickam, and A. Hilal-Alnaqbi, "Graphene-based 3D scaffolds in tissue engineering: fabrication, applications, and future scope in liver tissue engineering," *International journal of nanomedicine*, vol. 14, pp. 5753–5783, 2019.

[29] F. D'Angelo, I. Armentano, I. Cacciotti et al., "Tuning multi/-pluri-potent stem cell fate by electrospun poly(L-lactic acid)-calcium-deficient hydroxyapatite nanocomposite mats," *Biomacromolecules*, vol. 13, no. 5, pp. 1350–1360, 2012.

[30] S. C. Cox, J. A. Thornby, G. J. Gibbons, M. A. Williams, and K. K. Mallick, "3D printing of porous hydroxyapatite scaffolds intended for use in bone tissue engineering applications," *Materials science & engineering. C, Materials for biological applications*, vol. 47, pp. 237–247, 2015.

[31] H. Gong, M. Beauchamp, S. Perry, A. T. Woolley, and G. P. Nordin, "Optical approach to resin formulation for 3D printed microfluidics," *RSC Advances*, vol. 5, no. 129, pp. 106621–106632, 2015.

[32] S. Lou, L. Pagani, W. Zeng, M. U. Ghori, X. Jiang, and P. J. Scott, "Surface texture evaluation of additively manufactured metallic cellular scaffolds for acetabular implants using X-ray computed tomography," *Bio-Design and Manufacturing*, vol. 2, no. 2, pp. 55–64, 2019.

[33] L. Zhao, X. Pei, L. Jiang et al., "Bionic design and 3D printing of porous titanium alloy scaffolds for bone tissue repair," *Composites Part B: Engineering*, vol. 162, pp. 154–161, 2019.

[34] D. Yoo, "New paradigms in internal architecture design and freeform fabrication of tissue engineering porous scaffolds," *Medical engineering & physics*, vol. 34, no. 6, pp. 762–776, 2012.

[35] P. H. Warnke, T. Douglas, P. Wollny et al., "Rapid prototyping: porous titanium alloy scaffolds produced by selective laser melting for bone tissue engineering," *Tissue engineering Part C, Methods*, vol. 15, no. 2, pp. 115–124, 2009.

[36] D. Lai, J. M. Labuz, J. Kim, G. D. Luker, A. Shikanov, and S. Takayama, "Simple multi-level microchannel fabrication by pseudo-grayscale backside diffused light lithography," *RSC Advances*, vol. 3, no. 42, pp. 19467–19473, 2013.

[37] B. Zhang, X. Pei, P. Song et al., "Porous bioceramics produced by inkjet 3D printing: effect of printing ink formulation on the ceramic macro and micro porous architectures control," *Composites Part B: Engineering*, vol. 155, pp. 112–121, 2018.

[38] G. Ying, N. Jiang, C. Yu, and Y. S. Zhang, "Three-dimensional bioprinting of gelatin methacryloyl (GelMA)," *Bio-Design and Manufacturing*, vol. 1, no. 4, pp. 215–224, 2018.

[39] B. Zhang, X. Pei, C. Zhou et al., "The biomimetic design and 3D printing of customized mechanical properties porous Ti6Al4V scaffold for load-bearing bone reconstruction," *Materials & Design*, vol. 152, pp. 30–39, 2018.

[40] J. A. Paten, G. E. Tilburey, E. A. Molloy, R. Zareian, C. V. Trainor, and J. W. Ruberti, "Utility of an optically-based, micromechanical system for printing collagen fibers," *Biomaterials*, vol. 34, no. 11, pp. 2577–2587, 2013.

[41] S. Gura, M. Joshi, and J. R. Almirall, "Solid-phase microextraction (SPME) calibration using inkjet microdrop printing for direct loading of known analyte mass on to SPME fibers," *Analytical and bioanalytical chemistry*, vol. 398, no. 2, pp. 1049–1060, 2010.

[42] T. Serra, M. A. Mateos-Timoneda, J. A. Planell, and M. Navarro, "3D printed PLA-based scaffolds A versatile tool in regenerative medicine," *Organogenesis*, vol. 9, no. 4, pp. 239–244, 2013.

[43] R. Murugan and S. Ramakrishna, "Design strategies of tissue engineering scaffolds with controlled fiber orientation," *Tissue engineering*, vol. 13, no. 8, pp. 1845–1866, 2007.

[44] I. Garcia-Orue, G. Gainza, P. Garcia-Garcia et al., "Composite nanofibrous membranes of PLGA/Aloe vera containing lipid nanoparticles for wound dressing applications," *International journal of pharmaceutics*, vol. 556, pp. 320–329, 2019.

[45] J. Wang, C. Peng, Z. Chen et al., "Engineering antimicrobial and biocompatible electrospun PLGA fibrous membranes by irradiation grafting polyvinylpyrrolidone and periodate," *Colloids and surfaces B Biointerfaces*, vol. 181, pp. 918–926, 2019.

[46] K. E. Sullivan, L. J. Burns, and L. D. Black 3rd, "An _in vitro_ model for the assessment of stem cell fate following implantation within the infarct microenvironment identifies ISL-1 expression as the strongest predictor of c-Kit$^+$ cardiac progenitor cells' therapeutic potential," *Journal of molecular and cellular cardiology*, vol. 88, pp. 91–100, 2015.

[47] P. V. Kolluru, J. Lipner, W. Liu et al., "Strong and tough mineralized PLGA nanofibers for tendon-to-bone scaffolds," *Acta biomaterialia*, vol. 9, no. 12, pp. 9442–9450, 2013.

[48] X. Cheng, C. Tsao, V. L. Sylvia et al., "Platelet-derived growth-factor-releasing aligned collagen-nanoparticle fibers promote the proliferation and tenogenic differentiation of adipose-derived stem cells," *Acta biomaterialia*, vol. 10, no. 3, pp. 1360–1369, 2014.

[49] S. Yao, X. Liu, S. Yu et al., "Co-effects of matrix low elasticity and aligned topography on stem cell neurogenic differentiation and rapid neurite outgrowth," *Nanoscale*, vol. 8, no. 19, pp. 10252–10265, 2016.

[50] M. L. A. da Silva, A. Martins, A. R. Costa-Pinto et al., "Cartilage tissue engineering using electrospun PCL nanofiber meshes and MSCs," *Biomacromolecules*, vol. 11, no. 12, pp. 3228–3236, 2010.

[51] M. Mehrasa, M. A. Asadollahi, K. Ghaedi, H. Salehi, and A. Arpanaei, "Electrospun aligned PLGA and PLGA/gelatin nanofibers embedded with silica nanoparticles for tissue engineering," *International journal of biological macromolecules*, vol. 79, pp. 687–695, 2015.

[52] Y. Gui-Bo, Z. You-Zhu, W. Shu-Dong, S. De-Bing, D. Zhi-Hui, and F. Wei-Guo, "Study of the electrospun PLA/silk fibroin-gelatin composite nanofibrous scaffold for tissue engineering," *Journal of biomedical materials research Part A*, vol. 93, no. 1, pp. 158–163, 2010.

[53] K. A. Kilian, B. Bugarija, B. T. Lahn, and M. Mrksich, "Geometric cues for directing the differentiation of mesenchymal stem cells," *Proceedings of the National Academy of Sciences of the United States of America*, vol. 107, no. 11, pp. 4872–4877, 2010.

[54] S. H. McBride, T. Falls, and M. L. Knothe Tate, "Modulation of stem cell shape and fate B: mechanical modulation of cell shape and gene expression," *Tissue engineering Part A*, vol. 14, no. 9, pp. 1573–1580, 2008.

[55] R. McBeath, D. M. Pirone, C. M. Nelson, K. Bhadriraju, and C. S. Chen, "Cell shape, cytoskeletal tension, and RhoA regulate stem cell lineage commitment," *Developmental cell*, vol. 6, no. 4, pp. 483–495, 2004.

[56] M. Thery, A. Pepin, E. Dressaire, Y. Chen, and M. Bornens, "Cell distribution of stress fibres in response to the geometry of the adhesive environment," *Cell motility and the cytoskeleton*, vol. 63, no. 6, pp. 341–355, 2006.

[57] X. Chen, X. Chen, X. Zhu, B. Cai, H. Fan, and X. Zhang, "Effect of surface topography of hydroxyapatite on human osteosarcoma MG-63 cell," *Journal of Inorganic Materials*, vol. 28, no. 8, pp. 901–906, 2013.

[58] X. N. Chen, X. Zhu, H. S. Fan, and X. D. Zhang, "Rat bone marrow cell responses on the surface of hydroxyapatite with different topography," *Key Engineering Materials*, vol. 361-363, pp. 1107–1110, 2007.

[59] Z. Wang, Z.-W. Xiao, H.-S. Fan, and X.-D. Zhang, "Fabrication of micro-grooved patterns on hydroxyapatite ceramics and observation of earlier response of osteoblasts to the patterns," *Journal of Inorganic Materials*, vol. 28, no. 1, pp. 51–57, 2013.

[60] C. Zhao, L. Xia, D. Zhai et al., "Designing ordered micropatterned hydroxyapatite bioceramics to promote the growth and osteogenic differentiation of bone marrow stromal cells," *Journal of Materials Chemistry B*, vol. 3, no. 6, pp. 968–976, 2015.

[61] R. Wang and Y. X. Hu, "Patterning hydroxyapatite biocoating by electrophoretic deposition," *Journal of Biomedical Materials Research Part A*, vol. 67, no. 1, pp. 270–275, 2003.

[62] K. Teshima, S. Lee, K. Yubuta, S. Mori, T. Shishido, and S. Oishi, "Selective growth of highly crystalline hydroxyapatite in a micro-reaction cell of agar gel," *CrystEngComm*, vol. 13, no. 3, pp. 827–830, 2011.

[63] Y. Tseng, M. E. Birkbak, and H. Birkedal, "Spatial organization of hydroxyapatite nanorods on a substrate via a biomimetic approach," *Crystal Growth & Design*, vol. 13, no. 10, pp. 4213–4219, 2013.

[64] T. Ito and S. Okazaki, "Pushing the limits of lithography," *Nature*, vol. 406, no. 6799, pp. 1027–1031, 2000.

[65] M. Geissler and Y. Xia, "Patterning: principles and some new developments," *Advanced Materials*, vol. 16, no. 15, pp. 1249–1269, 2004.

[66] H. Xu, X. Y. Ling, J. van Bennekom et al., "Microcontact printing of dendrimers, proteins, and nanoparticles by porous stamps," *Journal of the American Chemical Society*, vol. 131, no. 2, pp. 797–803, 2009.

[67] T. Kraus, L. Malaquin, H. Schmid, W. Riess, N. D. Spencer, and H. Wolf, "Nanoparticle printing with single-particle resolution," *Nature Nanotechnology*, vol. 2, no. 9, pp. 570–576, 2007.

[68] H. Radman, M. Maghrebi, and M. Baniadam, "Inkjet printing of carbon nanotubes (CNTs) with a binary surfactant mixture: the effect of the nonionic surfactant on the uniformity of the printed surface," *Diamond and Related Materials*, vol. 100, p. 107550, 2019.

[69] X. Li, Y. Zhao, J. Yu et al., "Layer-by-layer inkjet printing GO film and Ag nanoparticles supported nickel cobalt layered double hydroxide as a flexible and binder-free electrode for supercapacitors," *Journal of Colloid and Interface Science*, vol. 557, pp. 691–699, 2019.

[70] E. Kaivosoja, G. Barreto, K. Levon, S. Virtanen, M. Ainola, and Y. T. Konttinen, "Chemical and physical properties of regenerative medicine materials controlling stem cell fate," *Annals of medicine*, vol. 44, no. 7, pp. 635–650, 2012.

[71] Y. Zhang, W. Fan, Z. Ma et al., "The effects of pore architecture in silk fibroin scaffolds on the growth and differentiation of mesenchymal stem cells expressing BMP7," *Acta biomaterialia*, vol. 6, no. 8, pp. 3021–3028, 2010.

[72] S. W. Choi, Y. Zhang, and Y. Xia, "Three-dimensional scaffolds for tissue engineering: the importance of uniformity in pore size and structure," *Langmuir*, vol. 26, no. 24, pp. 19001–19006, 2010.

[73] J. W. Lee, G. Ahn, J. Y. Kim, and D. W. Cho, "Evaluating cell proliferation based on internal pore size and 3D scaffold architecture fabricated using solid freeform fabrication technology," *Journal of Materials Science: Materials in Medicine*, vol. 21, no. 12, pp. 3195–3205, 2010.

[74] G. I. Im, J. Y. Ko, and J. H. Lee, "Chondrogenesis of adipose stem cells in a porous polymer scaffold: influence of the pore size," *Cell transplantation*, vol. 21, no. 11, pp. 2397–2405, 2012.

[75] S. Taqvi and K. Roy, "Influence of scaffold physical properties and stromal cell coculture on hematopoietic differentiation of mouse embryonic stem cells," *Biomaterials*, vol. 27, no. 36, pp. 6024–6031, 2006.

[76] V. Karageorgiou and D. Kaplan, "Porosity of 3D biomaterial scaffolds and osteogenesis," *Biomaterials*, vol. 26, no. 27, pp. 5474–5491, 2005.

[77] B. B. Mandal and S. C. Kundu, "Cell proliferation and migration in silk fibroin 3D scaffolds," *Biomaterials*, vol. 30, no. 15, pp. 2956–2965, 2009.

[78] P. Kasten, I. Beyen, P. Niemeyer, R. Luginbuhl, M. Bohner, and W. Richter, "Porosity and pore size of β-tricalcium phosphate scaffold can influence protein production and osteogenic differentiation of human mesenchymal stem cells: An in vitro and in vivo study," *Acta biomaterialia*, vol. 4, no. 6, pp. 1904–1915, 2008.

[79] J. van den Dolder, E. Farber, P. H. Spauwen, and J. A. Jansen, "Bone tissue reconstruction using titanium fiber mesh combined with rat bone marrow stromal cells," *Biomaterials*, vol. 24, no. 10, pp. 1745–1750, 2003.

[80] M. Wang, H. Pei, L. Zhang et al., "Hepatogenesis of adipose-derived stem cells on poly-lactide-co-glycolide scaffolds: in vitro and in vivo studies," *Tissue engineering Part C, Methods*, vol. 16, no. 5, pp. 1041–1050, 2010.

[81] S. W. Cho, I. K. Kim, S. H. Lim et al., "Smooth muscle-like tissues engineered with bone marrow stromal cells," *Biomaterials*, vol. 25, no. 15, pp. 2979–2986, 2004.

[82] T. Mygind, M. Stiehler, A. Baatrup et al., "Mesenchymal stem cell ingrowth and differentiation on coralline hydroxyapatite scaffolds," *Biomaterials*, vol. 28, no. 6, pp. 1036–1047, 2007.

[83] J. Yuan, L. Cui, W. J. Zhang, W. Liu, and Y. Cao, "Repair of canine mandibular bone defects with bone marrow stromal cells and porous _β_ -tricalcium phosphate," *Biomaterials*, vol. 28, no. 6, pp. 1005–1013, 2007.

[84] S. Diederichs, S. Roker, D. Marten et al., "Dynamic cultivation of human mesenchymal stem cells in a rotating bed bioreactor system based on the Z RP platform," *Biotechnology progress*, vol. 25, no. 6, pp. 1762–1771, 2009.

[85] H. J. Kim, J. H. Lee, and G. I. Im, "Chondrogenesis using mesenchymal stem cells and PCL scaffolds," *Journal of biomedical materials research Part A*, vol. 92, no. 2, pp. 659–666, 2010.

[86] A. J. Engler, S. Sen, H. L. Sweeney, and D. E. Discher, "Matrix elasticity directs stem cell lineage specification," *Cell*, vol. 126, no. 4, pp. 677–689, 2006.

[87] E. J. Semler and P. V. Moghe, "Engineering hepatocyte functional fate through growth factor dynamics: the role of cell morphologic priming," *Biotechnology and bioengineering*, vol. 75, no. 5, pp. 510–520, 2001.

[88] R. Olivares-Navarrete, E. M. Lee, K. Smith et al., "Substrate stiffness controls osteoblastic and chondrocytic differentiation of mesenchymal stem cells without exogenous stimuli," *PloS one*, vol. 12, no. 1, article e0170312, 2017.

[89] T. Zhang, S. Lin, X. Shao et al., "Regulating osteogenesis and adipogenesis in adipose-derived stem cells by controlling underlying substrate stiffness," *Journal of cellular physiology*, vol. 233, no. 4, pp. 3418–3428, 2018.

[90] N. Liu, M. Zhou, Q. Zhang et al., "Stiffness regulates the proliferation and osteogenic/odontogenic differentiation of human dental pulp stem cells via the WNT signalling pathway," *Cell proliferation*, vol. 51, no. 2, article e12435, 2018.

[91] A. J. Keung, P. Asuri, S. Kumar, and D. V. Schaffer, "Soft microenvironments promote the early neurogenic differentiation but not self-renewal of human pluripotent stem cells," *Integrative biology: quantitative biosciences from nano to macro*, vol. 4, no. 9, pp. 1049–1058, 2012.

[92] C. M. Lo, H. B. Wang, M. Dembo, and Y. L. Wang, "Cell movement is guided by the rigidity of the substrate," *Biophysical journal*, vol. 79, no. 1, pp. 144–152, 2000.

[93] K. Ghosh, Z. Pan, E. Guan et al., "Cell adaptation to a physiologically relevant ECM mimic with different viscoelastic properties," *Biomaterials*, vol. 28, no. 4, pp. 671–679, 2007.

[94] H. B. Wang, M. Dembo, and Y. L. Wang, "Substrate flexibility regulates growth and apoptosis of normal but not transformed cells," *American Journal of Physiology-Cell Physiology*, vol. 279, no. 5, pp. C1345–C1350, 2000.

[95] K. Saha, A. J. Keung, E. F. Irwin et al., "Substrate modulus directs neural stem cell behavior," *Biophysical journal*, vol. 95, no. 9, pp. 4426–4438, 2008.

[96] I. G. Kim, C. H. Gil, J. Seo et al., "Mechanotransduction of human pluripotent stem cells cultivated on tunable cell-derived extracellular matrix," *Biomaterials*, vol. 150, pp. 100–111, 2018.

[97] J. Fu, Y. J. Chuah, W. T. Ang, N. Zheng, and D. A. Wang, "Optimization of a polydopamine (PD)-based coating method and polydimethylsiloxane (PDMS) substrates for improved mouse embryonic stem cell (ESC) pluripotency maintenance and cardiac differentiation," *Biomaterials science*, vol. 5, no. 6, pp. 1156–1173, 2017.

[98] D. T. Butcher, T. Alliston, and V. M. Weaver, "A tense situation: forcing tumour progression," *Cancer*, vol. 9, no. 2, pp. 108–122, 2009.

[99] C. Zhou, Y. Jiang, Z. Sun, Y. Li, B. Guo, and Y. Hong, "Biological effects of apatite nanoparticle-constructed ceramic surfaces in regulating behaviours of mesenchymal stem cells," *Journal of Materials Chemistry B*, vol. 6, no. 35, pp. 5621–5632, 2018.

[100] A. Graziano, R. d'Aquino, M. G. Cusella-De Angelis et al., "Scaffold's surface geometry significantly affects human stem cell bone tissue engineering," *Journal of cellular physiology*, vol. 214, no. 1, pp. 166–172, 2008.

[101] J. Ji, X. Tong, X. Huang et al., "Sphere-shaped nano-hydroxyapatite/chitosan/gelatin 3D porous scaffolds increase proliferation and osteogenic differentiation of human induced pluripotent stem cells from gingival fibroblasts," *Biomedical Materials*, vol. 10, no. 4, p. 045005, 2015.

[102] A. Cooper, M. Leung, and M. Zhang, "Polymeric fibrous matrices for substrate-mediated human embryonic stem cell lineage differentiation," *Macromolecular bioscience*, vol. 12, no. 7, pp. 882–892, 2012.

[103] M. R. Lee, K. W. Kwon, H. Jung et al., "Direct differentiation of human embryonic stem cells into selective neurons on nanoscale ridge/groove pattern arrays," *Biomaterials*, vol. 31, no. 15, pp. 4360–4366, 2010.

[104] H. N. Kim, D. H. Kang, M. S. Kim, A. Jiao, D. H. Kim, and K. Y. Suh, "Patterning methods for polymers in cell and tissue engineering," *Annals of biomedical engineering*, vol. 40, no. 6, pp. 1339–1355, 2012.

[105] P. Y. Wang, D. T. Bennetsen, M. Foss, T. Ameringer, H. Thissen, and P. Kingshott, "Modulation of human mesenchymal stem cell behavior on ordered tantalum nanotopographies fabricated using colloidal lithography and glancing angle deposition," *ACS applied materials & interfaces*, vol. 7, no. 8, pp. 4979–4989, 2015.

[106] P. Y. Collart-Dutilleul, E. Secret, I. Panayotov et al., "Adhesion and proliferation of human mesenchymal stem cells from dental pulp on porous silicon scaffolds," *ACS applied materials & interfaces*, vol. 6, no. 3, pp. 1719–1728, 2014.

[107] J. E. Nichols, J. Cortiella, J. Lee et al., "_In vitro_ analog of human bone marrow from 3D scaffolds with biomimetic inverted colloidal crystal geometry," *Biomaterials*, vol. 30, no. 6, pp. 1071–1079, 2009.

[108] T. Sjostrom, M. J. Dalby, A. Hart, R. Tare, R. O. Oreffo, and B. Su, "Fabrication of pillar-like titania nanostructures on titanium and their interactions with human skeletal stem cells," *Acta biomaterialia*, vol. 5, no. 5, pp. 1433–1441, 2009.

[109] S. Thakur, S. Massou, A. M. Benoliel, P. Bongrand, M. Hanbucken, and K. Sengupta, "Depth matters: cells grown on nano-porous anodic alumina respond to pore depth," *Nanotechnology*, vol. 23, no. 25, p. 255101, 2012.

[110] M. Mehrali, A. Thakur, F. B. Kadumudi et al., "Pectin methacrylate (PEMA) and gelatin-based hydrogels for cell delivery: converting waste materials into biomaterials," *ACS applied materials & interfaces*, vol. 11, no. 13, pp. 12283–12297, 2019.

[111] F. A. Pennacchio, C. Fedele, S. De Martino, S. Cavalli, R. Vecchione, and P. A. Netti, "Three-dimensional microstructured azobenzene-containing gelatin as a photoactuable cell confining system," *ACS applied materials & interfaces*, vol. 10, no. 1, pp. 91–97, 2018.

[112] M. M. McCafferty, G. A. Burke, and B. J. Meenan, "Mesenchymal stem cell response to conformal sputter deposited calcium phosphate thin films on nanostructured titanium surfaces," *Journal of biomedical materials research Part A*, vol. 102, no. 10, pp. 3585–3597, 2014.

[113] M. A. Wood, "Colloidal lithography and current fabrication techniques producing in-plane nanotopography for biological applications," *Journal of the Royal Society, Interface*, vol. 4, no. 12, pp. 1–17, 2007.

[114] L. Ji, V. L. LaPointe, N. D. Evans, and M. M. Stevens, "Changes in embryonic stem cell colony morphology and early differentiation markers driven by colloidal crystal topographical cues," *European cells & materials*, vol. 23, pp. 135–146, 2012.

[115] M. J. Dalby, N. Gadegaard, R. Tare et al., "The control of human mesenchymal cell differentiation using nanoscale symmetry and disorder," *Nature materials*, vol. 6, no. 12, pp. 997–1003, 2007.

[116] C. Allan, A. Ker, C. A. Smith et al., "Osteoblast response to disordered nanotopography," *Journal of tissue engineering*, vol. 9, Article ID 2041731418784098, 2018.

[117] S. Fujita, M. Ohshima, and H. Iwata, "Time-lapse observation of cell alignment on nanogrooved patterns," *Journal of the Royal Society, Interface*, vol. 6, Supplement 3, pp. S269–S277, 2009.

[118] J. Kim, H. N. Kim, K. T. Lim et al., "Designing nanotopographical density of extracellular matrix for controlled morphology and function of human mesenchymal stem cells," *Scientific reports*, vol. 3, no. 1, p. 3552, 2013.

[119] G. Abagnale, M. Steger, V. H. Nguyen et al., "Surface topography enhances differentiation of mesenchymal stem cells towards osteogenic and adipogenic lineages," *Biomaterials*, vol. 61, pp. 316–326, 2015.

[120] L. E. McNamara, T. Sjostrom, K. Seunarine, R. D. Meek, B. Su, and M. J. Dalby, "Investigation of the limits of nanoscale filopodial interactions," *Journal of tissue engineering*, vol. 5, Article ID 2041731414536177, 2014.

[121] R. Umapathi, S. B. Vepuri, P. Venkatesu, and M. E. Soliman, "Comprehensive computational and experimental analysis of biomaterial toward the behavior of imidazolium-based ionic liquids: an interplay between hydrophilic and hydrophobic interactions," *J Phys Chem B*, vol. 121, no. 18, pp. 4909–4922, 2017.

[122] J. A. Braatz, A. H. Heifetz, and C. L. Kehr, "A new hydrophilic polymer for biomaterial coatings with low protein adsorption," *J Biomater Sci Polym Ed*, vol. 3, no. 6, pp. 451–462, 1992.

[123] L. R. C. Peng-Yuan Wang, H. Thissen, S.-C. Hung, N.-C. Cheng, W.-B. Tsai, and N. H. Voelcker, "Screening the attachment and spreading of bone marrow-derived and adipose-derived mesenchymal stem cells on porous silicon gradients," *RSC Advances*, vol. 2, no. 33, pp. 12857–12865, 2012.

[124] D. Carson, M. Hnilova, X. Yang et al., "Nanotopography-induced structural anisotropy and sarcomere development in human cardiomyocytes derived from induced pluripotent stem cells," *ACS applied materials & interfaces*, vol. 8, no. 34, pp. 21923–21932, 2016.

[125] L. Lv, Y. Liu, P. Zhang et al., "The nanoscale geometry of TiO_2 nanotubes influences the osteogenic differentiation of human adipose-derived stem cells by modulating H3K4 trimethylation," *Biomaterials*, vol. 39, pp. 193–205, 2015.

[126] P. Y. Wang, H. Thissen, and P. Kingshott, "Stimulation of early osteochondral differentiation of human mesenchymal stem cells using binary colloidal crystals (BCCs)," *ACS applied materials & interfaces*, vol. 8, no. 7, pp. 4477–4488, 2016.

[127] K. Yang, K. Jung, E. Ko et al., "Nanotopographical manipulation of focal adhesion formation for enhanced differentiation of human neural stem cells," *ACS applied materials & interfaces*, vol. 5, no. 21, pp. 10529–10540, 2013.

[128] R. Verloes and L. Kanarek, "Tumour microenvironment studies open new perspectives for immunotherapy," *Arch Int Physiol Biochim*, vol. 84, no. 2, pp. 420–422, 1976.

[129] H. Baharvand, S. M. Hashemi, S. Kazemi Ashtiani, and A. Farrokhi, "Differentiation of human embryonic stem cells into hepatocytes in 2D and 3D culture systems in vitro," *The International journal of developmental biology*, vol. 50, no. 7, pp. 645–652, 2006.

[130] C. Y. Lin, C. H. Huang, Y. K. Wu, N. C. Cheng, and J. Yu, "Maintenance of human adipose derived stem cell (hASC) differentiation capabilities using a 3D culture," *Biotechnology letters*, vol. 36, no. 7, pp. 1529–1537, 2014.

[131] C. R. Kothapalli and R. D. Kamm, "3D matrix microenvironment for targeted differentiation of embryonic stem cells into neural and glial lineages," *Biomaterials*, vol. 34, no. 25, pp. 5995–6007, 2013.

[132] T. Limongi, A. Rocchi, F. Cesca et al., "Delivery of brain-derived neurotrophic factor by 3D biocompatible polymeric scaffolds for neural tissue engineering and neuronal regeneration," *Molecular neurobiology*, vol. 55, no. 12, pp. 8788–8798, 2018.

[133] M. O. Lee, H. Jeon, M. Y. Son, S. C. Lee, and Y. S. Cho, "Clump-passaging-based efficient 3D culture of human pluripotent stem cells under chemically defined conditions," *Biochemical and biophysical research communications*, vol. 493, no. 1, pp. 723–730, 2017.

[134] M. M. Adil, G. M. C. Rodrigues, R. U. Kulkarni et al., "Efficient generation of hPSC-derived midbrain dopaminergic neurons in a fully defined, scalable, 3D biomaterial platform," *Scientific reports*, vol. 7, no. 1, p. 40573, 2017.

[135] T. B. Bertucci and G. Dai, "Biomaterial engineering for controlling pluripotent stem cell fate," *Stem cells international*, vol. 2018, Article ID 9068203, 12 pages, 2018.

[136] J. Pons, Y. Huang, J. Arakawa-Hoyt et al., "VEGF improves survival of mesenchymal stem cells in infarcted hearts," *Biochemical and biophysical research communications*, vol. 376, no. 2, pp. 419–422, 2008.

[137] W. L. Fu, Z. Xiang, F. G. Huang et al., "Coculture of peripheral blood-derived mesenchymal stem cells and endothelial progenitor cells on strontium-doped calcium polyphosphate scaffolds to generate vascularized engineered bone," *Tissue engineering Part A*, vol. 21, no. 5-6, pp. 948–959, 2015.

[138] H. Haider, S. Jiang, N. M. Idris, and M. Ashraf, "IGF-1-overexpressing mesenchymal stem cells accelerate bone marrow stem cell mobilization via paracrine activation of SDF-1alpha/CXCR4 signaling to promote myocardial repair," *Circ Res*, vol. 103, no. 11, pp. 1300–1308, 2008.

[139] H. Zhu, X. Wang, Y. Han et al., "Icariin promotes the migration of bone marrow stromal cells via the SDF-1α/HIF-1α/CXCR 4 pathway," *Drug Des Devel Ther*, vol. - Volume 12, pp. 4023–4031, 2018.

[140] T. Zhou, Y. Yan, C. Zhao, Y. Xu, Q. Wang, and N. Xu, "Resveratrol improves osteogenic differentiation of senescent bone mesenchymal stem cells through inhibiting endogenous reactive oxygen species productionviaAMPK activation," *Redox Rep*, vol. 24, no. 1, pp. 62–69, 2019.

[141] Y. Li, J. Wang, G. Chen et al., "Quercetin promotes the osteogenic differentiation of rat mesenchymal stem cells via mitogen-activated protein kinase signaling," *Exp Ther Med*, vol. 9, no. 6, pp. 2072–2080, 2015.

[142] Q. Gu, Y. Cai, C. Huang, Q. Shi, and H. Yang, "Curcumin increases rat mesenchymal stem cell osteoblast differentiation but inhibits adipocyte differentiation," *Pharmacogn Mag*, vol. 8, no. 31, pp. 202–208, 2012.

[143] S. Qin, W. Zhou, S. Liu, P. Chen, and H. Wu, "Icariin stimulates the proliferation of rat bone mesenchymal stem cells via ERK and p38 MAPK signaling," *Int J Clin Exp Med*, vol. 8, no. 5, pp. 7125–7133, 2015.

[144] P. C. Tseng, S. M. Hou, R. J. Chen et al., "Resveratrol promotes osteogenesis of human mesenchymal stem cells by upregulating RUNX2 gene expression via the SIRT1/-FOXO3A axis," *Journal of Bone and Mineral Research*, vol. 26, no. 10, pp. 2552–2563, 2011.

[145] D. Wang, S. P. Li, J. S. Fu, L. Bai, and L. Guo, "Resveratrol augments therapeutic efficiency of mouse bone marrow mesenchymal stem cell-based therapy in experimental autoimmune encephalomyelitis," *International journal of developmental neuroscience: the official journal of the International Society for Developmental Neuroscience*, vol. 49, pp. 60–66, 2016.

[146] Y. Zhou, Y. Wu, X. Jiang et al., "The effect of quercetin on the osteogenesic differentiation and angiogenic factor expression of bone marrow-derived mesenchymal stem cells," *PloS one*, vol. 10, no. 6, p. e0129605, 2015.

[147] S. J. Kim, T. G. Son, H. R. Park et al., "Curcumin stimulates proliferation of embryonic neural progenitor cells and neurogenesis in the adult hippocampus," *The Journal of biological chemistry*, vol. 283, no. 21, pp. 14497–14505, 2008.

[148] X. Wang, C. Liu, Y. Xu et al., "Combination of mesenchymal stem cell injection with icariin for the treatment of diabetes-associated erectile dysfunction," *PloS one*, vol. 12, no. 3, p. e0174145, 2017.

[149] D. Liu, Y. Ye, L. Xu, W. Yuan, and Q. Zhang, "Icariin and mesenchymal stem cells synergistically promote angiogenesis and neurogenesis after cerebral ischemia _via_ PI3K and ERK1/2 pathways," *Biomedicine & pharmacotherapy = Biomedecine & pharmacotherapie*, vol. 108, pp. 663–669, 2018.

[150] I. I. Suvorova, A. R. Knyazeva, A. V. Petukhov, N. D. Aksenov, and V. A. Pospelov, "Resveratrol enhances pluripotency of mouse embryonic stem cells by activating AMPK/Ulk1 pathway," *Cell death discovery*, vol. 5, no. 1, p. 61, 2019.

[151] X. Wang, S. Ma, B. Yang et al., "Resveratrol promotes hUC-MSCs engraftment and neural repair in a mouse model of Alzheimer's disease," *Behavioural Brain Research*, vol. 339, pp. 297–304, 2018.

[152] Z. Yuan, J. Min, Y. Zhao et al., "Quercetin rescued TNF-alpha-induced impairments in bone marrow-derived mesenchymal stem cell osteogenesis and improved osteoporosis in rats," *American journal of translational research*, vol. 10, no. 12, pp. 4313–4321, 2018.

[153] X. G. Pang, Y. Cong, N. R. Bao, Y. G. Li, and J. N. Zhao, "Quercetin stimulates bone marrow mesenchymal stem cell differentiation through an estrogen receptor-mediated pathway," *BioMed research international*, vol. 2018, 11 pages, 2018.

[154] J. Li, Y. Han, M. Li, and C. Nie, "Curcumin promotes proliferation of adult neural stem cells and the birth of neurons in Alzheimer's disease mice via Notch signaling pathway," *Cell Reprogram*, vol. 21, no. 3, pp. 152–161, 2019.

[155] R. Yang, J. Wang, Z. Zhou et al., "Curcumin promotes burn wound healing in mice by upregulating caveolin-1 in epidermal stem cells," *Phytotherapy research: PTR*, vol. 33, no. 2, pp. 422–430, 2019.

[156] X. X. Ma, J. Liu, C. M. Wang, J. P. Zhou, Z. Z. He, and H. Lin, "Low-dose curcumin stimulates proliferation of rat embryonic neural stem cells through glucocorticoid receptor and STAT3," *CNS Neuroscience & Therapeutics*, vol. 24, no. 10, pp. 940–946, 2018.

[157] S. Pirmoradi, E. Fathi, R. Farahzadi, Y. Pilehvar-Soltanahmadi, and N. Zarghami, "Curcumin affects adipose tissue-derived mesenchymal stem cell aging through TERT gene expression," *Drug Research*, vol. 68, no. 4, pp. 213–221, 2018.

[158] S. P. Palecek, J. C. Loftus, M. H. Ginsberg, D. A. Lauffenburger, and A. F. Horwitz, "Integrin-ligand binding properties govern cell migration speed through cell- substratum adhesiveness," *Nature*, vol. 385, no. 6616, pp. 537–540, 1997.

[159] R. O. Hynes, "Integrins: a family of cell surface receptors," *Cell*, vol. 48, no. 4, pp. 549–554, 1987.

[160] E. Ruoslahti, "RGD and other recognition sequences for integrins," *Annual review of cell and developmental biology*, vol. 12, no. 1, pp. 697–715, 1996.

[161] C. K. Choi, Y. J. Xu, B. Wang, M. Zhu, L. Zhang, and L. Bian, "Substrate coupling strength of integrin-binding ligands modulates adhesion, spreading, and differentiation of human mesenchymal stem cells," *Nano letters*, vol. 15, no. 10, pp. 6592–6600, 2015.

[162] U. Hersel, C. Dahmen, and H. Kessler, "RGD modified polymers: biomaterials for stimulated cell adhesion and beyond," *Biomaterials*, vol. 24, no. 24, pp. 4385–4415, 2003.

[163] Y. Luo and M. S. Shoichet, "A photolabile hydrogel for guided three-dimensional cell growth and migration," *Nature materials*, vol. 3, no. 4, pp. 249–253, 2004.

[164] X. Lin, K. Takahashi, Y. Liu, and P. O. Zamora, "Enhancement of cell attachment and tissue integration by a IKVAV containing multi-domain peptide," *Biochimica et biophysica acta*, vol. 1760, no. 9, pp. 1403–1410, 2006.

[165] Y. Kaneda, S. Yamamoto, T. Kihira et al., "Synthetic cell-adhesive laminin peptide YIGSR conjugated with polyethylene glycol has improved antimetastatic activity due to a longer half-life in blood," *Invasion Metastasis*, vol. 15, no. 3-4, pp. 156–162, 1995.

[166] C. C. DuFort, M. J. Paszek, and V. M. Weaver, "Balancing forces: architectural control of mechanotransduction," *Nature reviews Molecular cell biology*, vol. 12, no. 5, pp. 308–319, 2011.

[167] J. M. Stukel and R. K. Willits, "Mechanotransduction of neural cells through cell-substrate interactions," *Tissue engineering Part B, Reviews*, vol. 22, no. 3, pp. 173–182, 2016.

[168] L. S. Campos, "β1 integrins and neural stem cells: making sense of the extracellular environment," *BioEssays: news and reviews in molecular, cellular and developmental biology*, vol. 27, no. 7, pp. 698–707, 2005.

[169] P. Y. Wang, H. Thissen, and P. Kingshott, "Modulation of human multipotent and pluripotent stem cells using surface nanotopographies and surface-immobilised bioactive signals: a review," *Acta biomaterialia*, vol. 45, pp. 31–59, 2016.

[170] S. Chen, M. Lewallen, and T. Xie, "Adhesion in the stem cell niche: biological roles and regulation," *Development*, vol. 140, no. 2, pp. 255–265, 2013.

[171] H. Zhang, M. F. Liu, R. C. Liu, W. L. Shen, Z. Yin, and X. Chen, "Physical microenvironment-based inducible scaffold for stem cell differentiation and tendon regeneration," *Tissue engineering Part B, Reviews*, vol. 24, no. 6, pp. 443–453, 2018.

[172] A. L. Ponte, E. Marais, N. Gallay et al., "The in vitro migration capacity of human bone marrow mesenchymal stem cells: comparison of chemokine and growth factor chemotactic activities," *Stem Cells*, vol. 25, no. 7, pp. 1737–1745, 2007.

[173] S. H. Moon, C. M. Lee, S. H. Park, and M. Jin Nam, "Effects of hepatocyte growth factor gene-transfected mesenchymal stem cells on dimethylnitrosamine-induced liver fibrosis in rats," *Growth Factors*, vol. 37, no. 3-4, pp. 105–119, 2019.

[174] C. Knight, S. James, D. Kuntin et al., "Epidermal growth factor can signal via β-catenin to control proliferation of mesenchymal stem cells independently of canonical Wnt signalling," *Cellular signalling*, vol. 53, pp. 256–268, 2019.

[175] N. S. S. Halim, E. S. Ch'ng, E. Kardia, S. A. Ali, R. Radzi, and B. H. Yahaya, "Aerosolised mesenchymal stem cells expressing angiopoietin-1 enhances airway repair," *Stem cell reviews and reports*, vol. 15, no. 1, pp. 112–125, 2019.

[176] C. J. Taylor, J. E. Church, M. D. Williams et al., "Hypoxic preconditioning of myoblasts implanted in a tissue engineering chamber significantly increases local angiogenesis via upregulation of myoblast vascular endothelial growth factor-A expression and downregulation of miRNA-1, miRNA-206 and angiopoietin-1," *Journal of tissue engineering and regenerative medicine*, vol. 12, no. 1, pp. e408–e421, 2018.

[177] P. S. Lienemann, M. P. Lutolf, and M. Ehrbar, "Biomimetic hydrogels for controlled biomolecule delivery to augment bone regeneration," *Advanced drug delivery reviews*, vol. 64, no. 12, pp. 1078–1089, 2012.

[178] S. Kuttappan, D. Mathew, J. I. Jo et al., "Dual release of growth factor from nanocomposite fibrous scaffold promotes vascularisation and bone regeneration in rat critical sized calvarial defect," *Acta biomaterialia*, vol. 78, pp. 36–47, 2018.

[179] J. M. Tang, J. N. Wang, L. Zhang et al., "VEGF/SDF-1 promotes cardiac stem cell mobilization and myocardial repair in the infarcted heart," *Cardiovascular Research*, vol. 91, no. 3, pp. 402–411, 2011.

[180] J. Y. Kim, S. Y. Chun, J. S. Park et al., "Laminin and platelet-derived growth factor-BB promote neuronal differentiation of human urine-derived stem cells," *Tissue Engineering and Regenerative Medicine*, vol. 15, no. 2, pp. 195–209, 2018.

[181] F. Li, Y. Liu, Y. Cai et al., "Ultrasound irradiation combined with hepatocyte growth factor accelerate the hepatic differentiation of human bone marrow mesenchymal stem cells," *Ultrasound in Medicine & Biology*, vol. 44, no. 5, pp. 1044–1052, 2018.

[182] E. J. Lee, I. Hwang, J. Y. Lee et al., "Hepatocyte growth factor improves the therapeutic efficacy of human bone marrow mesenchymal stem cells via RAD51," *Molecular therapy: the journal of the American Society of Gene Therapy*, vol. 26, no. 3, pp. 845–859, 2018.

[183] P. Song, C. Hu, X. Pei et al., "Dual modulation of crystallinity and macro-/microstructures of 3D printed porous titanium implants to enhance stability and osseointegration," *Journal of Materials Chemistry B*, vol. 7, no. 17, pp. 2865–2877, 2019.

Hindawi
Stem Cells International
Volume 2019, Article ID 2382534, 21 pages
https://doi.org/10.1155/2019/2382534

Research Article

Genomics Analysis of Metabolic Pathways of Human Stem Cell-Derived Microglia-Like Cells and the Integrated Cortical Spheroids

Julie Bejoy,[1] Xuegang Yuan,[1] Liqing Song,[1] Thien Hua,[2] Richard Jeske,[1] Sébastien Sart,[3] Qing-Xiang Amy Sang,[2,4] and Yan Li[1,4]

[1]*Department of Chemical and Biomedical Engineering, FAMU-FSU College of Engineering, Florida State University, Tallahassee, FL, USA*
[2]*Department of Chemistry and Biochemistry, Florida State University, Tallahassee, Florida, USA*
[3]*Hydrodynamics Laboratory (LadHyX)-Department of Mechanics, Ecole Polytechnique, CNRS-UMR7646, 91128 Palaiseau, France*
[4]*Institute of Molecular Biophysics, Florida State University, Tallahassee, Florida, USA*

Correspondence should be addressed to Yan Li; yli4@fsu.edu

Received 1 August 2019; Revised 18 September 2019; Accepted 9 October 2019; Published 18 November 2019

Guest Editor: Monica Montesi

Brain spheroids or organoids derived from human pluripotent stem cells (hiPSCs) are still not capable of completely recapitulating *in vivo* human brain tissue, and one of the limitations is lack of microglia. To add built-in immune function, coculture of the dorsal forebrain spheroids with isogenic microglia-like cells (D-MG) was performed in our study. The three-dimensional D-MG spheroids were analyzed for their transcriptome and compared with isogenic microglia-like cells (MG). Cortical spheroids containing microglia-like cells displayed different metabolic programming, which may affect the associated phenotype. The expression of genes related to glycolysis and hypoxia signaling was increased in cocultured D-MG spheroids, indicating the metabolic shift to aerobic glycolysis, which is in favor of M1 polarization of microglia-like cells. In addition, the metabolic pathways and the signaling pathways involved in cell proliferation, cell death, PIK3/AKT/mTOR signaling, eukaryotic initiation factor 2 pathway, and Wnt and Notch pathways were analyzed. The results demonstrate the activation of mTOR and p53 signaling, increased expression of Notch ligands, and the repression of NF-κB and canonical Wnt pathways, as well as the lower expression of cell cycle genes in the cocultured D-MG spheroids. This analysis indicates that physiological 3-D microenvironment may reshape the immunity of *in vitro* cortical spheroids and better recapitulate *in vivo* brain tissue function for disease modeling and drug screening.

1. Introduction

Understanding the models established by human induced pluripotent stem cells (hiPSCs) requires genome-wide mapping to elucidate gene regulatory networks [1, 2]. Therefore, transcriptome analysis has been used to compare hiPSC-derived lineage-specific cells with somatic counterparts [3]. Recently, forebrain spheroids or organoids were derived from hiPSCs for disease modeling and as potential platforms for drug screening [4–7]. These spheroids need to contain critical components of the human brain, such as vascular cells and microglia, for proper function. Our previous study characterized microglia-like cells differentiated from hiPSCs and introduced isogenic microglia-like cells into forebrain spheroids [8]. The microglia-like cells were cocultured with isogenic dorsal cortical spheroids in order to build immune function within the spheroids. While extensive phenotypic characterizations were performed in our previous study, the fundamental metabolic pathways and signaling pathways in different culture systems were not analyzed yet. It is postulated that the microglia-like cells inside the spheroids retain more *in vivo*-like metabolic program and the associated phenotype due to the environmental change in intimate cell-cell and cell-matrix interactions compared to 2-D culture.

Metabolic programming was found to play important roles in homeostasis, tissue repair, immune function, epigenetic change, and cellular phenotype. For hiPSC reprogramming, the somatic cells with oxidative phosphorylation (OXPHOS) gain the glycolysis metabolism when they gain pluripotency [9, 10]. For human mesenchymal stem cell (MSC) aggregates, metabolic reconfiguration towards glycolysis supports reacquisition of the primitive stem cell phenotype [11]. Similarly, for microglia, limited data suggest that polarization to an M1 phenotype (proinflammatory) may be accompanied by a metabolic shift from oxidative phosphorylation to aerobic glycolysis for energy production [12, 13]. It has been suggested that default polarization of resident microglia uses OXPHOS (mitochondrial respiration, i.e., anti-inflammatory M2 phenotype) for the functions involved in tissue repair, while the metabolic program shifts towards glycolysis as well as nitric oxide and citrulline production for M1 polarization [12]. In addition, the metabolic environment of microglia can affect brain region-dependent gene regulation [13]. Therefore, modifications of immune response by the physiological 3-D microenvironment may reshape the innate immunity that gains the "memory" and "trained" inflammation response [12].

Based on the literature for metabolic programming of 3-D HepG2/C3A spheroids [14], this present study analyzed the genomics data for hiPSC-derived microglia-like cells (i.e., single cells in semiadherent culture) and the isogenic 3-D dorsal spheroids containing microglia-like cells. The focus is on changes in metabolic pathways and the signaling pathways that are involved in cell proliferation, cell death, inflammation, PIK3/AKT/mTOR signaling, and Wnt and Notch pathways in 3-D cortical spheroids derived from hiPSCs. This study provides global genomic details on the impact of 3-D culturing on the metabolic phenotype of cells inside the cortical spheroids. The analysis in this study can also help to establish better coculturing strategies for mimicking the *in vivo* structure and functions of the central nervous system *in vitro*.

2. Materials and Methods

2.1. Microglia-Like Cells Derived from iPSCs. Our lab has derived microglia-like cells from human iPSK3 cells free of feeders using a modified protocol [15]. Mesoderm induction was performed using activin A, BMP4, SCF, and VEGF, followed by SCF, Flt3L, IL-3, and GM-CSF treatment. Non-adherent cells were replated to tissue culture-treated plates in the presence of IL-3 and M-CSF. The day 23 cells expressed 48-59% CD11b and 52-64% CD45. Day 28 cells expressed $70 \pm 6\%$ CD11b and $80 \pm 5\%$ IBA-1. Day 30-33 cells expressed $68 \pm 12\%$ P2RY12 and $51 \pm 10\%$ CX3CR1 (Figure 1(a)) [8].

2.2. Generation of Isogenic Dorsal Cortical Spheroids and Coculturing with Microglia-Like Cells. Neural differentiation was induced using dual SMAD inhibitors LDN193189 (LDN) and SB431542 (SB) on human iPSK3 cells in low attachment 96-well plates. The neural progenitor spheres were treated with patterning factors cyclopamine (a sonic hedgehog inhibitor) and fibroblast growth factor- (FGF-) 2 [7, 16]. The dorsal identity is defined by TBR1, PAX6, BRN2, and SATB2.

Dorsal spheroids (day 30) were cocultured with isogenic microglia-like cells at a 4 : 1 ratio (8×10^5 neurons to 2×10^5 microglia-like cells, i.e., 20%) in 50% DMEM/10% FBS and 50% neural differentiation medium composed of DMEM/F12 plus 2% B27 (Figures 1(b) and 1(c)). The CellTracker Red-labeled MGs were observed to move into the D-MG spheroids (Figure 1(c)). After three days of coculture (day 33), the dorsal spheroids containing microglia-like cells (D-MG group) and the microglia cells only (MG group) were harvested for RNA isolation and RNA-sequencing.

2.3. RNA-Sequencing. mRNA was isolated from the total RNA using the NEBNext Poly(A) mRNA Magnetic Isolation Module (New England Biolabs). cDNA libraries were generated from the isolated mRNA using an NEBNext Ultra RNA Library Prep Kit for Illumina (New England Biolabs), with a unique 6-nucleotide index primer (NEBNext Multiplex Oligos for Illumina), using Beckman Biomek 4000. The multiplexed sample was quantified with qPCR (Kapa Biosystems) specific for Illumina sequencing primers, and the average fragment size was determined with a Bioanalyzer High-Sensitivity DNA Chip (Agilent Technologies). The sequencing was performed on Illumina HiSeq 2500 at the Translational Science Laboratory of Florida State University. The pooled data were demultiplexed into individual sample data, and adapter primer sequences were removed [17].

2.4. RNA-Sequencing Data Analysis. The sequencing reads were analyzed using RNA-Seq Alignment version 1.1.1 (Illumina BaseSpace application). The reads were aligned with TopHat 2 [18] to the human genome (genome release GRCh38) using default parameters, and counts for each gene were generated. This workflow uses Cufflinks to generate FPKM (fragments per kilobase per million reads) normalized values [19]. DESeq2 was used to determine statistically significant differentially expressed genes (a false discovery rate (FDR) of <0.05 was used). 15,585 genes were considered to be expressed in this study by the DESeq2 software [20]. The top 500 genes that were upregulated and downregulated (1000 total genes) in the microglial culture versus the D-MG group were assessed for GO, KEGG pathway, and phenotype pathway analysis using WebGestalt [21, 22]. Significant enrichment was determined in WebGestalt using the hypergeometric test and the Benjamini-Hochberg FDR method [23] for multiple testing adjustment.

2.5. Reverse Transcription Polymerase Chain Reaction (RT-PCR) Analysis. Total RNA was isolated from different cell samples using the RNeasy Mini Kit (Qiagen, Valencia, CA) according to the manufacturer's protocol followed by the treatment with a DNA-Free RNA Kit (Zymo, Irvine, CA) [24]. Reverse transcription was carried out using 2 g of total RNA, anchored oligo-dT primers (Operon, Huntsville, AL), and Superscript III (Invitrogen, Carlsbad, CA) (according to the protocol of the manufacturer). Primers specific for target genes (Supplementary Table S1) were designed using the

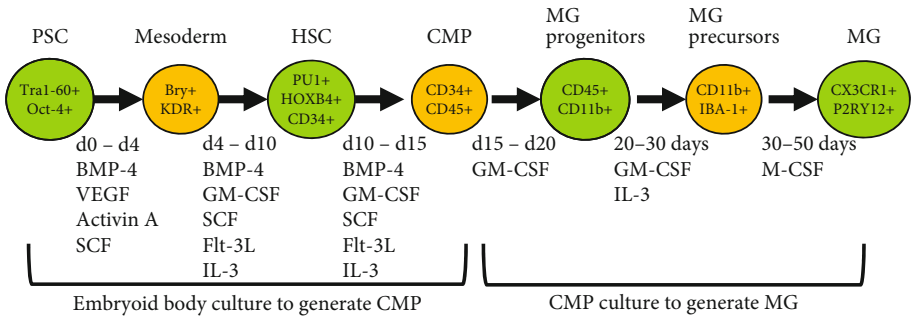

(a)

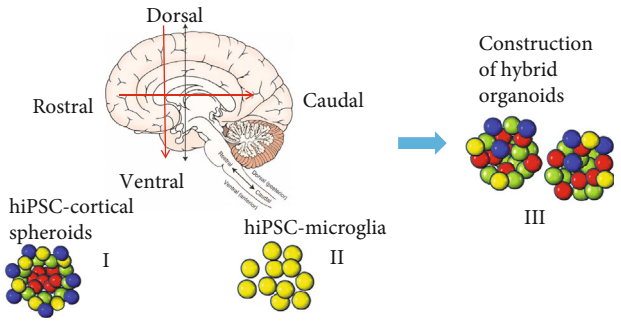

(b)

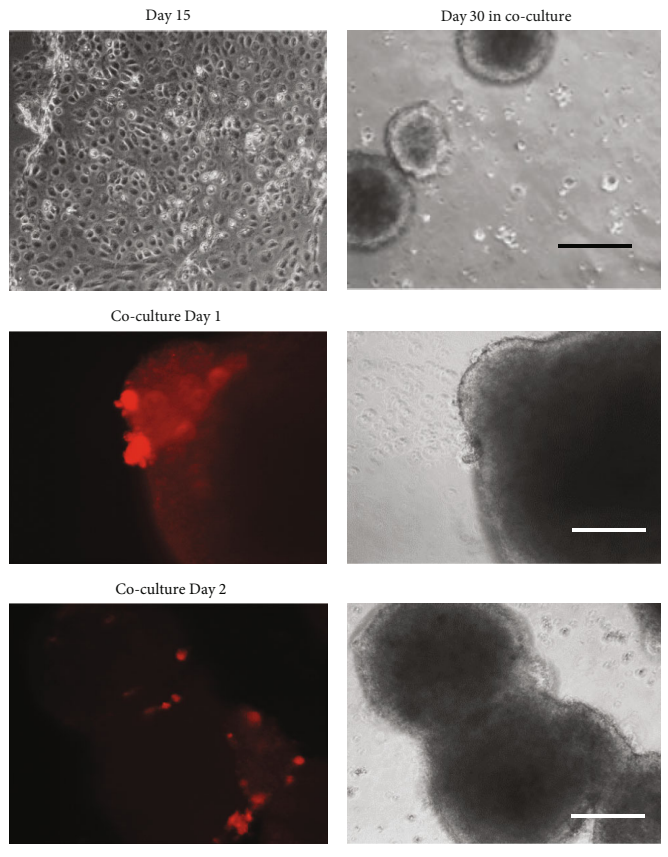

(c)

Figure 1: Illustration of the MG group and D-MG group. (a) Derivation of microglia-like cells (MG) from hiPSCs. (b) Incorporation of MG into the isogenic dorsal spheroids (DMG). (c) Morphology of the cells in microglial differentiation and the D-MG spheroids. Day 30 MGs were labeled with CellTracker Red. White scale bar: 100 μm. Black scale bar: 200 μm.

software Oligo Explorer 1.2 (GeneLink, Hawthorne, NY). The gene β-actin was used as an endogenous control for normalization of expression levels. Real-time RT-PCR reactions were performed on an ABI7500 instrument (Applied Biosystems, Foster City, CA), using SYBR1 Green PCR Master Mix (Applied Biosystems). The amplification reactions were performed as follows: 2 min at 50°C, 10 min at 95°C, and 40 cycles of 95°C for 15 sec and 55°C for 30 sec and 68°C for 30 sec. Fold variation in gene expression was quantified by means of the comparative Ct method: $2^{-(\Delta C_{t\,\text{treatment}} - \Delta C_{t\,\text{control}})}$, which is based on the comparison of expression of the target gene (normalized to the endogenous control β-actin) between the compared samples.

3. Results and Discussions

Previously, our study derived and characterized microglia-like cells from the healthy iPSK3 cells and Ep-iPSC cells [8]. The cells were cocultured and integrated with isogenic dorsal cortical spheroids (Supplementary Figure S1). The whole-cell transcriptome analysis was performed for the microglial phenotype, neural inflammation, and the genes involved in Alzheimer's disease. Our current study focuses on different attributes of the 3-D dorsal cortical spheroids containing isogenic microglia-like cells (D-MG group) vs. microglia-like cells (MG group), including metabolic pathways and the signaling pathways that are involved in cell proliferation, cell death, inflammation, PIK3/AKT/mTOR signaling, EIF2 pathway, and Wnt and Notch pathways, which were not reported previously.

3.1. Central Metabolic Pathway. The 3-D spheroid culture usually is associated with slow growth rates, cytoskeleton reorganization, enhanced tight junctions and polarity, and the relocated membrane transporters [25–27]. In aerobic glycolysis, glucose is consumed through the glycolytic pathway to produce lactic acid, nucleotides, amino acids, and other metabolites, while glutamine is converted through glutaminolysis to citrate for cholesterol and lipid production. In oxidative phosphorylation, the generated pyruvate is oxidized to CO_2 and water through the tricarboxylic (TCA) cycle, which produces ATP and coverts NADH to NADPH [28–30].

The central metabolic pathways are shown in Figure 2. The values were calculated using log2 (DMG/MG). Relative enzyme expression levels indicate an increase in glycolytic and pentose phosphate pathways in the D-MG group as well as the increased amino acid synthesis (Figure 2 and Supplementary Figure S2) [31]. The increased glycolysis is permissive to trigger microbiocidal activity of microglia and allows the cells to survive in the 3-D spheroids. However, enzymes in the glutaminolytic pathway, hexosamine, nucleotide, lipid synthesis, and TCA cycle have small differences among the two groups. Genes related to ATP synthesis and mitochondrial complexes I, III, and IV are shown in Supplementary Table S2 and Supplementary Figure S2. The differences between the two groups are small (within ±0.5 except NDUFA13 at -0.68). But the values are all negative for genes related to ATP synthesis and mitochondrial complexes I and III, indicating lower expression in the D-MG group. Together, these results indicate the different energetic/metabolic phenotypes between the D-MG and the MG groups.

Metabolic shift towards glycolysis usually results in the elevated dependence on glutaminolysis or fatty acid synthesis in cell metabolism [32]. However, in this study, the cells did not show a significant increase in glutaminolysis in the spheroids (Figure 2 and Supplementary Figure S2). Cytoplasmic isocitrate dehydrogenase 1 (IDH-1) is involved in the reaction of isocitrate production from α-ketoglutarate in the cytosol. IDH-1 expression is decreased in the D-MG spheroids, which may be associated with NF-κB activation in a hypoxia-inducible factor- (HIF-1α-) dependent manner [33].

Similarly, 3-D culture of iPSC-derived endothelial cells also showed the glycolysis-dominated metabolism compared to ones in 2-D culture [34]. Moreover, human MSCs treated with interferon gamma exert an immunosuppressive phenotype by secreting PGE2/IDO and reconfigure the metabolic phenotype to aerobic glycolysis [35]. It was also suggested that activation of the AKT/mTOR signaling pathway is required for metabolic shift under this immune polarization.

The 3-D cultures may not always enhance the glycolysis, which is dependent on a specific cell type. For example, it was reported that 3-D cultures of hiPSC-derived cardiomyocytes displayed downregulation of genes involved in glycolysis and lipid biosynthesis and upregulation of genes involved in oxidative phosphorylation. Accordingly, the 3-D cultures showed lower fluxes for fatty acid synthesis and the increased TCA cycle activity, which improved both cell purity and metabolic maturation [36].

3.2. Hypoxia (Glycolysis and Oxidative Phosphorylation)

3.2.1. HIF-1α Pathway. In 3-D spheroid culture, the inside of the spheroids is thought to be more hypoxic than the surface due to mass transfer limitation of oxygen [37], while this has been challenged by other studies as nonhypoxia-stabilized HIF expression [25]. Hypoxia is an important factor in regulating stem cell metabolism and phenotype [38]. When oxygen concentrations decrease, the oxygen-dependent prolyl hydroxylase domain proteins are inactivated and the HIF-1α protein is accumulated, which promotes HIF-1α translocation to the nucleus and its binding to hypoxia response elements, such as glucose transporters and glycolytic enzymes [39, 40]. Our results do not show the higher HIF-1α gene expression in the D-MG group but demonstrate the increased expression of HIF-1α pathway downstream genes, including SIAH2 (1.29), PDK1 (3.84), LDHA (1.99), LONP1 (1.94), and P4HA1 (1.79) (Figures 3(a)–3(c)). These results may indicate the nonhypoxia-stabilized HIF expression in the D-MG group. The downregulated HIF-1α gene expression in the D-MG group was also validated using RT-PCR, along with the upregulated glycolytic gene expression in the D-MG group (Figures 3(d) and 3(e)).

HIF-1α induces pyruvate dehydrogenase kinase 1 (PDK1) expression, which inhibits mitochondrial pyruvate dehydrogenase (PDH) [38, 41]. This reduces pyruvate flux into the TCA cycle and lowers the mitochondrial oxygen

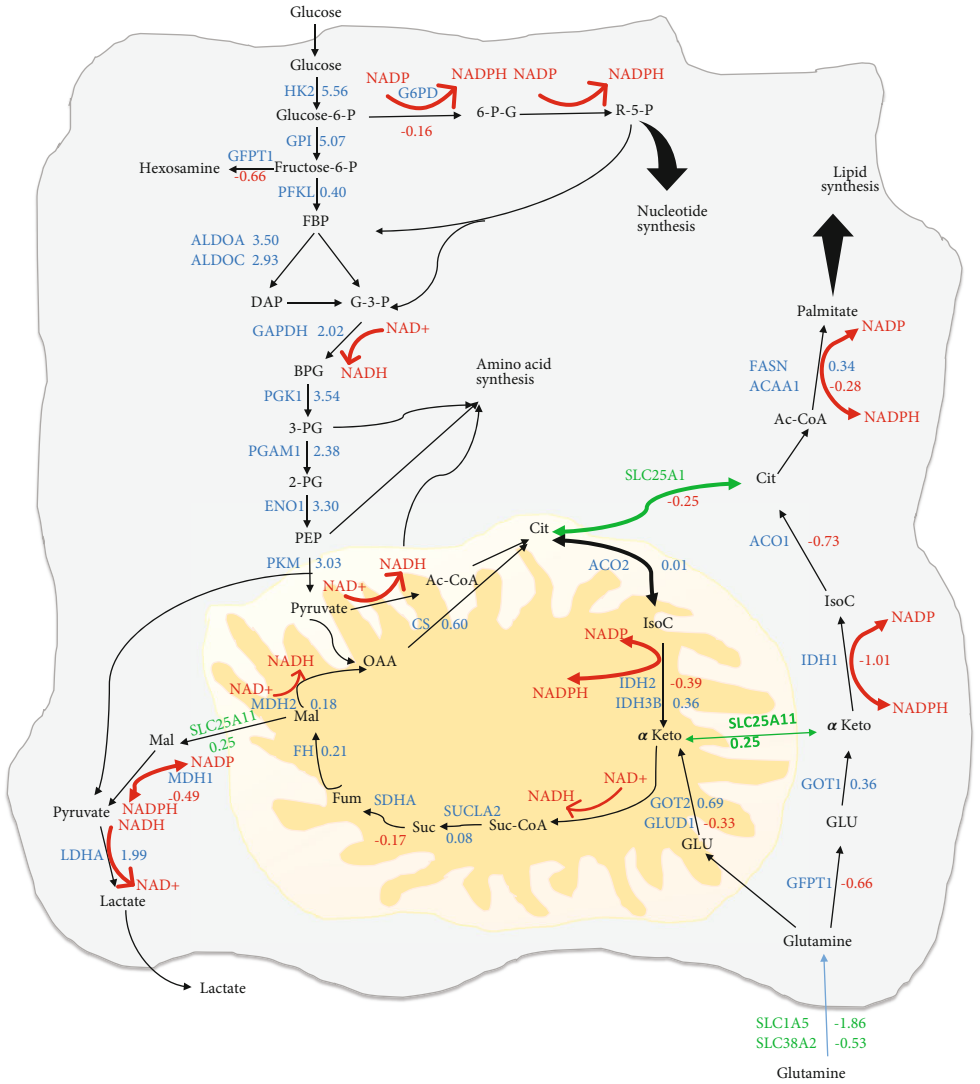

(a)

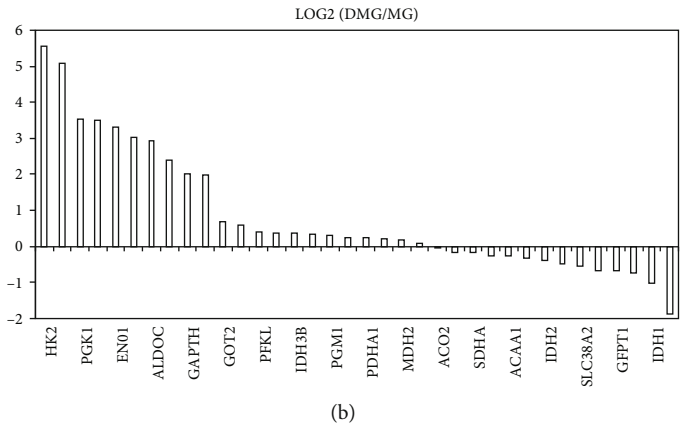

(b)

Figure 2: Ratios of gene abundance of central metabolic pathways in the D-MG group in comparison to the MG group. The FPKM (fragments per kilobase per million reads) normalized values for these genes are listed for both samples. The numbers are the log2 values of ratios of D-MG to MG. Negative values indicate that the genes are present in higher amounts in the MG group, while positive values indicate that the genes are present in higher amounts in the D-MG group. (a) Central metabolic pathways. (b) Log2 values of glycolysis genes of D-MG/MG ratios.

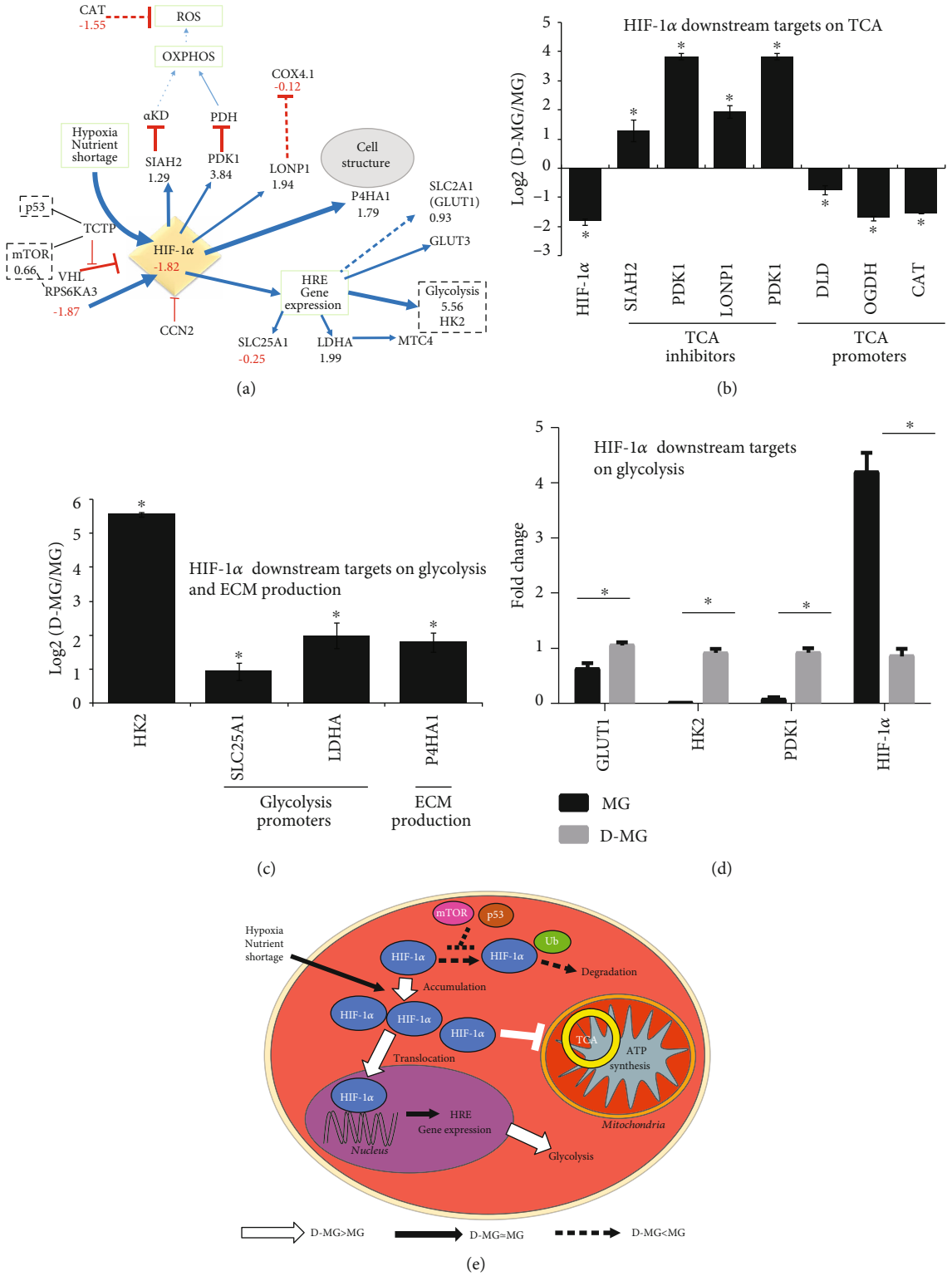

Figure 3: HIF-1α-related pathway. (a) RNA-sequencing results for glycolytic genes and HIF-1α; relative transcript expression between D-MG and MG for HIF-1α and its downstream targets (b) on tricarboxylic cycle (TCA) and (c) on glycolysis and extracellular matrix (ECM) production. ∗ indicates $p < 0.05$ ($n = 3$). (d) Validation of glycolytic genes using RT-PCR. ∗ indicates $p < 0.05$ ($n = 3$). (e) Schematic diagram showing the major changes in D-MG versus MG for HIF-1α signaling: D-MG shows enhanced HIF-1α activities that reduce TCA and ATP production, increasing glycolysis mediated by HIF-1α.

Table 1: Glycolysis vs. oxidative phosphorylation.

Gene name	MG-1	MG-2	MG-3	D-MG-1	D-MG-2	D-MG-3	MG ave	DMG ave	DMG/MG	LOG2 (DMG/MG)
P4HA1	140.340	135.633	141.039	389.230	546.723	505.399	139.004	480.451	3.456	1.79
SLC2A1 (GLUT1)	579.1676	469.9516	562.8377	912.218	1098.52	1056.15	537.319	1022.293	1.903	0.93
DLST	17.881	18.114	17.362	26.470	26.133	24.754	17.786	25.786	1.450	0.54
SLC16A3	304.016	219.663	293.687	255.760	244.563	255.972	272.455	252.098	0.925	-0.11
COX4I1	238.629	185.922	239.199	186.813	225.728	199.922	221.250	204.154	0.923	-0.12
SLC25A1	72.139	59.151	72.118	54.289	60.972	56.058	67.803	57.107	0.842	-0.25
DLD	22.476	21.521	21.854	12.507	12.003	14.700	21.950	13.070	0.595	-0.75
OGDH	28.692	23.353	27.126	8.233	7.421	8.492	26.390	8.049	0.305	-1.71

The FPKM (fragments per kilobase per million reads) normalized values for these genes are listed for both samples. The numbers are the log2 values of ratios of D-MG to MG. Negative values indicate that the genes are present in higher amounts in the MG group, while positive values indicate that the genes are present in higher amounts in the D-MG group. The value 1 indicates two-fold change.

requirements. The lactate production and secretion would be increased, as observed by Sart et al. [9]. HIF-1α also induces E3-ubiquitin ligase SIAH2 synthesis, which mediates the proteasomal degradation of the OGDH subunit of α-ketoglutarate dehydrogenase (α-KD) and forms a part of the feedback control of HIF-1α signaling. A modest reduction of the α-KD enzyme complex was observed in the D-MG group (DLD, -0.75, OGDH, -1.71) (Table 1), which may slow down TCA cycle activity. Interestingly, the citrate transportation into the cytoplasm by citrate transporter protein (SLC25A1, -0.25) was relatively comparable between these two groups. The extracellular matrix remodeling via collagen hydroxylases (P4HA1, 1.79) was upregulated in the D-MG group. The amounts of anabolic rate-limiting enzymes were increased or remained similar, while catabolic enzymes were unchanged between the two groups (Table 2). The rate-limiting glycolytic pathway steps (HK2, PKM, and PFKL) are the mostly increased enzymes of the pathway. These findings are consistent with the metabolic shift to aerobic glycolysis. In addition, high PFK level may also indicate high levels of AMP, since the spheroids usually have high ATP amounts [14].

HIF-1α signaling can induce the expression of the mitochondrial protease LONP1 (1.94) (Figure 3). LONP1 degrades cytochrome C oxidase 4 subunit 1 (COX4-1) through electron transport chain complex IV, allowing the replacement of COX4-1 by COX4-2 [42], which is more efficient in enzymatic reaction. LONP1 is an essential central regulator of mitochondrial activity and is overexpressed during oncogenesis [43]. Although LONP1 was increased (1.94) based on our results, there was little change in the level of COX4-1 (-0.12). Reduced mitochondrial respiration normally results in fewer reactive oxygen species (ROS), correlated with the reduced level of catalase (CAT, -1.55). The reduced oxidative stress results in the diminished hydrogen peroxide damage and less oxidized proteins [14].

3.2.2. Glutamine Metabolism and Hexosamine Pathway. While the D-MG group mainly uses glycolysis as its major energetic metabolism, our results did not show an increased reliance on glutamine metabolism (Figure 2 and Supplementary Figure S2). Intracellular glutamine levels are regulated by plasma membrane transporters SLC38A2 and SLC1A5 [14]. Endoplasmic reticulum stress would induce the degradation of transporters and ultimately autophagy and cell death [14]. In D-MG spheroids of this study, both SLC38A2 (-0.53) and SLC1A5 (-1.86) were decreased, which may suggest enhanced autophagy in D-MG spheroids.

(1) Conversion of Glutamine into Glutamate. The glutamate demand of the cells is indicated by the expression of GFPT1 (-0.66). GFPT1 is the first and rate-limiting step of the hexosamine pathway and catalyzes the conversion of fructose 6-phosphate and glutamine to glucosamine 6-phosphate and glutamate. Consistently in this study, several enzymes in polysaccharide, proteoglycan, and glycosylation synthetic pathways were downregulated in the D-MG spheroids, including UDP-glucose pyrophosphorylase UGP2 (-0.51), UDP-glucose 6-dehydrogenase UGDH (-1.18), and UDP-glucose 4-epimerase GALE (-1.31).

(2) α-Ketoglutarate. Glutamate can be converted to α-ketoglutarate by the mitochondrial GLUD1 (-0.33) or by cytoplasmic alanine or aspartate aminotransferases [44]. The cytoplasmic enzymes were slightly upregulated (GOT1, 0.36, GOT2, 0.69) in the D-MG group. There are three possible routes by which α-ketoglutarate can be converted to citrate (Figure 2) [1]. It can be converted through the TCA cycle [2]. It could be converted from isocitrate to citrate (by IDH2, -0.39, and ACO2, 0.01), which affects the normal TCA cycle flux by reductive glutamate metabolism [32]. In this study, IDH3B was slightly increased (0.36) and it can only catalyze the "forward" reaction [3]. Cytoplasmic α-ketoglutarate, produced through GFPT1 (-0.66) and GOT1 (0.36), can be converted by IDH1 (-1.01) and ACO1 (-0.73), which are both downregulated in the D-MG group compared to the MG group.

(3) NADH. NADH/NAD+ and NADPH/NADP+ conversions are critical in the central metabolic pathways (Figure 2 and Supplementary Figure S2). The reduction in the mitochondrial MDH1 (-0.49) and the downregulation of NAD(P) transhydrogenase (NNT, -1.24) suggest that the conversions in mitochondria may have some significance. MDH1 was decreased (-0.49) but lacked a malate source (e.g., the SLC25A11 transporter was essentially unchanged

Table 2: Rate-limiting enzymes for central metabolic pathways and the ratios of their expression in the D-MG group compared to the MG group.

Pathway	Gene name	MG-1	MG-2	MG-3	D-MG-1	D-MG-2	D-MG-3	MG ave	DMG ave	LOG2 (DMG/MG)
Glucose phosphorylation	HK2	8.057	7.382	8.514	373.333	367.184	391.036	7.984	377.184	5.56
Glycolysis	PKM	144.193	130.476	142.160	1071.419	1269.244	1061.022	138.943	1133.895	3.03
Glycine synthesis	SHMT2	34.121	29.636	33.060	146.550	175.435	141.673	32.272	154.553	2.26
Asparagine synthesis	ASNS	28.779	28.424	28.878	93.603	122.579	101.086	28.694	105.756	1.88
Glycogenolysis	PYGB	25.047	22.544	24.888	34.525	34.766	30.397	24.159	33.229	0.46
Pyrimidine synthesis	CAD	8.199	9.554	8.489	13.220	12.638	10.185	8.747	12.015	0.46
Glycolysis	PFKL	62.436	52.127	63.963	83.298	79.339	73.566	59.509	78.734	0.40
Aspartate synthesis	GOT1	16.089	14.826	14.507	18.869	20.440	19.010	15.141	19.439	0.36
Fatty acid synthesis	FASN	28.814	22.644	29.725	36.264	34.796	31.673	27.061	34.244	0.34
Purine synthesis	PRPS1	23.085	20.259	22.740	24.847	28.698	27.976	22.028	27.173	0.30
Pentose phosphate	G6PD	15.355	12.245	15.422	12.237	14.129	12.097	14.341	12.821	-0.16
Fatty acid synthesis	ACAA1	21.219	19.891	21.847	17.973	18.352	15.681	20.986	17.336	-0.28
Glutamine-glutamate conversion	GLUD1	49.375	44.127	51.590	35.530	41.837	38.198	48.364	38.522	-0.33
Methionine synthesis	MTR	7.799	9.359	8.511	7.162	5.777	6.920	8.556	6.620	-0.37
TCA cycle	IDH2	103.753	84.981	101.212	66.326	79.889	75.170	96.649	73.795	-0.39
Serine synthesis	PHGDH	141.285	116.771	138.838	92.636	114.237	92.781	132.298	99.884	-0.41
Hexose	GFPT1	46.208	45.599	46.304	26.099	32.086	29.340	46.037	29.175	-0.66
Fatty acid oxidation	CRAT	23.955	20.886	25.945	14.810	14.697	14.392	23.596	14.633	-0.69
Proline synthesis	PYCR1	102.329	84.127	98.191	46.173	65.047	53.249	94.883	54.823	-0.79
Urea synthesis	CPS1	7.949	7.541	8.583	4.041	3.943	4.177	8.024	4.054	-0.99
Tyrosine synthesis	PAH	0.441	0.551	0.468	0.171	0.184	0.224	0.487	0.193	-1.33
Cysteine synthesis	MAT1A	5.443	4.897	5.280	0.793	0.724	0.529	5.207	0.682	-2.93

The FPKM (fragments per kilobase per million reads) normalized values for these genes are listed for both samples. The numbers are the log2 values of ratios of D-MG to MG. Negative values indicate that the genes are present in higher amounts in the MG group, while positive values indicate that the genes are present in higher amounts in the D-MG group. The value 1 indicates two-fold change.

(0.25)). The conversion of cytoplasmic pyruvate to lactate would consume the produced NADH. The richest source of NADPH is the pentose phosphate pathway, where G6PD (-0.16) was essentially unchanged between the two groups. These results indicate the reliance on mitochondrial NAD +/NADH in the D-MG group.

(3) Citrate. Citrate can be used for fatty acid synthesis. ATP-citrate synthase uses citrate to generate cytosolic acetyl-CoA. Acetyl-CoA is used for (1) histone acetylation by acetyl-CoA acyltransferase (ACAA1, -0.28), (2) fatty acid synthesis (FASN, 0.34), and (3) synthesis of cholesterol, steroid hormones, and other biomolecules. Glutamine is as important as glucose in metabolism, and it can block glutamate-dependent cellular pathways at either IDH1 or ACL step [14].

3.3. Signaling Pathways Involved in Metabolic Reprogramming. The analysis so far shows the metabolic shift to aerobic glycolysis in the 3-D spheroids, which may be driven by diffusion gradients [30, 37]. In order to investigate how metabolic reprogramming is orchestrated, the status of critical pathways for cellular function, including PI3K/AKT/mTOR, Myc, p53, NF-κB, EIF2, Wnt, and Notch, was analyzed.

3.3.1. PIK3/AKT/mTOR Signaling. PI3K (a class I phosphoinositide 3-kinase) is one of the key signaling enzymes that are activated in 3-D spheroid cultures [45]. And the PIK3 pathway is directly related to cellular metabolism and growth. When cells consume the nutrients and growth factors, they generate amino acids, glucose, oxygen, and energy (i.e., ATP) and use these products to activate GTPase, such as Rheb, through PI3K. One key regulator of metabolism and growth-activated downstream of PI3K signaling is the mechanistic target of rapamycin (mTOR) [46]. Our results showed that the expression of mTOR (0.66) was slightly elevated in the D-MG spheroids and the downstream effectors were inhibited (e.g., ribosomal protein s6 kinase RPS6KA3, -1.87) (Figure 4(a)). mTOR stimulates pyrimidine synthesis via the RPS6KA-mediated phosphorylation of CAD (0.46), whereas AKT can phosphorylate ACL, enhancing its lipogenic activities and mTOR signaling. The expression of ACLY (-0.13) indicates that the activity of the AKT pathway was similar in the two groups. mTOR regulates several anabolic and catabolic pathways through fatty acid and cholesterol biosynthetic genes via the SREBP family (SREBP1 and SREBP2) [47].

mTOR signaling was reported to increase the translation of HIF-1α, glucose transporters, and glycolytic enzymes and

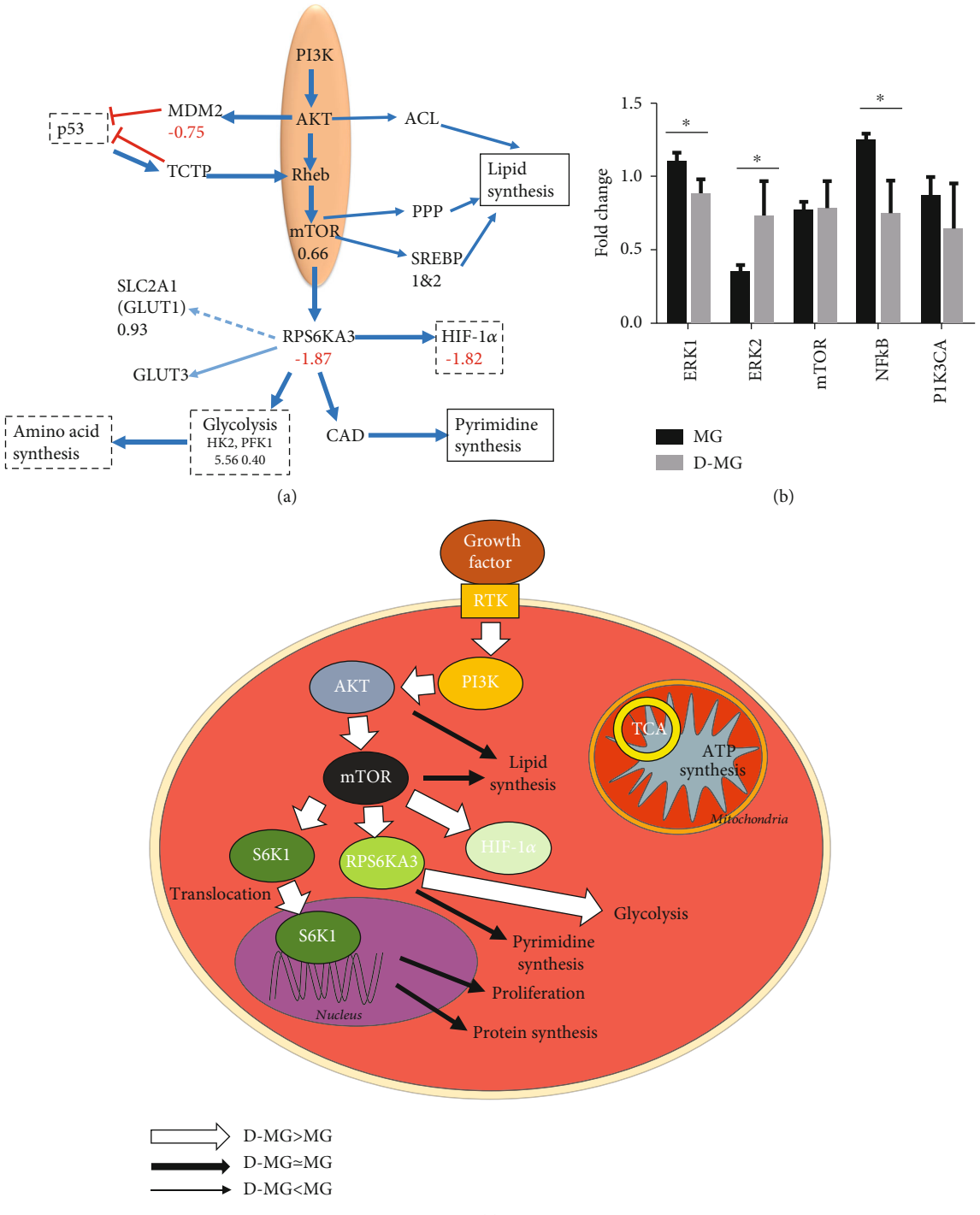

Figure 4: mTOR signaling in the D-MG group. (a) RNA-sequencing results. (b) Validation of ERK genes using RT-PCR. ∗ indicates $p < 0.05$ ($n = 3$). (c) Schematic diagram showing the major changes in D-MG versus MG condition for mTOR signaling. D-MG shows enhanced mTOR activities that reduce tricarboxylic cycle (TCA), and D-MG shows increased glycolysis mediated by mTOR.

promote metabolic reprogramming. The activation of the mTOR protein complex mTORC1 leads to the induction of genes encoding the enzymes of glycolysis, the pentose phosphate pathway, and lipid and sterol biosynthesis [35, 48]. mTOR was also reported to coordinate the activation of cell growth machinery together with amino acids in the presence of growth signals [49]. However, in the RT-PCR validation, mTOR gene expression was statistically insignificant, possibly due to assay variations (Figures 4(b) and 4(c)). In addition, ERK1 was downregulated while ERK2 was upregulated in the D-MG group.

3.3.2. Myc Signaling. Myc is a transcription factor that dimerizes with MAX to bind to DNA and regulate gene expression

involved in metabolism (glycolysis and glutaminolysis) and biosynthesis (nucleotide and lipid synthesis) [50]. Myc supports specific mRNA splice variants, such as glycolysis-affecting PKM2 over PKM1. Myc targets glucose membrane transporters such as GLUT1 (or SLC2A1) and glutamine transporter SLC1A5, which are important in cell proliferation [50]. Myc transactivates the gene expression of PFK, ENO, and LDHA (1.99) and indirectly increases GAPDH and PGK1, based on our genomics analysis (PGK1, 3.54; GPI, 5.07; ENO1, 3.30; and GAPDH, 2.02), indicating the relation between Myc and glycolysis (Figure 5). The gene expression of Myc-related proteins was downregulated in the D-MG spheroids including PTBP1 (-0.60), SLC1A5 (-1.86), and PRDX3 (-1.77) (Figure 5). The low Myc activity inside the D-MG spheroids might indicate the slow proliferation of cells.

3.3.3. p53 Signaling. In addition, the expression of the transcriptional suppressor CDK5RAP3 is comparable between the D-MG group and the MG group (0.34). CDK5RAP3 is a novel activator of PAK4 and processes important prometastatic function [51]. It has been reported that CDK5RAP3 knockdown upregulated the tumor suppressor p14ARF at protein and mRNA levels, and ectopic expression of CDK5RAP3 repressed the transcription of p14ARF [51]. Therefore, the CDK5RAP3 expression may allow for the synthesis of p14ARF and its binding to MDM2. The MDM2 (-0.75) expression was decreased in the D-MG spheroids (Figure 6). The MDM2 expression can release p53 from inhibition and thereby lead to the stabilization, accumulation, and activation of p53. Also, the negative regulators of p53 are subjected to tight feedback regulation. For example, BCCIPβ overexpression delays the G1 to S progression and results in an elevated p21 expression, which would inhibit CDK1 induction of cell cycle progression. Though the D-MG spheroids did not show a significant increase in BCCIPβ expression (0.13) compared to the MG group (Figure 6), the expression of CDK1 was decreased (-1.72) in the D-MG group, which indicated a potential cell cycle arrest.

3.3.4. Wnt Pathway. In the canonical Wnt pathway, Wnt interacts with the Frizzled receptor that results in the inhibition of glycogen synthase kinase-3β (GSK-3β) [52]. Due to the inhibition, GSK-3β would not be able to phosphorylate β-catenin, leading to the nuclear entry of β-catenin. In the nucleus, β-catenin interacts with members of TCF transcriptional factors (i.e., T cell factor/lymphoid enhancer factor) and modulates target gene expression [53]. In our D-MG spheroids, the expression of β-catenin was slightly reduced compared to that in the MG group (CTNNB1, -0.66) (Figure 7). Wnt 3 (-1.06) and Wnt 5B (-1.55) were also decreased. The histidine triad nucleotide-binding protein 1 (HINT1, 0.23), which keeps the Wnt/β-catenin pathway inactive [54], and protein phosphorylase 2A (PPP2RA1, 0.28) were comparable in the two groups. Our previous studies evaluated the influence of the canonical Wnt pathway on neural patterning of hiPSCs [55, 56]. The reduced canonical Wnt/β-catenin signaling at a late stage of neural differentiation of hiPSCs can enrich cells with rostral forebrain identity [57]. In the noncanonical pathway, Wnt binds to the Frizzled receptor which activates Dishevelled and forms a complex with RAC1, mediating profilin binding to actin [58]. In the current study, the noncanonical Wnt pathway activity was comparable for the D-MG spheroids and MG group (RAC1, 0.27).

3.3.5. NF-κB Pathway. NF-κB was found to be involved in cellular responses to various stimuli such as stress, cytokines, free radicals, and viral antigens [59, 60]. The two classes of NF-κB proteins (p50/p52 and ReIA/ReIB) form heterodimers to function as transcriptional activators. In an inactive state, NF-κB dimers are sequestered in the cytoplasm by IkB inhibitors. They mask the nuclear localization signals of NF-κB proteins and keep NF-κB signaling in the inactive state. When active, NF-κB proteins enter the nucleus and turn on the IkBα repressor. It has been reported that hypoxia upregulated PRMT1 which asymmetrically methylated ReIA, inhibiting the binding of ReIA to DNA and further repressing NF-κB [61]. NF-κB signaling was found to be dysregulated in TGFβR3 epicardial cells, which also showed the impaired cell invasion and revealed the role of NF-κB signaling in TGFβR3 activation [62]. In our D-MG spheroids, the lower expression of TGFβR3 (-2.61) and TGFB1 (-0.60) indicates the less activated NF-κB pathway (Supplementary Table S3 and Figure 4(b)). TGFBI expression is essentially similar (0.03), and PRMT1 expression (0.63) is slightly upregulated.

Microglial M1 immune response usually involves NF-κB signaling [59]. Knocking down of LRP1 in primary microglia led to the activation of both c-Jun N-terminal kinase and NF-κB pathways. The sensitivity to lipopolysaccharide (LPS) stimulation in the production of proinflammatory cytokines was also enhanced. The NF-κB inhibitor was shown not only to suppress the production of cytokines induced by the knockdown of LRP1 but also to restore the downregulated expression of LRP1 due to LPS stimulation.

3.3.6. Notch Pathway. Most Notch receptors were upregulated in the D-MG group, including DLL1 (5.85), DLL3 (2.84), DLL4 (1.49), JAG1 (2.55), JAG2 (1.70), HES1 (0.62), HES4 (2.44), and HES5 (7.93) (Figure 8(a)), indicating the enhanced cell-cell communications in 3-D culture. Our previous study also showed that Notch-1 expression was upregulated in the hybrid stem cell spheroids [63]. In addition, Notch signaling regulates the balance between the progenitor pool and the neuron pool, preventing premature neurogenesis [64]. Global deletion of Notch signaling leads to the accelerated differentiation into neurons. The activation of Notch by DLL1 causes neural stem cells to irreversibly commit to a glial fate and prevents the stem cells from adopting a neuronal fate [65]. When a Notch receptor interacts with its ligands, Delta and Serrate, it activates the membrane-tethered transcription factor and leads to the release of intracellular domain (NICD) and its translocation to the nucleus. Then, NICD interacts with CSL family regulators and transcript Hes1 and Hes5 expression. Notch signaling also promotes Wnt expression in Drosophila development [66]. Conversely, Wnt protein can promote the expression of

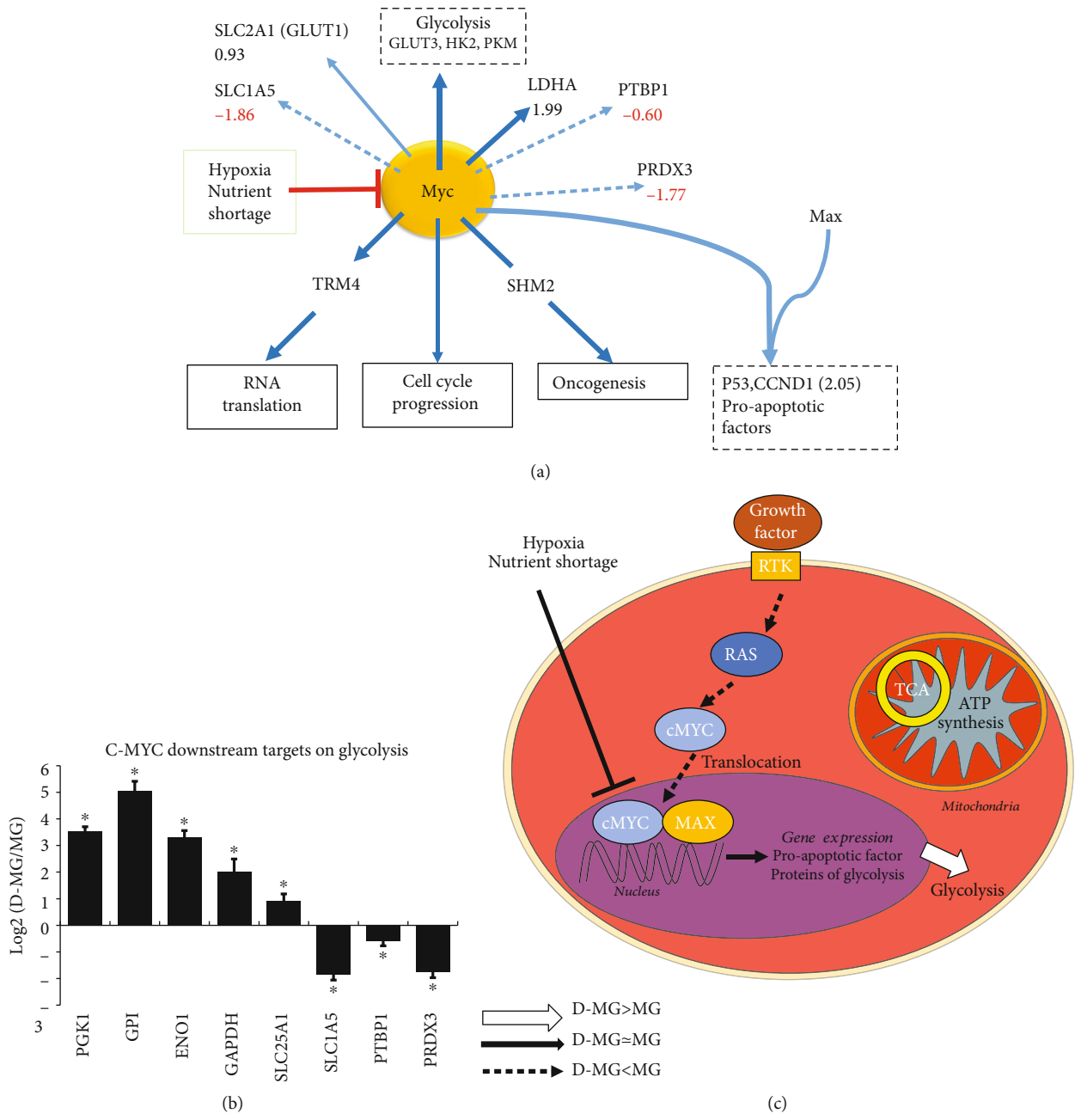

FIGURE 5: c-Myc signaling in the D-MG group. (a) RNA-sequencing results related to Myc. (b) Relative transcript expression between D-MG and MG conditions for c-Myc and its downstream targets; ∗ indicates $p < 0.05$ ($N = 3$). (c) Schematic diagram showing the major changes in D-MG versus MG for c-Myc signaling: D-MG shows enhanced c-Myc that mediates increased glycolysis.

Notch ligands DLLs, forming a positive feedback loop to maintain Notch signaling and Wnt protein expression.

3.3.7. Cell Death and Cell Cycle. It is important to evaluate cell death pathways (necrosis or apoptosis) in the 3-D spheroids. The major changes associated with cell death are free radical damage, swelling, rupture, and cytolysis. Under stress, the cells sense DNA damage by the serine/threonine kinase ATM and p53 [67]. p53 accumulates in the mitochondrial matrix and triggers mitochondrial permeability transition (MPT) pore (PTP) opening. Then, p53 physically interacts with anti- and proapoptotic Bcl-2 and BAX family members to inhibit or activate their respective functions, leading to mitochondrial outer membrane permeabilization (MOMP) and apoptosis [68]. From our results, PPID (0.74), the essential component of the MPT pore located in the mitochondrial matrix, is slightly increased in the D-MG group (Figure 8(b)).

The exact molecular composition of the MOMP complex is assumed to contain hexokinase, voltage-dependent anion channel (VDAC, on the outer membrane), the adenine nucleotide translocase (ANT, in the inner membrane), and cyclophilin D (a peptidyl-prolyl isomerase in the matrix).

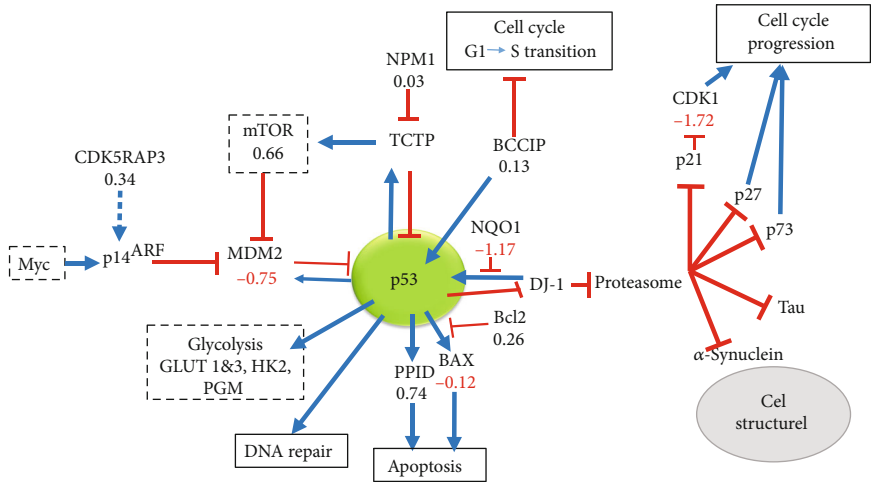

(a)

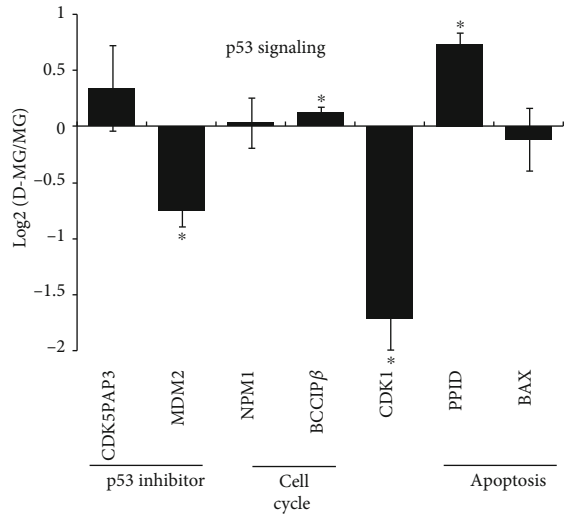

(b)

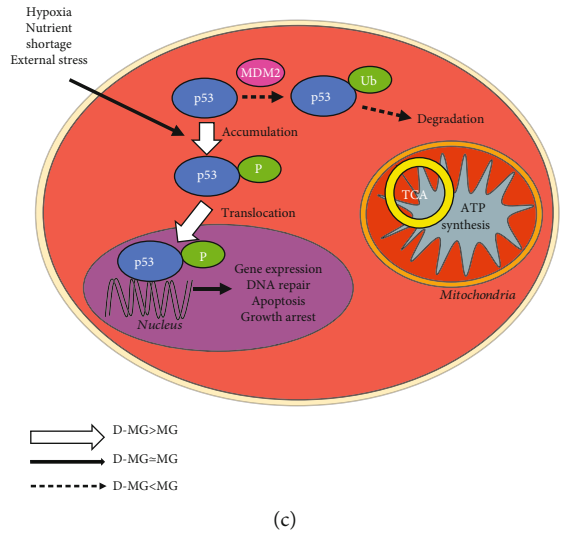

(c)

FIGURE 6: p53 signaling in the D-MG group. (a) RNA-sequencing results related to p53. (b) Relative transcript expression between D-MG and MG for p53 and its downstream targets; ∗ indicates $p < 0.05$ ($N = 3$). (c) Schematic diagram showing the major changes in D-MG versus MG for p53 signaling: D-MG shows the increased p53 activities, which results in the decreased expression of proteins related to cell proliferation.

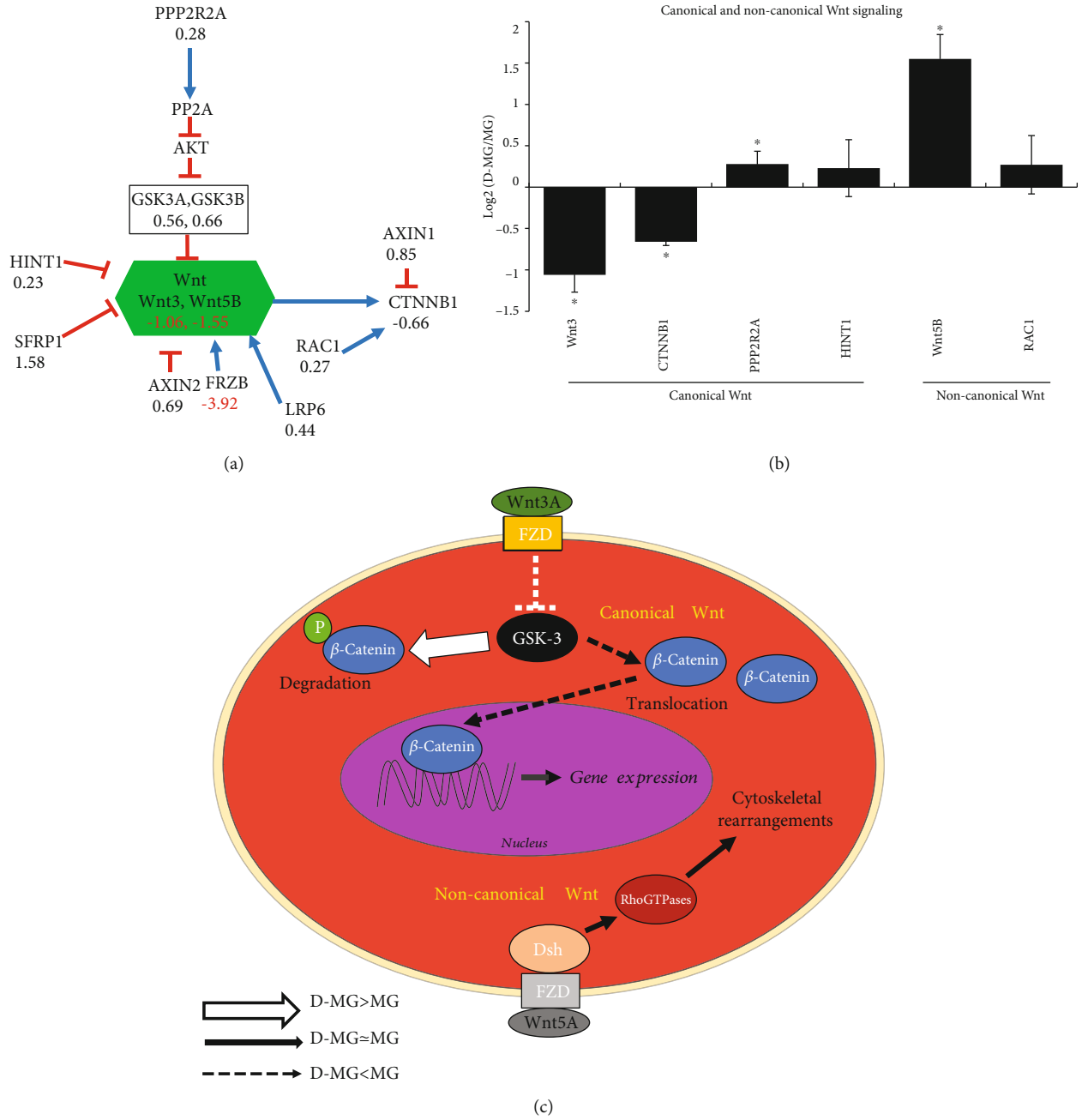

Figure 7: Wnt signaling in the D-MG group. (a) RNA-sequencing results related to Wnt. (b) Relative transcript expression between D-MG and MG for Wnt and its downstream targets. ∗ indicates $p < 0.05$ ($N = 3$). (c) Schematic diagram showing the major changes in D-MG versus MG conditions for Wnt signaling; i.e., D-MG shows the decreased canonical Wnt signaling while noncanonical Wnt is increased, which results in the increased cytoskeletal rearrangement.

When PTP opens, it leads to matrix swelling and depolarization of the membrane potential, causing subsequent rupture of the outer membrane and consequently apoptosis [68]. Based on our results, VDACs were increased (VDAC1, 1.84; VDAC3, 0.90) in the D-MG group (Figure 8(b)). MPT-driven necrosis works not only by the dissipation of mitochondrial transmembrane potential but also by the latent chromatinolytic activity of AIFM1 (apoptosis-inducing factor mitochondrion-associated 1) [69]. The slightly decreased AIFM1 (-0.38) in the D-MG spheroids indicates that necrosis is favored over apoptosis.

The mitochondrial HINT2 promotes angiogenesis via p53 and BAX. The activated NF-κB pathway also leads to the increased expression of antiapoptotic proteins, including Bcl-XL-binding protein v68 (PGAM5, 1.09) and Bcl-2-associated transcription factor 1 (BCLAF1, 0.96) in the D-MG spheroids (Figure 8(b)). The defender against apoptotic cell death (DAD1, 0.11) and Bcl-2 inhibitor of transcription

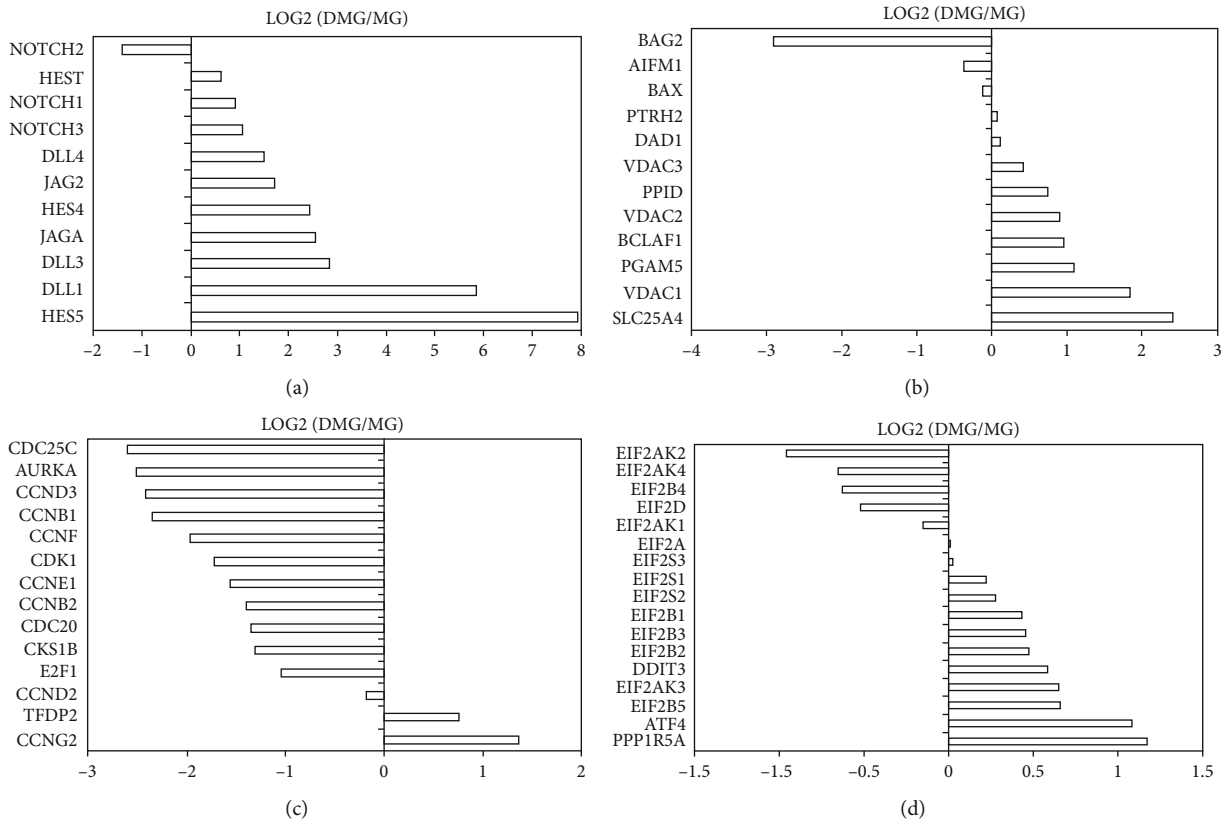

Figure 8: Log2 expression levels of the D-MG/MG ratios for genes about cell-cell interactions, cell death, and cell cycle. (a) Notch signaling. (b) Cell death. (c) Cell cycle and cell proliferation. (d) EIF2 signaling as a part of integrated stress response (ISR).

1 (PTRH2, 0.07) were unchanged. These antiapoptotic proteins can bind to and inactivate proapoptotic proteins. The proapoptotic protein BAX, Bcl-2-like protein 4, was unchanged (-0.02), but Bcl-2-associated athanogene 2 (BAG2, -2.90) was decreased in the D-MG spheroids. Consistent with higher expression of death genes in the D-MG group, the cell cycle-related genes were downregulated in the D-MG spheroids but highly expressed in the MG group (Figure 8(c)).

The sirtuin signaling proteins SIRT1 (0.48) and SIRT6 (1.01) were upregulated in the D-MG spheroids (Table 3), which regulate DNA damage and oxidative stress. The autophagy-related genes were essentially similar between the two groups. Poly (ADP-ribose) polymerase (PARP) is a family of proteins involved in a number of cellular processes such as DNA repair, genomic stability, and programmed cell death [70]. PARP6 (1.32), PARP3 (1.12), and PARP2 (0.97) were upregulated while PARP4 (-1.34), PARP14 (-2.44), PARP12 (-2.54), and PARP9 (-2.76) were downregulated in the D-MG group (Table 4). PARP1 (-0.01) was essentially unchanged between the two groups.

3.3.8. Eukaryotic Initiation Factor 2 (eIF2) Pathway. eIF2 is one of the critical translation G proteins that are tightly regulated in the integrated stress response. In response to stress stimuli, eIF2α undergoes phosphorylation via different kinases, such as PKR-like endoplasmic reticulum kinase (PERK), which results in the formation of eIF2B. This blocks the p-eIF2 from its active GTP-bound state, causing a reduction of the translation of most mRNAs [71]. In the operative nervous systems, the eIF pathway was found to support the connectivity between neurons. The physiological extracellular cue Sema3A can trigger rapid and transient phosphorylation of eIF2a in axons for the axonal translational changes [72]. The D-MG group displayed the slightly elevated expression of eIF proteins, such as eIF-2α/EIF2S1 (0.220), eIF2-β/EIF2S2 (0.274), and eIF2B proteins, such as EIF2B1 (0.43), EIF2B2 (0.47), EIF2B3 (0.45), and EIF2B5 (0.66) (Figure 8(d)), indicating potential stress such as hypoxia or insufficient nutrient uptake in the D-MG group. Also, the expression of EIF2AK3 (0.64), a stress sensing protein kinase that phosphorylates the alpha subunit of eIF2, was slightly elevated in the D-MG group. DDIT3 (0.58), which plays an essential role in inducing cell cycle arrest and apoptosis in response to ER stress, was also slightly elevated in the D-MG group. PPP1R15A (1.17) dephosphorylates the eIF-2α/EIF2S1, thereby reversing the shutoff of protein synthesis initiated by stress-inducible kinases and then facilitating cell recovery from stress.

3.3.9. Extracellular Matrix. The extracellular matrix- (ECM-) related genes were found to be differentially expressed in the two groups (Supplementary Figure S3) [1]. The D-MG group had higher expression of some collagen genes including COL7A1, COL20A1, COL9A1, and COL11A2. The MG group expressed high levels of different types of collagens,

Table 3: Sirtuin signaling and autophagy.

Gene name	MG-1	MG-2	MG-3	D-MG-1	D-MG-2	D-MG-3	MG ave	DMG ave	DMG/MG	LOG2 (D-MG/MG)
Sirtuin signaling										
SIRT6	11.268	9.088	9.289	20.250	21.520	17.741	9.882	19.837	2.007	1.01
SIRT1	8.625	8.714	9.529	12.048	12.060	13.258	8.956	12.455	1.391	0.48
SIRT4	3.945	5.113	3.877	5.457	4.254	5.735	4.312	5.148	1.194	0.26
SIRT7	7.837	8.696	7.100	8.127	7.686	7.362	7.877	7.725	0.981	-0.03
SIRT5	1.763	2.161	1.591	1.743	1.551	1.505	1.838	1.599	0.870	-0.20
SIRT3	13.160	13.397	12.523	8.864	7.755	8.300	13.027	8.306	0.638	-0.65
SIRT2	50.715	42.689	48.365	27.236	31.360	27.618	47.256	28.738	0.608	-0.72
Autophagy										
TFEB	5.357	4.069	5.025	4.723	5.425	5.416	4.817	5.188	1.077	0.11
BECN1	13.675	11.764	13.135	12.298	12.239	12.236	12.858	12.257	0.953	-0.07
LAMP1	57.074	48.954	58.426	46.114	51.499	47.309	54.818	48.307	0.881	-0.72

The FPKM (fragments per kilobase per million reads) normalized values for these genes are listed for both samples. The numbers are the log2 values of ratios of D-MG to MG. Negative values indicate that the genes are present in higher amounts in the MG group, while positive values indicate that the genes are present in higher amounts in the D-MG group. The value 1 indicates two-fold change.

Table 4: Gene expression of poly (ADP-ribose) polymerase (PARP) family proteins.

Gene name	MG-1	MG-2	MG-3	D-MG-1	D-MG-2	D-MG-3	MG ave	DMG ave	DMG/MG	LOG2 (D-MG/MG)
PARP6	19.908	24.159	20.683	55.689	59.154	54.018	21.583	56.287	2.608	1.38
PARP3	3.171	3.020	3.221	6.723	7.323	6.366	3.137	6.804	2.169	1.12
PARP2	17.659	22.634	16.142	35.570	39.811	34.828	18.812	36.736	1.953	0.97
PARP11	3.485	3.789	3.403	6.320	6.097	6.702	3.559	6.373	1.791	0.84
PARP15	0.163	0.124	0.127	0.286	0.263	0.179	0.138	0.243	1.759	0.81
PARP8	2.142	2.526	2.428	3.305	3.204	3.578	2.365	3.362	1.422	0.51
PARP1	42.914	40.611	42.447	41.423	43.048	40.686	41.990	41.719	0.994	-0.01
PARP10	1.451	1.234	1.709	1.518	1.198	1.385	1.465	1.367	0.933	-0.10
PARP16	12.871	12.281	11.812	7.840	8.730	9.558	12.321	8.709	0.707	-0.50
PARP4	8.746	9.413	8.348	3.874	3.104	3.526	8.836	3.501	0.396	-1.34
PARP14	7.616	10.770	8.298	1.482	1.613	1.818	8.895	1.638	0.184	-2.44
PARP12	1.519	1.168	1.288	0.182	0.274	0.228	1.325	0.228	0.172	-2.54
PARP9	3.633	3.688	3.397	0.533	0.460	0.586	3.573	0.526	0.147	-2.76

The FPKM (fragments per kilobase per million reads) normalized values for these genes are listed for both samples. The numbers are the log2 values of ratios of D-MG to MG. Negative values indicate that the genes are present in higher amounts in the MG group, while positive values indicate that the genes are present in higher amounts in the D-MG group. The value 1 indicates two-fold change.

including COL23A1, COL6A1, COL4A1, COL13A1, COL5A2, COL5A1, COL14A1, and COL4A1 [2]. The D-MG group mainly enriched laminin LAMB4, while the MG group enriched LAMA3, LAMB1, LAMC1, LAMA2, LAMA1, etc. [3]. The D-MG group expressed higher levels of specific integrins, including ITGA7, ITGB8, ITGA2, and ITGAB3, while the MG group enriched ITGA6, ITGA11, ITGA8, ITGB6, ITGA1, ITGB5, etc. [4]. For ECM remodeling genes, the D-MG group enriched proteases MMP17, MMP10, MMP24, MMP7, and MMP1; the MG group had higher expression of proteases MMP23, MMP2, MMP14, TIMP1, MMP28, MMP26, and MMP15, etc.

Other pathways of our interests are shown in Supplementary Table S4, which include the AMPK pathway and PDL1/PD1 pathway (Figure 9 shows the relationship between miRNAs and PDL1/PD1 interactions) (Figure 9) [73]. Microglia, the main antigen-presenting cells in the human brain, maintain the equilibrium with T cells through the PD1 pathway as reported [74].

4. Conclusions

The genomics data reveal that the D-MG spheroids have higher expression of genes for glycolysis and hypoxia signaling, showing the metabolic shift to aerobic glycolysis, consistent with M1 polarization of microglia. However, glutamine conversion is not activated. The signaling pathway activities (activation of mTOR and p53, repression of NF-κB and canonical Wnt) are consistent with the slower proliferation rate and the accumulation of differentiated cells. The

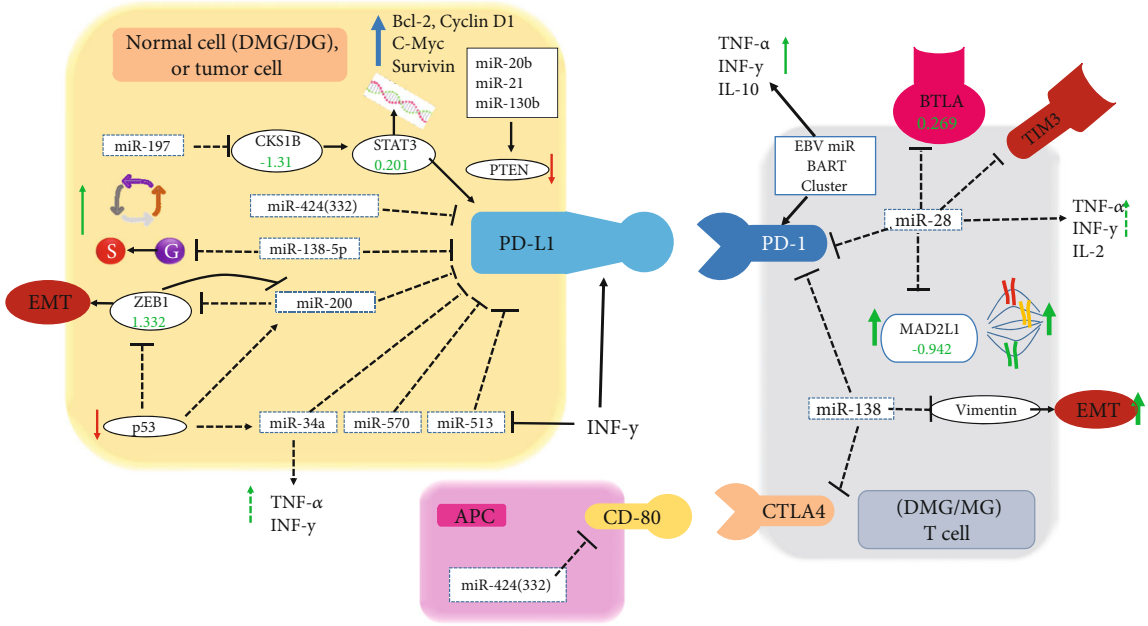

Figure 9: Illustration of microglia with PDL1/PD1 interactions. The numbers in the illustration are from the normal DMG/MG ratios. The arrows show the ways of tumor cell and T cell interactions. MGs act as antigen-presenting cells (APC).

additional NADPH needed for citrate and lipid synthesis is mainly generated by pentose phosphate pathway activation. The reduction in the proliferation rate allows the cells to achieve higher ATP levels in the spheroids. The D-MG group enriches genes for NOTCH signaling, but not canonical Wnt signaling. The MG group has higher expression of genes related to cell cycle and proliferation. These results can help to establish better coculturing methods for efficiently mimicking the *in vivo* structure of the central nervous system.

Abbreviations

6PD: 6-Phosphate dehydrogenase
ACAA1: Acetyl-CoA acyltransferase
ACL: ATP citrate lyase
ACO2: Aconitase 2
ADP: Adenosine diphosphate
AIFM1: Apoptosis-inducing factor mitochondrion-associated 1
AKT: Protein kinase B
AMP: Adenosine monophosphate
AMPK: AMP-activated protein kinase
ANT: Adenine nucleotide translocase
APC: Antigen-presenting cells
ARF: ADP ribosylation factor
ASNS: Asparagine synthetase
ATP: Adenosine triphosphate
BAG2: Bcl-2-associated athanogene 2
BAX: Bcl-2-associated X
BCCIPβ: BRCA2 and CDKN1A-interacting protein isoform β
Bcl-2: B-cell lymphoma 2
BCLAF1: Bcl-2-associated transcription factor 1
Bcl-XL: B-cell lymphoma-extra large
BECN1: Beclin 1
BMP4: Bone morphogenetic protein 4
BRN2: POU class 3 homeobox 2
CAD: Carbamoyl-phosphate synthetase 2
CAT: Catalase
CD11b: Integrin alpha M
CD45: Protein tyrosine phosphatase receptor type C
CDK: Cyclin-dependent kinase
CDK5RAP3: CDK5 regulatory subunit-associated protein 3
cDNA: Complementary DNA
CM: Cardiomyocytes
COL: Collagen
COX4-1: Cytochrome C oxidase 4 subunit 1
CPS1: Carbamoyl-phosphate synthase 1
CRAT: Carnitine O-acetyltransferase
CSL: Recombination signal binding protein for immunoglobulin kappa J region
CX3CR1: C-X3-C motif chemokine receptor 1
DAD1: Defender against apoptotic cell death
DDIT3: DNA damage inducible transcript 3
DLD: Dihydrolipoamide dehydrogenase
DLL: Delta-like canonical Notch ligand
DLST: Dihydrolipoyllysine-residue succinyltransferase
DMEM: Dulbecco's modified Eagle's medium
DMG/D-MG: Coculture of the dorsal forebrain spheroids with isogenic microglia-like cells
EC: Endothelial cells
ECM: Extracellular matrix
eIF2: Eukaryotic initiation factor 2
ENO: Enolase
Ep-iPSC: Episomal-induced pluripotent stem cells
ER: Endoplasmic reticulum
ERK: Extracellular signal-regulated kinases

FASN: Fatty acid synthase
FBS: Fetal bovine serum
FDR: False discovery rate
FGF: Fibroblast growth factor
FLT3L: FMS-like tyrosine kinase 3 ligand
FPKM: Fragments per kilobase per million reads
G6PD: Glucose-6-phosphate dehydrogenase
GALE: UDP-glucose 4-epimerase
GAPDH: Glyceraldehyde-3-phosphate dehydrogenase
GFPT1: Glucosamine-fructose-6-phosphate aminotransferase isomerizing 1
GLUD1: Glutamate dehydrogenase 1
GLUT1: Glucose transporter 1
GM-CSF: Granulocyte-macrophage colony-stimulating factor
GO: Gene Ontology
GOT: Glutamic-oxaloacetic transaminase
GPI: Phosphor-glucose isomerase
GSK-3β: Glycogen synthase kinase-3β
GTP: Guanosine triphosphate
HES: Hairy and enhancer of split 1
HIF-1α: Hypoxia-inducible-factor 1α
HINT: Histidine triad nucleotide-binding protein
hiPSCs: Human induced pluripotent stem cells
HK2: Hexokinase 2
IBA-1: Allograft inflammatory factor 1
IDH: Cytoplasmic isocitrate dehydrogenase
IDO: Indoleamine-pyrrole 2,3-dioxygenase
IkB: Nuclear factor of kappa light polypeptide gene enhancer in B-cell inhibitor
IL: Interleukin
ISR: Integrated stress response
ITG: Integrins
JAG: Jagged
KEGG: Kyoto Encyclopedia of Genes and Genomes
LAM: Laminin
LAMP1: Lysosomal-associated membrane protein 1
LDHA: Lactate dehydrogenase A
LDN: SMAD inhibitor LDN193189
LONP1: Lon protease homolog, mitochondrial
LPS: Lipopolysaccharide
LRP1: Low-density lipoprotein receptor-related protein 1
MAT1A: Methionine adenosyltransferase 1A
MAX: Myc-associated factor X
MDH1: Malate dehydrogenase 1
MDM2: Mouse double minute 2 protooncogene
MG: Microglia-like cells
MMP: Matrix metalloproteinase
MOMP: Mitochondrial outer membrane permeabilization
MPT: Mitochondrial permeability transition
MSC: Human mesenchymal stem cell
mTOR: Mechanistic target of rapamycin
MTR: 5-Methyltetrahydrofolate-homocysteine methyltransferase
Mxi-1: MAX-interacting protein 1
Myc: Myelocytomatosis
NADH: Nicotinamide adenine dinucleotide
NADPH: Nicotinamide adenine dinucleotide phosphate
NANS: Sialic acid synthase
NDUFA13: NADH dehydrogenase 1 alpha subcomplex subunit 13
NF-κB: Nuclear factor kappa-B
NICD: Notch intracellular domain
NNT: NAD(P) transhydrogenase
OGDH: Oxoglutarate dehydrogenase
OXPHOS: Oxidative phosphorylation
P4HA1: Prolyl 4-hydroxylase subunit alpha 1
PAH: Phenylalanine hydroxylase
PAK4: p21-activated kinase 4
PARP: Poly (ADP-ribose) polymerase
PD1: Programmed cell death protein 1
PDH: Mitochondrial pyruvate dehydrogenase
PDK1: Pyruvate dehydrogenase kinase 1
PDL1: Programmed death-ligand 1
PERK: PKR-like endoplasmic reticulum kinase
PFK: Phosphofructokinase
PFKL: 6-Phosphofructokinase, liver type
PGAM5: Bcl-XL-binding protein v68
PGE2: Prostaglandin E2
PGK1: Phosphoglycerate kinase
PHD: Prolyl hydroxylase domain
PHGDH: Phosphoglycerate dehydrogenase
PIK3: Phosphoinositide 3-kinase
PKM: Pyruvate kinase isozymes M
PPID: Peptidyl-prolyl isomerase D
PPP1R15A: Protein phosphatase 1 regulatory subunit 15A
PPP2RA1: Protein phosphorylase 2A
PRDX3: Peroxiredoxin 3
PRMT1: Protein arginine methyltransferase 1
PRPS1: Phosphoribosyl pyrophosphate synthetase 1
PTBP1: Polypyrimidine tract-binding protein 1
PTP: Mitochondrial permeability transition pore
PTRH2: Bcl-2 inhibitor of transcription 1
PYCR1: Pyrroline-5-carboxylate reductase 1
PYGB: Glycogen phosphorylase B
qPCR: Quantitative polymerase chain reaction
RAC1: Ras-related C3 botulinum toxin substrate 1
Rheb: Ras homolog enriched in brain
ROS: Reactive oxygen species
RPS6KA: Ribosomal protein S6 kinase alpha
RT-PCR: Reverse transcription polymerase chain reaction
SATB2: Special AT-rich sequence-binding protein 2
SB: SMAD inhibitor SB431542
SCF: Stem cell factor
Sema3A: Semaphorin-3A
SHMT2: Serine hydroxymethyltransferase 2
SIAH2: Seven in absentia homolog 2
SIRT: Sirtuin
SLC16A3: Solute carrier family 16 member 3 (similar for SLC1A5, SLC25A1, and SLC38A2)
SREBP: Sterol regulatory element-binding protein
TBR1: T-box, brain 1
TCA: Tricarboxylic cycle

TCF: T cell factor/lymphoid enhancer factor
TFEB: Transcription factor EB
TGFBI: Transforming growth factor beta induced
TGFβR3: Transforming growth factor beta receptor 3
TIMP: Tissue inhibitor of metalloproteinases
UDP: Uridine diphosphate
UGDH: UDP-glucose 6-dehydrogenase
UGP2: UDP-glucose pyrophosphorylase
VDAC: Voltage-dependent anion channel
VEGF: Vascular endothelial growth factor
α-KD: α-Ketoglutarate dehydrogenase.

Data Availability

Data is available by contacting the corresponding author.

Additional Points

Significance. Most current forebrain spheroids or organoids lack the components of microglia. This study uses the genomics tool to analyze various pathways of dorsal forebrain spheroids/organoids integrated with isogenic microglia-like cells derived from human induced pluripotent stem cells. The metabolic shift to aerobic glycolysis, consistent with M1 polarization of microglia, in the cocultured spheroids was observed. This study enhances our understanding of 3-D coculturing impacts on the metabolic programming of cells inside the forebrain spheroids. The results can be used to establish better coculturing methods for efficiently mimicking *in vivo* structure of the central nervous system.

Disclosure

Liqing Song's current address is College of Medicine, Vanderbilt University, Nashville, Tennessee, USA. Julie Bejoy's current address is Department of Chemical Engineering, Carnegie Mellon University, Pittsburgh, Pennsylvania, USA. The content is solely the responsibility of the authors and does not necessarily represent the official views of the National Institutes of Health. Part of the results of this study will be presented in 2019 Annual Meeting of American Institute of Chemical Engineers (AIChE), Nov 10-15, 2019, Orlando, FL.

Conflicts of Interest

No competing financial interests exist.

Authors' Contributions

JB wrote the first version of the manuscript, did some analysis, and prepared most figures. XY did critical reviews and prepared some figures. LS performed the differentiation procedure and prepared genomics samples. TH and QS helped in microglial differentiation. RJ helped in data analysis and manuscript review. SS reanalyzed the results for figures and validated the statistical analysis. YL conceived the projects and wrote and revised the manuscript.

Acknowledgments

The authors thank Dr. Brian K. Washburn in the FSU Department of Biological Sciences for his help with RNA-sequencing and RT-PCR analysis and Dr. Cynthia Vied in the FSU Translational Science Laboratory for the initial genomics analysis. This work is supported by the FSU Bridge Grant, NSF Career Award (No. 1652992 to YL), and by NIH R03EB020770 (YL).

Supplementary Materials

Supplementary Table S1: primer sequence for target genes, Supplementary Table S2: genes related to ATP synthesis and mitochondrial complexes I, III, and IV. Supplementary Table S3: genes related to the NF-κB pathway. Supplementary Table S4: AMPK pathway and PDL1/PD1 pathway. Supplementary Figure S1: microglial differentiation using additional human iPSC line: Ep-iPSC. Supplementary Figure S2: regulation of central metabolism in D-MG. Supplementary Figure S3: log2 gene expression levels of D-MG/MG ratios for ECM-related genes. *(Supplementary Materials)*

References

[1] E. Lau, D. T. Paik, and J. C. Wu, "Systems-wide approaches in induced pluripotent stem cell models," *Annual Review of Pathology*, vol. 14, pp. 395–419, 2019.

[2] R. Brandenberger, H. Wei, S. Zhang et al., "Transcriptome characterization elucidates signaling networks that control human ES cell growth and differentiation," *Nature Biotechnology*, vol. 22, no. 6, pp. 707–716, 2004.

[3] J. Muffat, Y. Li, B. Yuan et al., "Efficient derivation of microglia-like cells from human pluripotent stem cells," *Nature Medicine*, vol. 22, no. 11, pp. 1358–1367, 2016.

[4] F. Birey, J. Andersen, C. D. Makinson et al., "Assembly of functionally integrated human forebrain spheroids," *Nature*, vol. 545, no. 7652, pp. 54–59, 2017.

[5] S. P. Pasca, "The rise of three-dimensional human brain cultures," *Nature*, vol. 553, no. 7689, pp. 437–445, 2018.

[6] Y. Yan, L. Song, J. Bejoy et al., "Modeling neurodegenerative microenvironment using cortical organoids derived from human stem cells," *Tissue Engineering Part A*, vol. 24, no. 13-14, pp. 1125–1137, 2018.

[7] Y. Yan, L. Song, J. Madinya, T. Ma, and Y. Li, "Derivation of cortical spheroids from human induced pluripotent stem cells in a suspension bioreactor," *Tissue Engineering Part A*, vol. 24, no. 5-6, pp. 418–431, 2018.

[8] L. Song, X. Yuan, Z. Jones et al., "Functionalization of brain region-specific spheroids with isogenic microglia-like cells," *Scientific Reports*, vol. 9, no. 1, pp. 11055–11072, 2019.

[9] S. Sart, S. N. Agathos, and Y. Li, "Process engineering of stem cell metabolism for large scale expansion and differentiation in bioreactors," *Biochemical Engineering Journal*, vol. 84, pp. 74–82, 2014.

[10] T. Perestrelo, M. Correia, J. Ramalho-Santos, and D. Wirtz, "Metabolic and mechanical cues regulating pluripotent stem cell fate," *Trends in Cell Biology*, vol. 28, no. 12, pp. 1014–1029, 2018.

[11] Y. Liu, N. Munoz, A. C. Tsai, T. M. Logan, and T. Ma, "Metabolic reconfiguration supports reacquisition of primitive

phenotype in human mesenchymal stem cell aggregates," *Stem Cells*, vol. 35, no. 2, pp. 398–410, 2017.

[12] R. Orihuela, C. A. McPherson, and G. J. Harry, "Microglial M1/M2 polarization and metabolic states," *British Journal of Pharmacology*, vol. 173, no. 4, pp. 649–665, 2016.

[13] K. Grabert, T. Michoel, M. H. Karavolos et al., "Microglial brain region–dependent diversity and selective regional sensitivities to aging," *Nature Neuroscience*, vol. 19, no. 3, pp. 504–516, 2016.

[14] K. Wrzesinski and S. J. Fey, "Metabolic reprogramming and the recovery of physiological functionality in 3D cultures in micro-bioreactors," *Bioengineering*, vol. 5, no. 1, p. 22, 2018.

[15] H. Pandya, M. J. Shen, D. M. Ichikawa et al., "Differentiation of human and murine induced pluripotent stem cells to microglia-like cells," *Nature Neuroscience*, vol. 20, no. 5, pp. 753–759, 2017.

[16] Y. Yan, J. Bejoy, J. Xia, J. Guan, Y. Zhou, and Y. Li, "Neural patterning of human induced pluripotent stem cells in 3-D cultures for studying biomolecule-directed differential cellular responses," *Acta Biomaterialia*, vol. 42, pp. 114–126, 2016.

[17] C. Vied, S. Ray, C. D. Badger, J. L. Bundy, M. N. Arbeitman, and R. S. Nowakowski, "Transcriptomic analysis of the hippocampus from six inbred strains of mice suggests a basis for sex-specific susceptibility and severity of neurological disorders," *The Journal of Comparative Neurology*, vol. 524, no. 13, pp. 2696–2710, 2016.

[18] C. Trapnell, L. Pachter, and S. L. Salzberg, "TopHat: discovering splice junctions with RNA-Seq," *Bioinformatics*, vol. 25, no. 9, pp. 1105–1111, 2009.

[19] C. Trapnell, B. A. Williams, G. Pertea et al., "Transcript assembly and quantification by RNA-Seq reveals unannotated transcripts and isoform switching during cell differentiation," *Nature Biotechnology*, vol. 28, no. 5, pp. 511–515, 2010.

[20] M. I. Love, W. Huber, and S. Anders, "Moderated estimation of fold change and dispersion for RNA-seq data with DESeq2," *Genome Biology*, vol. 15, no. 12, p. 550, 2014.

[21] J. Wang, D. Duncan, Z. Shi, and B. Zhang, "WEB-based GEne SeT AnaLysis Toolkit (WebGestalt): update 2013," *Nucleic Acids Research*, vol. 41, Web Server issue, pp. W77–W83, 2013.

[22] B. Zhang, S. Kirov, and J. Snoddy, "WebGestalt: an integrated system for exploring gene sets in various biological contexts," *Nucleic Acids Research*, vol. 33, pp. W741–W748, 2005.

[23] Y. Benjamini and Y. Hochberg, "Controlling the false discovery rate: a practical and powerful approach to multiple testing," *Journal of the Royal Statistical Society: Series B (Methodological)*, vol. 57, no. 1, pp. 289–300, 1995.

[24] L. Song, K. Wang, Y. Li, and Y. Yang, "Nanotopography promoted neuronal differentiation of human induced pluripotent stem cells," *Colloids and Surfaces B: Biointerfaces*, vol. 148, pp. 49–58, 2016.

[25] B. M. Bijonowski, S. I. Daraiseh, X. Yuan, and T. Ma, "Size-dependent cortical compaction induces metabolic adaptation in mesenchymal stem cell aggregates," *Tissue Engineering Part A*, vol. 25, no. 7-8, pp. 575–587, 2019.

[26] S. Sart, A.-C. Tsai, Y. Li, and T. Ma, "Three-dimensional aggregates of mesenchymal stem cells: cellular mechanisms, biological properties, and applications," *Tissue Engineering Part B: Reviews*, vol. 20, no. 5, pp. 365–380, 2014.

[27] S. Sart, J. Bejoy, and Y. Li, "Characterization of 3D pluripotent stem cell aggregates and the impact of their properties on bioprocessing," *Process Biochemistry*, vol. 59, pp. 276–288, 2017.

[28] S. Varum, A. S. Rodrigues, M. B. Moura et al., "Energy metabolism in human pluripotent stem cells and their differentiated counterparts," *PLoS One*, vol. 6, no. 6, article e20914, 2011.

[29] J. Zhang, E. Nuebel, D. R. R. Wisidagama et al., "Measuring energy metabolism in cultured cells, including human pluripotent stem cells and differentiated cells," *Nature Protocols*, vol. 7, no. 6, pp. 1068–1085, 2012.

[30] R. J. McMurtrey, "Analytic models of oxygen and nutrient diffusion, metabolism dynamics, and architecture optimization in three-dimensional tissue constructs with applications and insights in cerebral organoids," *Tissue Engineering Part C: Methods*, vol. 22, no. 3, pp. 221–249, 2016.

[31] L. Jiang, A. A. Shestov, P. Swain et al., "Reductive carboxylation supports redox homeostasis during anchorage-independent growth," *Nature*, vol. 532, no. 7598, pp. 255–258, 2016.

[32] C. M. Metallo, P. A. Gameiro, E. L. Bell et al., "Reductive glutamine metabolism by IDH1 mediates lipogenesis under hypoxia," *Nature*, vol. 481, no. 7381, pp. 380–384, 2011.

[33] G. Wang, K. Sai, F. Gong, Q. Yang, F. Chen, and J. Lin, "Mutation of isocitrate dehydrogenase 1 induces glioma cell proliferation via nuclear factor-κB activation in a hypoxia-inducible factor 1-α dependent manner," *Molecular Medicine Reports*, vol. 9, no. 5, pp. 1799–1805, 2014.

[34] H. Lin, Q. Du, Q. Li et al., "A scalable and efficient bioprocess for manufacturing human pluripotent stem cell-derived endothelial cells," *Stem Cell Reports*, vol. 11, no. 2, pp. 454–469, 2018.

[35] Y. Liu, X. Yuan, N. Munoz, T. M. Logan, and T. Ma, "Commitment to aerobic glycolysis sustains immunosuppression of human mesenchymal stem cells," *Stem Cells Translational Medicine*, vol. 8, no. 1, pp. 93–106, 2019.

[36] C. Correia, A. Koshkin, P. Duarte et al., "3D aggregate culture improves metabolic maturation of human pluripotent stem cell derived cardiomyocytes," *Biotechnology and Bioengineering*, vol. 115, no. 3, pp. 630–644, 2018.

[37] A. P. Van Winkle, I. D. Gates, and M. S. Kallos, "Mass transfer limitations in embryoid bodies during human embryonic stem cell differentiation," *Cells, Tissues, Organs*, vol. 196, no. 1, pp. 34–47, 2012.

[38] T. Ma, W. L. Grayson, M. Frohlich, and G. Vunjak-Novakovic, "Hypoxia and stem cell-based engineering of mesenchymal tissues," *Biotechnology Progress*, vol. 25, no. 1, pp. 32–42, 2009.

[39] J. Mathieu, W. Zhou, Y. Xing et al., "Hypoxia-inducible factors have distinct and stage-specific roles during reprogramming of human cells to pluripotency," *Cell Stem Cell*, vol. 14, no. 5, pp. 592–605, 2014.

[40] T. Mutoh, T. Sanosaka, K. Ito, and K. Nakashima, "Oxygen levels epigenetically regulate fate switching of neural precursor cells via hypoxia-inducible factor 1α-Notch signal interaction in the developing brain," *Stem Cells*, vol. 30, no. 3, pp. 561–569, 2012.

[41] W. L. Grayson, F. Zhao, R. Izadpanah, B. Bunnell, and T. Ma, "Effects of hypoxia on human mesenchymal stem cell expansion and plasticity in 3D constructs," *Journal of Cellular Physiology*, vol. 207, no. 2, pp. 331–339, 2006.

[42] R. Fukuda, H. Zhang, J. W. Kim, L. Shimoda, C. V. Dang, and G. L. Semenza, "HIF-1 regulates cytochrome oxidase subunits to optimize efficiency of respiration in hypoxic cells," *Cell*, vol. 129, no. 1, pp. 111–122, 2007.

[43] P. M. Quirós, Y. Español, R. Acín-Pérez et al., "ATP-dependent Lon protease controls tumor bioenergetics by reprogramming mitochondrial activity," *Cell Reports*, vol. 8, no. 2, pp. 542–556, 2014.

[44] F. Weinberg, R. Hamanaka, W. W. Wheaton et al., "Mitochondrial metabolism and ROS generation are essential for Kras-mediated tumorigenicity," *Proceedings of the National Academy of Sciences of the United States of America*, vol. 107, no. 19, pp. 8788–8793, 2010.

[45] J. Chen, R. Crawford, C. Chen, and Y. Xiao, "The key regulatory roles of the PI3K/Akt signaling pathway in the functionalities of mesenchymal stem cells and applications in tissue regeneration," *Tissue Engineering Part B: Reviews*, vol. 19, no. 6, pp. 516–528, 2013.

[46] J. Zhou, P. Su, L. Wang et al., "mTOR supports long-term self-renewal and suppresses mesoderm and endoderm activities of human embryonic stem cells," *Proceedings of the National Academy of Sciences of the United States of America*, vol. 106, no. 19, pp. 7840–7845, 2009.

[47] T. R. Peterson, S. S. Sengupta, T. E. Harris et al., "mTOR complex 1 regulates lipin 1 localization to control the SREBP pathway," *Cell*, vol. 146, no. 3, pp. 408–420, 2011.

[48] K. Düvel, J. L. Yecies, S. Menon et al., "Activation of a metabolic gene regulatory network downstream of mTOR complex 1," *Molecular Cell*, vol. 39, no. 2, pp. 171–183, 2010.

[49] A. R. Tee, "The target of rapamycin and mechanisms of cell growth," *International Journal of Molecular Sciences*, vol. 19, no. 3, p. 880, 2018.

[50] Z. E. Stine, Z. E. Walton, B. J. Altman, A. L. Hsieh, and C. V. Dang, "MYC, metabolism, and cancer," *Cancer Discovery*, vol. 5, no. 10, pp. 1024–1039, 2015.

[51] G. W.-Y. Mak, W.-L. Lai, Y. Zhou, M. Li, I. O.-L. Ng, and Y.-P. Ching, "CDK5RAP3 is a novel repressor of p14ARF in hepatocellular carcinoma cells," *PLoS One*, vol. 7, no. 7, article e42210, 2012.

[52] X. Zhang, K. A. Peterson, X. S. Liu, A. P. McMahon, and S. Ohba, "Gene regulatory networks mediating canonical Wnt signal directed control of pluripotency and differentiation in embryo stem cells," *Stem Cells*, vol. 31, no. 12, pp. 2667–2679, 2013.

[53] L. Azzolin, T. Panciera, S. Soligo et al., "YAP/TAZ incorporation in the β-catenin destruction complex orchestrates the Wnt response," *Cell*, vol. 158, no. 1, pp. 157–170, 2014.

[54] L. Wang, H. Li, Y. Zhang, R. M. Santella, and I. B. Weinstein, "HINT1 inhibits β-catenin/TCF4, USF2 and NFκB activity in human hepatoma cells," *International Journal of Cancer*, vol. 124, no. 7, pp. 1526–1534, 2009.

[55] J. Bejoy, L. Song, Y. Zhou, and Y. Li, "Wnt/Yes-Associated protein interactions during neural tissue patterning of human induced pluripotent stem cells," *Tissue Engineering Part A*, vol. 24, no. 7-8, pp. 546–558, 2018.

[56] J. Bejoy, Z. Wang, B. Bijonowski et al., "Differential effects of heparin and hyaluronic acid on neural patterning of human induced pluripotent stem cells," *ACS Biomaterials Science & Engineering*, vol. 4, no. 12, pp. 4354–4366, 2018.

[57] N. Moya, J. Cutts, T. Gaasterland, K. Willert, and D. A. Brafman, "Endogenous WNT signaling regulates hPSC-derived neural progenitor cell heterogeneity and specifies their regional identity," *Stem Cell Reports*, vol. 3, no. 6, pp. 1015–1028, 2014.

[58] E. D. Cohen, Y. Tian, and E. E. Morrisey, "Wnt signaling: an essential regulator of cardiovascular differentiation, morphogenesis and progenitor self-renewal," *Development*, vol. 135, no. 5, pp. 789–798, 2008.

[59] L. Yang, C. C. Liu, H. Zheng et al., "LRP1 modulates the microglial immune response via regulation of JNK and NF-κB signaling pathways," *Journal of Neuroinflammation*, vol. 13, no. 1, p. 304, 2016.

[60] Y. Zhang, J. Liu, S. Yao et al., "Nuclear factor kappa B signaling initiates early differentiation of neural stem cells," *Stem Cells*, vol. 30, no. 3, pp. 510–524, 2012.

[61] K. Wrzesinski, A. Rogowska-Wrzesinska, R. Kanlaya et al., "The cultural divide: exponential growth in classical 2D and metabolic equilibrium in 3D environments," *PLoS One*, vol. 9, no. 9, article e106973, 2014.

[62] C. R. Clark, J. Y. Robinson, N. S. Sanchez et al., "Common pathways regulate type III TGFβ receptor-dependent cell invasion in epicardial and endocardial cells," *Cellular Signalling*, vol. 28, no. 6, pp. 688–698, 2016.

[63] L. Song, X. Yuan, Z. Jones et al., "Assembly of human stem cell-derived cortical spheroids and vascular spheroids to model 3-D brain-like tissues," *Scientific Reports*, vol. 9, no. 1, article 5977, 2019.

[64] J. Hatakeyama, Y. Wakamatsu, A. Nagafuchi, R. Kageyama, R. Shigemoto, and K. Shimamura, "Cadherin-based adhesions in the apical endfoot are required for active Notch signaling to control neurogenesis in vertebrates," *Development*, vol. 141, no. 8, pp. 1671–1682, 2014.

[65] L. Grandbarbe, J. Bouissac, M. Rand, M. Hrabé de Angelis, S. Artavanis-Tsakonas, and E. Mohier, "Delta-Notch signaling controls the generation of neurons/glia from neural stem cells in a stepwise process," *Development*, vol. 130, no. 7, pp. 1391–1402, 2003.

[66] P. Hayward, T. Kalmar, and A. M. Arias, "Wnt/Notch signalling and information processing during development," *Development*, vol. 135, no. 3, pp. 411–424, 2008.

[67] L. Galluzzi, J. M. Bravo-San Pedro, O. Kepp, and G. Kroemer, "Regulated cell death and adaptive stress responses," *Cellular and Molecular Life Sciences*, vol. 73, no. 11-12, pp. 2405–2410, 2016.

[68] C. Wang and R. J. Youle, "The role of mitochondria in apoptosis," *Annual Review of Genetics*, vol. 43, pp. 95–118, 2009.

[69] L. Galluzzi, J. M. Bravo-San Pedro, and G. Kroemer, "Organelle-specific initiation of cell death," *Nature Cell Biology*, vol. 16, no. 8, pp. 728–736, 2014.

[70] S. Beneke and A. Burkle, "Poly(ADP-ribosyl)ation in mammalian ageing," *Nucleic Acids Research*, vol. 35, no. 22, pp. 7456–7465, 2007.

[71] R. E. Hodgson, B. A. Varanda, M. P. Ashe, K. E. Allen, and S. G. Campbell, "Cellular eIF2B subunit localization: implications for the integrated stress response and its control by small molecule drugs," *Molecular Biology of the Cell*, vol. 30, no. 8, pp. 942–958, 2019.

[72] R. Cagnetta, H. H. W. Wong, C. K. Frese, G. R. Mallucci, J. Krijgsveld, and C. E. Holt, "Noncanonical modulation of

the eIF2 pathway controls an increase in local translation during neural wiring," *Molecular Cell*, vol. 73, no. 3, pp. 474–489.e5, 2019.

[73] M. A. Smolle, H. N. Calin, M. Pichler, and G. A. Calin, "Non-coding RNAs and immune checkpoints-clinical implications as cancer therapeutics," *The FEBS Journal*, vol. 284, no. 13, pp. 1952–1966, 2017.

[74] S. T. T. Schetters, D. Gomez-Nicola, J. J. Garcia-Vallejo, and Y. Van Kooyk, "Neuroinflammation: microglia and T cells get ready to tango," *Frontiers in Immunology*, vol. 8, 2018.